OPTICAL DETECTION OF AZITHROMYCIN IN WATER AND URINE USING MOLECULARLY IMPRINTED POLYMER-MICROFLUIDICS INTEGRATION

NOHA HASANEEN

A THESIS SUBMITTED TO THE FACULTY OF GRADUATE STUDIES IN PARTIAL FULFILLMENT OF THE REQUIREMENTS FOR THE DEGREE OF MASTER OF APPLIED SCIENCE

GRADUATE PROGRAM IN

Civil Engineering

YORK UNIVERSITY

TORONTO, ONTARIO

September 2024

Abstract

Azithromycin (AZM) is one of the most used antibiotics worldwide. Monitoring antibiotic concentration in urine and environmental samples is essential to control the spread of antibiotic-resistant bacteria. Analysis of AZM in environmental and biological samples is usually done by conventional methods such as High-performance liquid chromatography (HPLC) and liquid chromatography-mass spectrometry (LC-MS). These methods are time and chemical consuming, mostly laboratory-based, and require trained personnel. As for most modern sensors in recent literature, they typically suffer from one or more disadvantages such as exhibiting low sensitivity, consuming many chemicals, requiring long analysis time, or demanding expensive supporting instruments. On the other hand, optical sensors are known for their ease of use, low cost, effective portability (as they miniaturize easily), and good sensitivity. Several optical methods have been developed for AZM detection; however, they mostly require some reaction time between AZM and reagents which can reach up to 30 min, and sometimes they require derivatization using harsh acidic conditions. Therefore, there is a need for a direct, fast, and sensitive optical technique for AZM detection with reasonable chemical usage.

In this work, two new methods for AZM analysis in artificial urine were developed using direct fluorescence microscopic and spectrophotometric techniques. These methods involve forming an ion-pair complex with fluorescein isothiocyanate (FITC), thus enhancing the fluorescence intensity at a wavelength of 520 nm and the absorbance at a wavelength of 480 nm. The fluorescence method showed higher sensitivity and precision, with a linear range of 0-31.25 µg/mL, limit of detection (LOD) of 0.41 µg/mL, and limit of quantification (LOQ) of 1.23 µg/mL. This is in comparison to the spectrophotometric method's LOD of 0.82 µg/mL and LOQ of 2.49 µg/mL. The fluorescence microscopic method showed an improved AZM recovery from the artificial urine samples, suggesting higher precision in complex matrices compared to the spectrophotometric one. For enhanced selectivity, molecularly imprinted polymer (MIP) as a synthetic receptor was prepared inside a microfluidic device. In literature, MIP has been used as a stationary phase for AZM extraction prior to its detection using conventional analytical techniques. It has also been integrated with electrochemical, not optical, sensors for AZM extraction and detection. Herein, a study on using MIP as a stationary phase for AZM extraction then applying FITC as a reagent on the polymer for fluorescence-based detection was performed inside a

microfluidic device. The MIP was synthesized using photo-initiated polymerization and the template was removed using two washing approaches. First, by immersing the glass with the MIP attached in 1:9 acetic acid/methanol and using ultrasonic waves for 20 minutes. Second, by continuous flow of the washing solution in the channels containing the MIP using a syringe pump. After applying the sample on the resulting MIP for extraction followed by FITC application, higher fluorescence intensity was observed on the MIP compared to the non-imprinted polymer (NIP) for polymers washed by aid of ultrasonication. A few challenges related to repeatability, thickness control, and solution leakage still persist in the trials with ultrasonication washing. Therefore, the second approach for washing using syringe pump was used for a more controlled experiment. After extraction and FITC application on the resulted polymer, both MIP and NIP showed high fluorescence intensity when using 100 µg/mL AZM in the water samples. This can be a result of non-specific adsorption on the NIP, while in the MIP, it can be attributed to the presence of complimentary cavities as well as the non-specific adsorption. Despite the challenges with specificity, the study constitutes a promising detailed investigation where both extraction and detection of AZM can be done on the same platform using optical techniques. This approach can be potentially extended to enable multiplexing, where a microfluidic device with multiple channels, each containing an MIP specific for a different target compound can be used.

Acknowledgement

I would like to express my sincere gratitude to ALLAH, the Almighty, the Most Gracious and the Most Merciful for granting me the strength and knowledge needed to complete this work.

I would like to extend my appreciation and gratitude to my supervisors Prof. Satinder Kaur Brar and Prof. Pouya Rezai, and my mentor Dr. Rama Pulicharla for their valuable advice and continuous and unconditional support throughout my academic journey. I would like to thank all my colleagues in the Inzymes and Acute labs for their support, assistance, and stimulating discussion that enriched my study.

I would like to thank my parents and all family members for their unconditional love, support, and encouragement throughout my life. I would like also to thank all my dear Egyptian friends who made Canada feel like home and were always there, supporting and pushing me forward.

Finally, no words can describe my deepest and heartfelt gratitude to my husband Dr. Mohamed Abdelhamid, whose support has been my greatest source of strength throughout my life. Your patience, support and sacrifices have made all the difference. Thank you for being my partner in this endeavor and for making every step of this journey a shared experience. I would like also to thank my son Malik and daughter Maryam for filling my life with joy and love. Your presence has enriched my life in a way that could hardly be captured in words.

Table of Contents

List of Tables

List of Figures

List of Abbreviations

AA	Acrylic acid
ABA	Aminobenzoic acid
AEAPMS	3-(2-Aminoethylamino) propyl-dimethoxy methyl
AIBN	Azobis(isobutryonitrile)
AM	Acrylamide
AP	Aptamer
APCI	Atmospheric pressure chemical ionization
APTES	3-Aminopropyltriethoxysilane
ATR	Attenuated total reflection
AuNCs	Gold nanoclusters
AZM	Azithromycin
4BA6FPh	Tetrabutylammonium hexafluoro-phosphate
BPO	Benzoyl peroxide
CAP	Chloramphenicol
CDs	Carbon dots
CDT	Circular DNA template
CG	Colloidal gold
CL	Chemiluminescence
CLA	Clarithromycin
COOH@MWCNT	Carboxylic functionalized multiwall carbon nanotubes
CQDs	Carbon quantum dots

CV	Cyclic voltammetry
DDQ	2,3-Dichloro-5,6-dicyano-p-benzoquinone
DI	Deionized water
DMF	Dimethylformamide
DNA	Deoxyribonucleic acid
DPV	Differential pulse voltammetry
EDC	1-(3-Dimethylaminopropyl)-3-ethylcarbodiimide hydrochloride
EDTA	Ethylenediaminetetraacetic acid
EGDMA	Ethylene glycol dimethacrylate
Eu(DBM)3Phen	Tris(dibenzoylmethane)(1,10-phenanthroline) europium(III)
ELISA	Enzyme-linked immunosorbent assay
EM	Emission
ERY	Erythromycin
ESI	Electrospray ionization
ESM	Eggshell membrane
FI	Fluorescence intensity
FITC	Fluorescein isothiocyanate
FP-ICA	Filter paper immunochromatographic assay
FTIR	Fourier transform infrared
GC	Gas chromatography
GCE	Glassy carbon electrode

GFP	Green fluorescence protein
GNP	Gold nano particles
GO	Graphene oxide
GQD	Graphene oxide quantum dots
HEMA	hydroxyethyl methacrylate
HMIP	single-hole hollow molecularly imprinted polymer
HPLC	High-performance liquid chromatography
ICH	International Conference on Harmonization
JOS	Josamycin
KIT	Kitasamycin
LC-MS	Liquid chromatography-mass spectrometry
LFIA	Lateral flow immunoassay
LOD	Limit of detection
LOQ	Limit of quantification
LSPR	Localized surface plasmon resonance
MAA	Methacrylic acid
MAGA	N-methacryloyl-(L)-glutamic acid
MALDI	Matrix-assisted laser desorption/ionization
MCL	Microtiter chemiluminescence
MES	2-Morpholinoethanesulfonic acid
MIP@CQD-PCM	Molecularly imprinted polymer@carbon quantum dot-phase change microcapsules

MIP	Molecularly imprinted polymer
MOF	Metal-organic framework
MPS	3-Mercapto-propyltriethoxysilane
MRL	Maximal residual limit
MS	Mass spectrometry
MWCNT	Multiwall carbon nanotubes
NHS	1-Hydroxy-5-pyrrolidinedione
NIP	Non imprinted polymer
NOR	Norfloxacin
NPs	Nanoparticles
OVA	Ovalbumin
OVDAC	Octadecyl-4-vinylbenzyl dimethylammonium chloride
PAD	Paper-based device
PBS	Phosphate buffer saline
PCB	Printed circuit board
PCM	Phase change microcapsules
PDA	Polydopamine
PDMS	Polydimethylsiloxane
POCT	Point-of-care testing
PP	Pre -primer
PS	Polystyrene
PVDF	Poly vinylidene fluoride

QCM	Quartz crystal microbalance
QDs	Quantum dots
QDM	Quantum dot microsphere
Q-TOF	Quadrupole Time-of-Flight
RGB	Red, green, and blue
ROX	Roxithromycin
RPD-DFD	Ratiometric paper-based device- digital fluorescence detector
RSD	Relative standard deviation
SALDI	Surface-assisted laser desorption/ionization
SD	Standard deviation
SEM	Scanning electron microscopy
SERS	Surface-enhanced Raman spectrum
SMIP	Surface molecularly imprinted polymer
SPE	Solid-phase extraction
SPR	Surface plasmon resonance
TBA	3-Thienyl boronic acid
TEOS	Tetraethoxysilane
TET	Tetracycline
TFQ	Tetrafluoro-1,4-benzoquinone
TGA-capped CdTe	Thioglycolic acid-capped cadmium telluride
TLM	Tilmicosin
TrFM	Time-resolved fluorescent microsphere

TYL	Tylosin
UV-Vis	Ultraviolet-visible
VPY	2-Vinyl pyridine
WHO	World Health Organization
WWTP	Wastewater treatment plant
ZIF-8	Zeolitic imidazolate

Publications Within the Thesis

1. **Hasaneen, N.**, Pulicharla, R., Brar, S. K. & Rezai, P. Direct fluorescence and spectrophotometric-based detection of azithromycin using fluorescein isothiocyanate: Method development and comparative analysis. J. Environ. Chem. Eng. 12, 112803 (2024). **(Research paper)**
2. **Hasaneen, N.**, Akhtarian, S., Pulicharla, R., Brar, S. K. & Rezai, P. Surface molecularly imprinted polymer-based sensors for antibiotic detection. TrAC - Trends Anal. Chem. 170, 117389 (2024). **(Review paper)**
3. **Hasaneen, N.**, Khurana, P., Pulicharla, R., Rezai, P. & Brar, S. K. Nanomaterial-Based Sensors for Macrolide Sensing - Nanoscale Matter and Principles for Sensing and Labeling Applications. in (eds. Mohanta, D. & Chakraborty, P.) 513–535 (Springer Nature Singapore, 2024). **(Book chapter)**

Conferences

1. **Hasaneen N.**, Pulicharla R., Rezai P., Brar S.K. (2024). Direct Fluorescence and Spectrophotometric-based Detection of Azithromycin Using Fluorescein Isothiocyanate: Method Development and Comparative Analysis. **CREATE Annual Summit**, April 30, 2024, York University, Toronto, Ontario, Canada. **(Oral presentation)**
2. **Hasaneen N.**, Pulicharla R., Rezai P., Brar S.K. (2023). Optical sensor for azithromycin detection in water samples. **TECHNOSCAPE 2023, International Conference on Sustainable Technologies for Water and Wastewater Treatment**, December 14-16, 2023, Vellore, India. **(Oral presentation, peer-reviewed)**
3. **Hasaneen N.**, Pulicharla R., Rezai P., Brar S.K. (2023). A proof of concept for Azithromycin detection in water using molecularly imprinted polymer in a microfluidic device. **CREATE Annual Summit**, May 1, 2023, York University, Toronto, Ontario, Canada. **(Presentation)**
4. **Hasaneen N.**, Pulicharla R., Rezai P., Brar S.K. (2023). A proof of concept for antibiotics detection in water using molecularly imprinted polymer in microfluidic device. **58th Annual Central Canadian Symposium on Water Quality Research**, March 21, 2023, York University, Toronto, Ontario, Canada. **(Oral presentation, peer-reviewed)**
5. **Hasaneen N.**, Khurana P., Pulicharla R., Rezai P., Brar S.K. (2023). The Antibiotic Apocalypse': Surrendering to superbugs? **World Water Day Celebrations** at York University, March 20, 2023, York University, Toronto, Ontario, Canada. **(Infographic poster)**
6. **Hasaneen N.**, Pulicharla R., Rezai P., Brar S.K. (2022). Detection of azithromycin in wastewater and surface water using microfluidics. **TABES Annual Summit**, May 18, 2022, York University, Toronto, Ontario, Canada. **(Oral presentation)**

Publication Outside the Thesis

Khurana, P., **Hasaneen, N.**, Pulicharla, R., Kaur, G. & Brar, S. K. Co-transport of PFCs in the environment- An interactive story. Curr. Res. Green Sustain. Chem. 5, 100302 (2022).

Chapter 1: Introduction, Literature Review, and Proposed Research

1.1. Introduction

AZM is one of the most essential antibiotics globally, ranking as the second-highest purchased antibiotic in Canadian hospitals in 2018, after ceftriaxone [1]. It is known for its broad-spectrum antimicrobial efficiency starting from respiratory tract infections to sexually transmitted diseases. However, the detection of antibiotics, including AZM, in environmental and urine samples raises environmental concerns, particularly as urine is recently reused as fertilizer for its nitrogen and phosphorous contents [2–4]. Over 50% of AZM is excreted in feces and 6-14% is excreted unchanged in urine [5–7]. This highlights the need for monitoring its presence in urine to prevent soil and plant contamination which potentially enhances the development of antimicrobial resistant genes and bacteria. Although techniques such as high-performance liquid chromatography (HPLC) [8–11], capillary electrophoresis [12], liquid chromatography-mass spectrometry (LC-MS) [13–16], and electrochemistry [17–22] have been used for the detection of AZM traces in complex samples, they are laborious, expensive, and require experienced professionals. Optical detection of antibiotics has gained intensive attention, offering simple, cost-effective, and sensitive sensing techniques. Fluorescence and absorbance-based methods have been investigated for rapid, on-site detection of different antibiotics in environmental and food samples [23–25]. In addition, they can be integrated into smartphone applications that enable portable and disposable sensors for qualitative, semiquantitative or quantitative analysis of antibiotics in the field of food safety as well as public health [26–30]. Few studies have been conducted on fluorescence-based detection of AZM due to its poor optical properties where it has no fluorescence emission and only absorbs light at around 210 nm. AZM was found to quench the fluorescence of nitrogen sulfur carbon quantum dots (N,S-CQDs) [31]. Moreover, owing to the presence of tertiary amine groups in AZM, it can catalyze the condensation of malonic acid anhydride and acetic acid anhydride, producing a fluorescent product [32]. This was successfully applied to detect AZM in dosage forms and biological samples. Moreover, AZM was found to form a fluorescent ion-pair complex with eosin-G dye at pH 5-6 which was used for its detection in pharmaceutical dosage forms [33]. AZM derivatization under harsh acidic conditions was successfully applied for its detection in pharmaceutical dosage forms using both spectrofluorometric and spectrophotometric techniques [34]. Various reagents such as quinalizarin [35], methyl orange [36], bromophenol blue [37],

bromothymol blue, bromocresol green, bromocresol purple [38], and eosin Y were studied to form colored ion-pair or charge transfer complexes with AZM that can be detected using spectrophotometry [39]. Other studies were conducted on the characterization of the colored charge transfer complex formed between AZM and various reagents such as iodine [40], picric acid, chloranilic acid, chloranil [41], tetracyanoethylene [42], 2,3-dichloro-5,6-dicyano-p-benzoquinone (DDQ), and tetrafluoro-1,4-benzoquinone (TFQ) [43]. Moreover, AZM and other macrolide antibiotics were explored to react with haematoxylin in the presence of boric acid producing a colored product [44] and to form colored ternary complexes with rose Bengal and copper [45]. Despite the sensitivity of some of these methods and the ability to produce colored products with detectable optical responses, they suffer from one or more disadvantages such as the necessity of pH adjustment, some expensive and harsh chemicals, or long reaction time before measuring the response.

In addition to laboratory-based methods, the need for on-site monitoring of antibiotics, including AZM, has prompted the development of microfluidics sensors [46]. Microfluidic sensors with miniaturized systems have been tremendously studied where portable, easily operated, time and chemical-saving, and on-site devices can be developed for antibiotic analysis [47–49]. These sensors have gained extensive attention as successful tools in several fields including forensic [50], environmental [51], and food analysis [52]. Microfluidics can be integrated with optical [53], electrochemical [54], or mass spectrometric techniques [55] for analysis, offering state-of-the-art chips or paper-based devices for detection [56]. To extract antibiotics from complex matrices, sensors use selective recognition elements like antibodies [57,58], aptamers [59,60], enzymes [61], or molecularly imprinted polymers (MIPs) [62]. MIPs have aroused extensive attention as a new solid phase extraction technique for target capturing from complex matrices [63]. In contrast to biological receptors, MIPs reveal better thermal and physical stability with good selectivity and ease of preparation [64]. MIPs have been used as synthetic receptors for AZM detection in diverse media in several studies using electrochemical, piezoelectric, or electrochemiluminescence sensors for AZM detection as summarized in Table 1-1. However, most of these studies relied on electrochemical detection which requires expensive and specific tools for signal measurements. Different monomers, cross linkers, initiators, and solvents were used to synthesize MIP for AZM in a trial to enhance the sensors' selectivity and sensitivity. For MIP preparation, a template which

is AZM or a dummy template such as erythromycin which is a structurally related compound was mixed with the monomers in a solvent for a period of time to form some bonds between the template and the monomers. Afterwards, initiator and cross-linker can be added and polymerization can be performed. Polymerization can be electro-polymerization, photo-initiated polymerization, or thermal polymerization. Methacrylic acid (MAA) and ethylene glycol dimethacrylate (EGDMA) were the most used monomer and crosslinker for AZM's MIP [17,65–71].

In this thesis, an innovative approach for AZM detection in artificial urine samples has been developed based on the formation of an ion-pair complex between AZM and FITC. FITC, an acidic organic dye, is known for its strong and stable green fluorescence when excited with blue light. This property makes it a powerful tool for fluorescence-based analysis and applications in fluorescence microscopic applications. It is widely used as a fluorescent pH indicator to label biological molecules such as proteins and antibodies in various studies. Moreover, Its isothiocyanate functional group allows easy conjugation with amino groups of other molecules, enabling the analysis of different targets [72–74]. AZM-FITC ion-pair complex enabled simple, rapid, and sensitive spectrophotometric and fluorescence-based analysis of AZM in artificial urine samples with no need for long reaction time, harsh acid use, or compound derivatization. Moreover, by combining fluorescence-based detection using FITC, microfluidics, and MIP using MAA and EGDMA, this thesis has taken a step forward towards developing an efficient approach for AZM detection in artificial urine and water samples with the possibility of portability. This innovative integration not only extends the scope of monitoring antibiotic traces but also gives rise to a broad range of applications in protecting the environment and health.

Table 1-1: MIP integrated sensors for AZM detection

Fabrication method	Probe	Detection	Template	Monomers	Cross linker	Initiator	Solvent	Matrix	LOD (nM)	Linear range (nM)	Selectivity	Ref.
Electro polymerization by cyclic voltammetry (CV)	MIP/ glassy carbon electrode (GCE)	Square Wave Voltammetry	AZM (1 mmol)	benzothiophene-3-boronic acid (Ph-3-TBA) (1 mmol)	4,4'-dibromo-3,3'-bithiophene (4,4'-Br-3,3'-Bth) (2mmol) and 3-Me-Th (2 mmol) as linker		Acetonitrile + 5%DMF	Tap water, sewage	120	400-100000	AZM and erythromycin (40.6% relative response)	[65]
Electro polymerization by CV	MIP/GCE	Electrochemical impedance spectroscopy	AZM (10 mmol)	3-thienyl boronic acid (3-TBA) (20 mmol)	2,20-bithiophene (Bth) (5 mmol)	Tetrabutylammonium hexafluoro-phosphate (4BA6FPh) (50 mmol)	Methanol	Urine, plasma, tears	0.85	13.33 - 66670	Selective for AZM over other drugs, only clarithromycin shows 17% relative response	[66]
Electro polymerization by CV	MIP/gold nanourchin/graphene oxide modified GCE	Differential pulse voltammetry (DPV)	AZM (5 mmol)	Aniline (0.1 mol)			0.075M HNO_3, 0.025M H_2SO_4	Serum	0.1	0.3-920	More selective for AZM than erythromycin and penicillin	[67]
Electro polymerization by CV	MIP/screen printed electrode	DPV	AZM (0.05 mmol)	4-aminobenzoic acid (4-ABA) (5 mmol)			phosphate buffer (pH 7)	tap water, water samples collected upstream of	80	500-10000	CLA and ERY have relative response 48.1 and 58.4% of	[17]

								a WWTP output			AZM, respectively	
Thermal polymerization	MIP/graphite coated electrode	potentiometric	AZM (0.5mmol)	Acrylic acid (AA) Or 2-vinyl pyridine (VPY) (3 mmol)	ethylene glycol dimethacrylate (EGDMA) (15 mmol)	benzoyl peroxide (BPO) (0.32 mmol)	Methanol	Tablets, capsules	1000		Not studied for other antibiotics	[68]
Thermal polymerization	MIP/modified carbon paste electrode	Electrochemiluminescence	Erythromycin (1.5mmol)	Methacrylic acid (MAA) (6 mmol)	EGDMA (15 mmol)	2, 2-azobisisobutyronitrile (AIBN) (40 mg)	methanol/acetonitrile (1/4, v/v)	Urine, plasma	0.023	0.1-400	Other macrolides have response up to 50% of that of AZM	[69]
Thermal polymerization	MIP/acetylene black-modified carbon paste electrode	DPV	Erythromycin (1.5 mmol)	MAA (6 mmol)	(EGDMA) (15 mmol)	AIBN (40 mg)	methanol/acetonitrile (1/4, v/v)	Serum, urine, tablets	11	100-2000 and 2000-20000	Other macrolides have response up to more than 50% of that of AZM	[70]
Thermal polymerization	MIP@SiO_2/magnetic carbon nanocomposites	Piezoelectric sensor	AZM (0.06 g)	MAA (0.1 mmol)	(EGDMA) (0.8 mmol)	AIBN (0.0985 g)	Acetonitrile /toluene (3:1, v/v)	Pork, chicken meat	667.6	6676-213618	Selective for macrolide group over other antibiotics	[71]

1.2. Literature Review [1]

AZM is one of the most used antibiotics all over the world. It is classified under a large group of antibiotics called macrolide. Macrolide is a class of antibiotics used in the management and treatment of various bacterial infections, such as upper and lower respiratory tract bacterial infections including, pharyngitis, tonsilitis, otitis, sinusitis, bronchitis, *Mycobacteria* infections, community-acquired pneumonia, and *Legionella pneumophila* infection. Moreover, they are well-known for the treatment of sexually transmitted diseases such as chancroid, *Neisseria gonorrhea* infection, and *Chlamydia trachomatis* infections. They can also be used as a moderate treatment and a prophylactic drug for the traveler's diarrhea. They are categorized as the highest priority, critically important antibiotics by the WHO (World Health Organization) due to their ability to treat severe, life-threatening, rare diseases both in humans and animals [75]. Moreover, recent injectable macrolides have a long half-life, which allows for once-only dosing regimens. They are primarily bacteriostatic and prevent bacterial multiplication by binding to the 50S subunit of the ribosome and inhibiting bacterial protein synthesis [76].

Chemically, macrolides possess a macrocyclic lactone ring containing between 12 to 17 atoms, attached to one or more deoxy sugars via glycosidic bonds, and are classified based on the size of the macrocyclic ring. For instance, a 14-membered ring (e.g., erythromycin and clarithromycin consist of two sugar moieties attached to a 14-atom lactone ring), 15- (e.g., AZM), and 16- (e.g., tylosin and josamycin) membered macrolide antibiotics are the most common. The large lactone ring is substituted by hydroxyl, alkyl, or acyl groups, contains one ketone at C7 for 12-membered macrolides, and at C9 for 14-member analogues, and one aldehyde functionality in 16-membered rings. AZM contains a 15-member ring with a tertiary amino-group methyl-substituted nitrogen) as shown in Figure 1-1. The substitution of hydroxyl groups by neutral or basic sugars renders basic character to the macrolides.

[1] *Some extracts in this section were taken from the published book chapter* ***"Hasaneen, N.****, Khurana, P., Pulicharla, R., Rezai, P. & Brar, S. K. Nanomaterial-Based Sensors for Macrolide Sensing - Nanoscale Matter and Principles for Sensing and Labeling Applications. in (eds. Mohanta, D. & Chakraborty, P.) 513–535 (Springer Nature Singapore, 2024)"* [77] *and the review paper "****Hasaneen, N.****, Akhtarian, S., Pulicharla, R., Brar, S. K. & Rezai, P. Surface molecularly imprinted polymer-based sensors for antibiotic detection. TrAC - Trends Anal. Chem. 170, 117389 (2024)"*[187]

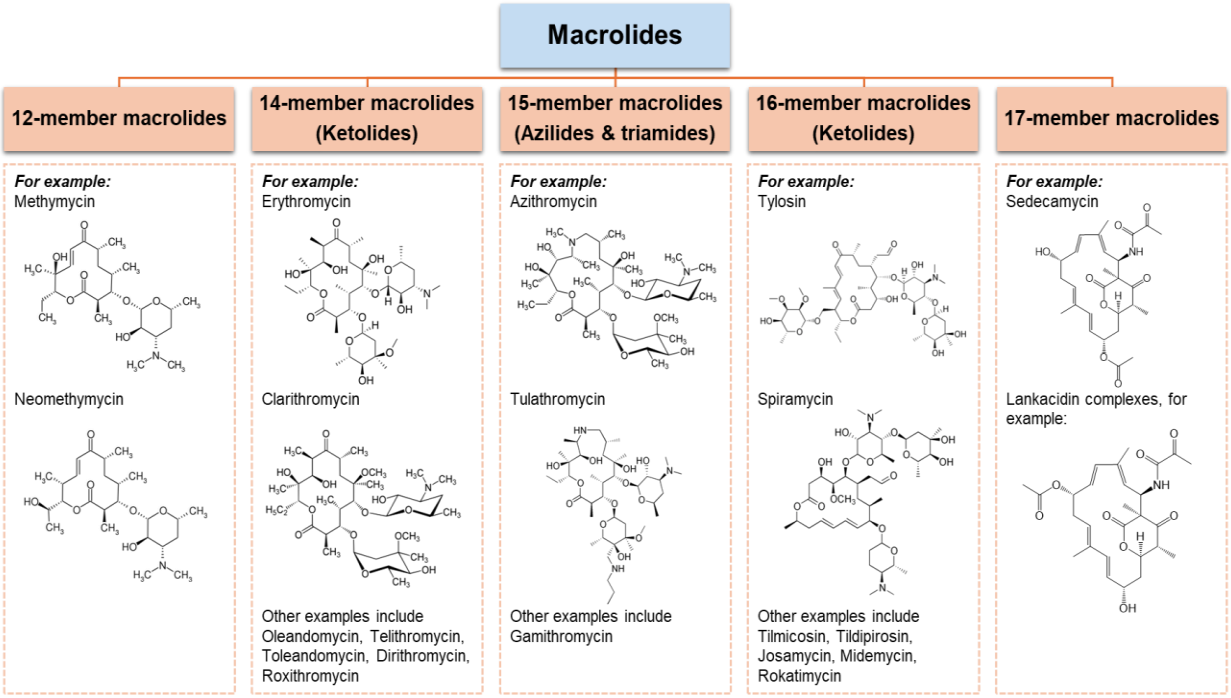

Figure 1-1: Classification of macrolide antibiotics. The figure was reprinted with permission from Springer Nature Singapore [77].

A study has revealed up to 7000, 1300, and 270 ng/L of macrolide antibiotics, including AZM, clarithromycin, and erythromycin, in effluents from six wastewater treatment plants (WWTPs) in Canada, with their concentrations ranging from 850-81, 580-4.6, 92-1.4 ng/g dw (dry weight) biosolids, respectively [78]. Similarly, their widespread applications to prevent and treat infections in poultry and livestock have resulted in their occurrence in food samples, such as honey, milk, eggs, and meat products. This continuous exposure to macrolides through water/food sources can trigger the development and dissemination of antibiotic resistance at a faster rate, which is alarming. Therefore, many countries have established maximal residual limits (MRL) of the most used macrolides in different types of food products to monitor their spread. For example, the MRL of erythromycin in Canadian animal food products is 0.05 ppm in cattle milk, 0.2 ppm in sheep muscles, 0.125 ppm in chicken muscles, and 0.2 ppm for tylosin in different food products [79]. In this sense, it becomes imperative to develop sensitive and robust on-site detection techniques for macrolides in varying samples, such as urine, milk, plasma, water, wastewater, soil, and sediments.

1.2.1. Conventional methods for detection of macrolides

Conventional methods for the detection of macrolide antibiotic residues are primarily based on HPLC, LC-MS, and gas chromatography-mass spectrometry (GC-MS). For instance, Amelin *et al.* (2019) developed a sensitive HPLC-Q-TOF MS method to accurately detect and quantify 12 macrolides in food materials, with limits of detection (LODs) and limits of quantification (LOQs) as 0.01-0.50 ng/g and 0.04-2.0 ng/g, respectively [80]. Similarly, a study by Thangadurai S. (2015) developed a method with GC-MS to analyze AZM in biological fluids, with an LOD of 2 ug/mL [81]. LC-MS has also been utilized to detect macrolides in various matrices, including food, biological samples, and environmental matrices. To improve the detection of these trace pollutants, sample preparation, which comprises extraction and concentration of the analyte from our sample, is performed first. This is often done by conventional extraction (dissolution, precipitation, filtration), solid-phase extraction (SPE) and its variants, electro-membrane extraction, QuEChERS (Quick, Easy, Cheap, Effective, Rugged and Safe), ultrasonication-assisted extraction (UAE), etc. [82]. Sample treatment is typically followed by LC-MS analysis, which has been a premier analytical tool for quantification and qualitative analysis of analytes. Generally, reverse phase columns, such as Zorbax SB-Aq C18 column, Hypersil gold C18, Eclipse XDB-C18, and C8 columns, are the most used stationary phases due to their good hydrophobicity, selectivity and high efficiency, along with acetonitrile or methanol as the mobile phase [14,83,84]. Soft ionization techniques such as electrospray ionization (ESI) and atmospheric pressure chemical ionization (APCI), matrix-assisted laser desorption/ionization (MALDI), and a newer technique called surface-assisted laser desorption/ionization (SALDI), can be used for macrolides. All these methods have been comprehensively discussed in a recent review by C. Hu, Y. Zhang, Y. Zhou *et al.* (2020) [82]. These methods are accurate and quantitative - with an LOD ranging from ng/L to ug/L, however, they necessitate highly qualified individuals and costly, sophisticated equipment. Also, extensive sample preparation- extraction and concentration make the processing time-consuming and labor-intensive.

Various attempts have been made to overcome these limitations of traditional methods and for the development and standardization of rapid, inexpensive, robust, and sensitive detection technologies for antibiotics including AZM. Consequently, researchers have been directed towards exploring new types of sensors, mostly using optical and electrochemical transduction modalities,

to address the limitations of traditional antibiotic detection techniques. To enhance sensor selectivity towards targets such as AZM, specific receptors such as antibodies, enzymes, aptamers, or MIPs can be used. However, MIP, being synthetic not biological, offers enhanced thermal, chemical, and physical stability.

1.2.2. Molecularly imprinted polymers (MIPs) for selective capturing and optical detection of antibiotics

MIPs are synthetic receptors, providing low-cost alternatives with better thermal and chemical stability compared to biomolecules [64]. They are formed of monomers, crosslinkers, initiator, solvent, and template molecules (e.g., AZM). Template molecules are eluted after the polymerization, leaving cavities specific for their shape, size, and function groups. Extraction of the target compounds can be through the formation of covalent, semi-covalent, or non-covalent bonding between the monomers and the target molecules [85].

MIPs can be synthesized through various methods including bulk polymerization, suspension polymerization, dispersion polymerization, precipitation polymerization, or surface molecularly imprinted polymerization [86]. Surface molecularly imprinted polymers (SMIPs) offer several advantages such as strong binding kinetics where target compounds can bind to the polymer quickly and efficiently, fast mass transfer, and minimum embedding problems as the polymerization is performed on the surface of solid substrates. In SMIP fabrication, as illustrated in Figure 1-2, a polymer with complementary cavities to the target analyte can be developed. This is achieved by mixing the analyte (e.g., an antibiotic referred to as the template) with one or multiple monomers, cross-linkers, and initiators to prepare the pre-polymerization solution. This solution is subsequently applied to the substrate surface [63,87]. Various materials can serve as a substrate for polymerization and may be pre-treated with different chemicals to introduce specific function groups such as -OH, -NH_2, -COOH. In some cases, initiators or monomers can be immobilized on the surface. On the substrate, a pre-polymerization solution containing the template compound is applied, followed by polymerization using different techniques. The template is then washed away, leaving behind a layer of MIP with specific cavities designed for capturing the analyte. Electrochemical sensors often employ electrodes or nano-materials as the substrate [88], while optical sensors can utilize microparticles, nanoparticles, or nanofilms. Various techniques for SMIP fabrication have been extensively reviewed [85], covering the

different types of interactions between monomers and template molecules, various polymerization techniques, and different applications of SMIP in different fields. In this context, we focus on optical sensors integrated with SMIP for different antibiotics.

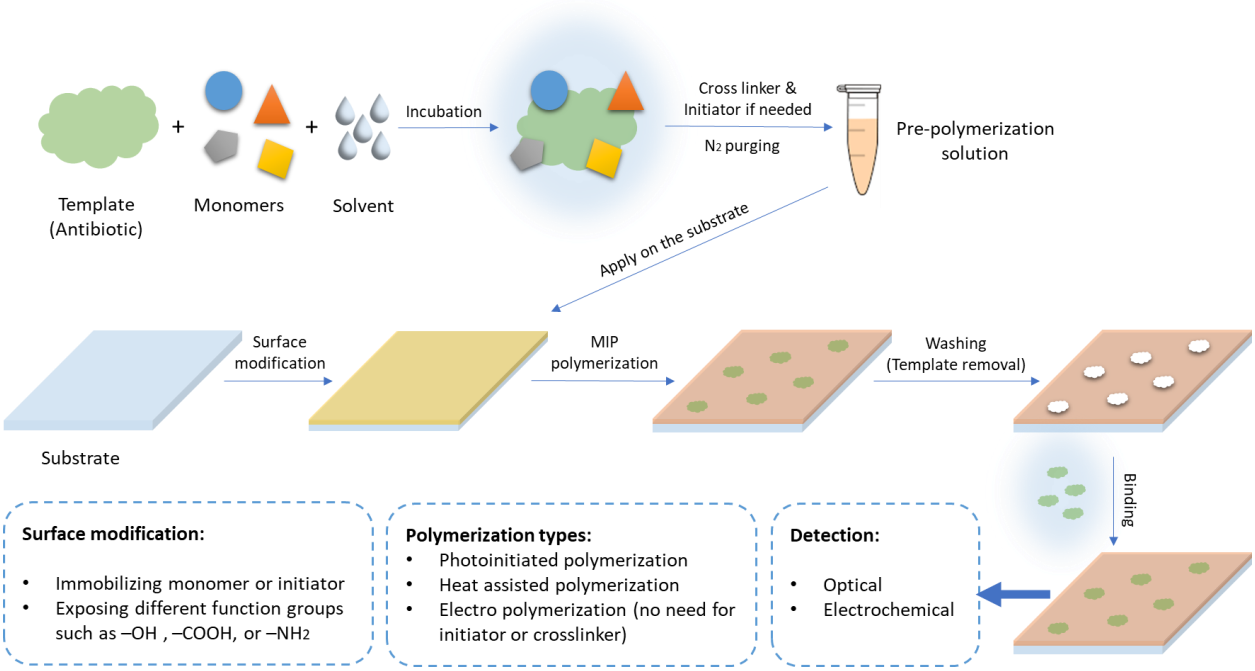

Figure 1-2: Surface molecularly imprinted polymerization technique involving preparation of the pre-polymerization solution, substrate surface modification, different polymerization techniques, washing step for template removal, rebinding of target compounds, and detection methods.

Optical sensors have been widely recognized for their ability to provide rapid, simple, low-cost, and sensitive analysis of antibiotics [89–92]. Among the different types of optical sensors used for antibiotic detection, colorimetric, fluorescence, chemiluminescent, surface plasmon resonance (SPR), and surface-enhanced Raman spectrum (SERS) sensors have been successfully utilized [93]. However, not all these optical sensor types have been integrated with SMIP technology, where the polymerization step takes place on the substrate surface. For example, a colorimetric MIP sensor has been developed by coating a pre-made MIP nanoparticles onto the substrate surface to act as synthetic receptors [27]. MIP particles have also been used in conjunction with a competitive dye displacement strategy for colorimetric detection of various chemical compounds including aryl amines, amoxicillin, and 2-methoxiphenidine [94–96]. This section provides a comprehensive overview of recent advances in optical sensing of antibiotics that have been

coupled with SMIPs as synthetic receptors. This is summarized in Table 1-2, which lists MIP composition, substrates, detection techniques with LODs, linear ranges and practical applications.

1.2.2.1. SMIP fluorometric sensors

Fluorescence-based sensors are one of the most widely used optical sensors and are highly sensitive and provide a rapid response. Also, they can be implemented for non-destructive visual recognition. They rely on the use of fluorophores which are molecules that exhibit ascending or descending fluorescence upon exposure to target analytes, which are also known as turn-on (increasing) and turn-off (quenching) mechanisms, respectively. To increase the stoke shift, which is the difference in wavelength between the maximum absorption and emission, many researchers have investigated fluorophores other than organic dyes to avoid self-quenching problems, with enhanced stability and fluorescence lifetime. These include quantum dots, gold nanoclusters, and Europium ions. Environmentally friendly fluorophores such as carbon dots and carbon nanomaterials have also attracted much attention [97,98] to avoid the potential toxicity of synthetic organic dyes on aquatic organisms [99] such as mutagenicity [100] and increased oxidative stress [101]. These new approaches have successfully enhanced sensitivity, lowered LOD and increased the linear range of fluorescence-based antibiotic analysis. Integrating SMIP with these nanomaterials offers both sensitivity and selectivity for target detection, as discussed below. SMIP used for fluorometric sensors can be categorized into two types based on the polymer matrix: vinyl-based MIP and silicon-based MIP.

Vinyl-based SMIP fluorometric sensors

Vinyl-based SMIPs are prepared using different types of monomers, each containing only one vinyl group in their chemical structure. These monomers include acrylic acid, methacrylic acid (MAA), acrylamide (AM), N-vinylpyrrolidone, methyl methacrylate, and hydroxyethyl methacrylate (HEMA). Cross-linking agents with two or more vinyl groups, such as ethylene glycol dimethacrylate (EGDMA), N, N-methylene-bis-acrylamide, divinylbenzene, methylene bis acrylamide, and trimethylolpropane trimethacrylate, are used to crosslink these monomers. These polymers are synthesized using the free radical polymerization technique, in which a photo or thermal initiator generates a free radical to initiate polymerization. Vinyl-based SMIPs have been employed as synthetic receptors for various antibiotics and they have been coated onto different types of fluorescent materials.

One of the most commonly used MIP recipes includes MAA, EGDMA, and azobisisobutyronitrile (AIBN) as the monomer, cross-linker, and thermal initiator, respectively. Z. Li et al. [102] used this recipe with ciprofloxacin as the template molecule to coat fluorescent microparticles with SMIP synthetic receptors for the detection of ciprofloxacin. They embedded tris (dibenzoyl methane) (1,10-phenanthroline) europium (III) (Eu(DBM)3Phen) as a fluorophore in carboxylic polystyrene microparticles to enhance their photostability using a swelling-shrinking technique. Rare earth ion composites, such as (Eu(DBM)3Phen) have garnered attention as novel fluorophores for fluorescence-based sensors due to their exceptional fluorescence intensity, energy transfer, distinct color, and extended fluorescence lifetime [103]. The binding of ciprofloxacin into the complementary cavities resulted in fluorescence quenching of the coated microparticles, successfully exhibiting an LOD of 92 ng/L [102]. Another study by Wei and Chen [104] was conducted on tetracycline detection using tetracycline as a template, acrylamide as a monomer, EGDMA as a crosslinker, AIBN as initiator and a combination of two types of cadmium telluride quantum dots (QDs) (green QDs (g-QDs) and red QDs (r-QDs)) as fluorophores. QDs are among the promising fluorophores in optical sensors, known for their unique luminescent and electronic properties, including a narrow emission band, a broad excitation range, and a large surface area-to-volume ratio [105]. Although this fluorescence probe exhibited dual emission, only the green fluorescence was quenched by binding tetracycline into the SMIP cavities. This can be attributed to the MIP@QDs fabrication design where the r-QDs were embedded inside the silica layer, forming the core. However, the modified g-QDs were included in the MIP polymerization solution as an auxiliary monomer. This resulted in the possibility of electron transfer occurring exclusively between tetracycline and the g-QDs, not the r-QDs. One advantage of this technique is the ability to visually observe a change in the solution colour from yellowish green to red by increasing the tetracycline concentration in the test solution [104]. Furthermore, tetracycline traces in food products were detected using blue, fluorescent N and Mg co-doped carbon dots (CDs) coated with SMIP layer. MAA was used as a monomer, tetracycline as the template with EGDMA and AIBN as cross-linker and initiator, respectively [106]. CDs have recently emerged as a viable alternative to QDs. Despite the successful applications of QDs in the detection of antibiotics, they contain heavy metals such as cadmium which are well known for their environmental and health hazards even at low concentrations [107–109]. Therefore, more efforts have been made to fabricate environmentally friendly fluorescent probes. CDs can be easily synthesized through top-down or

bottom-up techniques using various types of precursors, including natural and green sources [110–112]. This probe was successfully used for the detection of tetracycline at a very low LOD of 0.79 ng/mL through fluorescence quenching, which occurred due to both charge transfer and inner filter effect quenching mechanisms[106].

Silicon-based SMIP fluorometric sensors

Unlike vinyl-based SMIP, silicon-based SMIP can be synthesized at room temperature in water and ethanol as solvents, without the need for other organic solvents. The fabrication of this type of polymer involves a sol-gel polymerization mechanism, where silicon-containing monomers such as 3-aminopropyltriethoxysilane (APTES) and crosslinkers such as tetraethoxysilane (TEOS) are used as precursors for the polymerization. This polymerization process begins with the hydrolysis of silicon alkoxide groups Si-OR into silanol groups Si-OH in an acidic or basic medium followed by polycondensation of silanol groups from different molecules to form siloxane bond Si-O-Si [113].

Silicon-based SMIP layers can be fabricated over different types of fluorescent materials. For example, Yufeng Zhang et al. [114] developed an SMIP fluorescence-based sensor for the detection of erythromycin. They used APTES, TEOS, erythromycin, and ammonium hydroxide as the monomer, crosslinker, template, and catalyst respectively. Carboxylic gold nano clusters (AuNCs) with sizes of 2-4 nm were used as fluorophores. AuNCs have generated considerable attention in optical sensing due to their exceptional optical and physical properties, including excellent emission and the high surface-to-volume ratio [115]. These carboxylic AuNCs were immobilized onto amino-functionalized silica nanoparticles (80 nm) through carbodiimide coupling, which involved using 1-(3-dimethylaminopropyl)-3-ethylcarbodiimide hydrochloride (EDC) and 1-hydroxy-5-pyrrolidinedione (NHS) in 2-morpholinoethanesulfonic acid (MES) to form an amide bond between carboxylic and amino functional groups. The resulting AuNCs@SIO2 were then coated with the silicon-based SMIP. Fluorescence quenching occurred with selective rebinding of erythromycin to SMIP recognition sites, resulting in an LOD of 9.2 μg/L [114]. Additionally, based on the sol-gel polymerization using APTES and TEOS with ciprofloxacin as a template, Yuphintharakun et al. [116] developed a new method for ciprofloxacin detection. Carboxylic acid functionalized multiwall carbon nanotubes (COOH@MWCNTs) were incorporated with thioglycolic acid-capped cadmium telluride (TGA-capped CdTe) QDs as a

substrate for detection. Using 0.0005% w/v of COOH@MWCNTs provided higher binding efficiency and sensitivity because COOH@MWCNTs possess extended sp^2 hybridized bonds that can interact with aromatic rings in the ciprofloxacin structure through π-π interaction. However, a higher amount of MWCNTs could disrupt the polymerization process and result in fewer recognition sites.

In this context, capturing ciprofloxacin with the fluorescent probe resulted in fluorescence quenching through charge transfer since there is no overlapping between the absorption spectrum of ciprofloxacin and the emission spectrum of the fluorescent probe. This enabled the detection of ciprofloxacin at a low LOD of 0.006 μg/L and a wide linear range of 1-100 μg/L [116]. A silica layer can be beneficial for coating QDs as it helps prevent photodegradation and leakage of CdTe nanoparticles, as demonstrated by Shi et al. [117] in the detection of norfloxacin. They found that norfloxacin could quench the fluorescence of MIP-coated 3-mercaptopropionic acid-capped CdTe QDs, which were protected with a silica layer before polymerization using norfloxacin as the template, APTES as a monomer, and TEOS as a crosslinker. They employed a reverse microemulsion technique to coat QDs with the MIP layer [117]. Moreover, silicon-based SMIP coated on CDs synthesized from citric acid by pyrolysis were successfully used to capture ceftazidime from urine samples, achieving an LOD of 0.06 μg/L. Ceftazidime was found to quench the fluorescence of these carbon dots in a linear range of 0.18 - 1.27 μg/L through electron transfer between the CDs and the antibiotic [118].

Likewise, Jalili et al. [119] synthesized yellow and blue CDs (Y-CDs and B-CDs) for the detection of penicillin G in milk samples. They coated the MIP layer with APTES, TEOS, Y-CDs and penicillin G onto the surface of the silica-coated B-CDs. Penicillin G was found to quench the fluorescence of the Y-CDs, but it did not affect the B-CDs' fluorescence, as the latter was embedded inside silica coating as a core substrate. This resulted in a nanosensor with fluorescence colour changed from yellow to blue as the penicillin G concentration increased, with an LOD of 0.34 nM [119]. These Y/B-CDs were also used for detecting chloramphenicol in milk samples following the same mechanism as penicillin G but using chloramphenicol as a template in the MIP coating layer, with an LOD of 0.035 μg/L [120]. Moreover, Jinli Fu et al. [121] combined zeolitic imidazolate (ZIF-8) metal-organic framework (MOF) with 2 types of carbon dots for fluorescence-based detection of thiamphenicol. TEOS and APTES were used to coat this probe with a selective

layer of MIP. ZIF-8 was found to reduce the required reaction time for thiamphenicol with the fluorescence probe from 4 to 2 min, as it increases the surface area and the porosity of the sensing probe. They successfully detected thiamphenicol in different spiked complex samples such as fish, beef, and milk with an LOD of 1.9 nM [121]. Furthermore, Xiaodan Wu et al. [122] combined a luminescent zirconium-based MOF (NH_2-UiO-66) with two types of QDs, green and red, for the detection of chloramphenicol in meat, milk and honey samples using silicon-based MIP for selectivity. This ternary emission MIP sensor exhibited a wide range of color changes, ranging from yellowish green to blue color, which was observed by the naked eye. The addition of chloramphenicol to this probe resulted in fluorescence enhancement of the MOF's emission peak and fluorescence quenching of emission peaks of both the red and the green QDs achieving an LOD of 3.8 pM [122]. APTES can be used to modify the substrate material such as CDs to improve their interaction with the silicon-based MIP layer. An MIP coating was applied to APTES-CDs using oxytetracycline as a template for the selective detection of oxytetracycline in honey samples through the electron transfer quenching mechanism, achieving a LOD of 15.3 ng/mL [123]. To further improve the synthesis technique of CDs@MIP, microwave-assisted preparation has been investigated as a time-saving method. While CD preparation through the hydrothermal method may take some hours, microwave-assisted preparation only takes a few minutes. Microwaves can be utilized not only for CD preparation but also for MIP layer formation. For example, Hou et al. [124] synthesized CDs from citric acid and dipotassium hydrogen phosphate in water within 2 minutes and 30 seconds in a conventional microwave oven for the detection of tetracycline. Then these CDs were modified with APTES using a microwave for 4 minutes. Finally, CDs-APTES were coated with a silica MIP layer using tetracycline as a template with a programmed heating control in the microwave for only 68 minutes. Under optimum conditions, tetracycline quenched the fluorescence of the CDs with an LOD of 5.48 nM [124]. Furthermore, APTES and TEOS can be combined with graphene oxide quantum dots (GQDs) as another example for eco-friendly fluorophores to form a layer of MIP. These were used by Zhou et al. [125] for the detection of tetracycline in milk samples. Tetracycline can only quench the fluorescence intensity of MIP-coated COOH-GQDs through static quenching as there is a change in the absorbance spectrum of the GQDs after mixing with tetracycline. However, it has no effect on the fluorescence intensity of the MIP-coated NH2-GQDs. This depicts that functional groups on GQDs play a significant role in the interaction between the target analyte and the fluorophore and choosing the right

fluorophore is critical to ensure the interaction with the analyte. This environmentally friendly synthesized nanosensor could detect trace amounts of tetracycline with an LOD of 1 µg/L [125].

To evaluate the functioning of vinyl-based SMIP and silicon-based SMIP, Chao et al. [126] reported a comparative study between three different SMIP coatings on thioglycolic acid-capped CdTe QDs for the detection of tetracycline, based on its fluorescence quenching effect on these QDs. Although particles coated with vinyl-based SMIP required a longer equilibrium time for binding with tetracycline than those with silicon-based SMIP, they achieved better recognition and recovery, as well as reduced protein adsorption. This is because the vinyl-based MIP, where MAA and EGDMA were used, is hydrophilic compared to the hydrophobic silicon-based MIP [126]. All these studies have been using the fluorescence spectrophotometer for the detection step; however recently smartphones have been used as an alternative for on-site portable sensors. For example, Tang k et al. [127] developed a silicon -based MIP tri-color fluorescence-based sensor for the detection of chloramphenicol and florfenicol antibiotics, alongside ibuprofen anti-inflammatory drugs. Herein, images of the color changes were taken by the smartphone and then processed by converting them into RGB (red, green, and blue) values. This technique where MOF has been used with QDs as fluorescence probes was able to detect florfenicol and chloramphenicol in different sample types with LOD of 7 nM and 0.012 nM, respectively [127]. Although incorporating SMIP improves the selectivity of the above-mentioned fluorescent probes towards specific antibiotics, further modifications are necessary to increase their selectivity and eliminate interference from other structurally related compounds that may be present in the real samples. One disadvantage of these types of sensing probes is that most of them are highly affected by changes in pH. Therefore, further studies are necessary to develop signal transducers that are resistant to pH changes.

1.2.2.2. SMIP surface plasmon resonance-based (SPR) sensors

The SPR method, which is known for its high sensitivity and selectivity, has been successfully integrated with SMIP to create optical antibiotic sensors. In this technique, the SPR occurs when polarized light at a certain incident angle produces a total internal reflection that encounters a thin metal film. The reflected light intensity, which can be detected within a few seconds is dependent on the refractive index of the medium. This label-free and real-time technique involves coating a metal film (typically gold nanofilm) on a chip with a thin layer of SMIP to selectively capture the target analyte [128,129]. The thickness of the MIP layer is a crucial factor in this type of detection,

as the evanescent waves generated by the incident light can only travel to a short distance of about 200 nm on the SPR chip surface. The binding of target molecules to the SMIP cavities results in a change in the refractive index on the imprinted SPR chip, which can be detected [130].

Erythromycin, one of the commonly used macrolide antibiotics was detected in an aqueous solution with an LOD of 0.29 μg/mL using a gold SPR chip with a thin layer of MIP. Imprinted nanoparticles were first prepared using a mini-emulsion polymerization technique, in which organic and aqueous phases containing monomer, surfactants, cross-linker, and template were mixed. A first polymerization was done after adding the initiator to obtain 40 nm nanoparticles with erythromycin bound inside the cavities. A second polymerization was done on the surface of the SPR chip using UV to form a layer of these nanoparticles on the gold film. SPR detection using this technique provides higher selectivity and sensitivity compared to other spectrophotometric methods [131]. While this technique required two-step and took a long time, Luo et al. [130] used only one-step photo-initiated polymerization to synthesize a thin MIP layer on SPR modified gold chip on which benzophenone initiator was localized for detecting ciprofloxacin in an aqueous solution. This only required 100 seconds for the synthesis of an MIP layer of 50-100 nm thickness. SPR measurements were performed using their custom-built SPR sensor and images were acquired by a high-resolution camera. One advantage of photo-initiated polymerization is that it can be used for fabricating different MIP spots for different antibiotics on the same chip using a photo mask, as demonstrated for ciprofloxacin and AZM [130]. Additionally, amoxicillin was detected in egg samples using the SPR technique with a commercial SPR imager. A MIP layer was produced on allyl-modified gold chip using UV light (365 nm) for 45 minutes, where amoxicillin was used as a template, HEMA and MAA as monomers, AIBN as initiator, and EGDMA as a cross-linker. This MIP layer exhibited higher selectivity for amoxicillin over structurally related antibiotics such as cephalexin and ampicillin [132]. The same recipe was used for the detection of sulfamethoxazole in milk samples with sulfamethoxazole as a template which describes the MIP preparation technique and the SPR detection mechanism as mentioned above. This MIP was able to selectively capture sulfamethoxazole over amoxicillin and cephalexin [133]. Using the same technique, but with N-methacryloyl-(L)-glutamic acid (MAGA) as monomer instead of MAA, amoxicillin was detected in milk sample by SPR technique using a commercial SPR imager with high selectivity and a very low LOD of 0.0012 ng /mL [134].

In addition to the direct detection of target compounds using SPR sensors, where the sample containing the analyte is directly injected into the flow cell and the SPR signal is detected after binding into the selective cavities, competitive detection techniques can be used for enhancing the sensitivity. One such technique is the competitive SPR method, which was used for the detection of enrofloxacin in chicken muscle samples. The LOD was 61.1 ng/mL after pre-treatment. In this technique, enrofloxacin competes with enrofloxacin-protein conjugate for the MIP cavities. This MIP was fabricated using enrofloxacin as a template, which makes them more specific for enrofloxacin than its conjugate. The enrofloxacin-conjugate SPR signal decreased linearly from 25 to 1000 ng/mL as the concentration of enrofloxacin increased [135].

1.2.2.3. SMIP surface enhanced Raman spectrum-based (SERS) sensors

Similar to the SPR technique, the SERS technique is a label-free, ultrasensitive, and non-destructive analytical method based on enhancing the Raman spectrum. This enhancement of the Raman signal happens as a combination of electromagnetic and chemical enhancements. In SERS, a rough metallic surface is essential for producing a perpendicular plasmon oscillation on the surface and obtaining the scattering signal. When a molecule is adsorbed on this roughened metallic surface, electromagnetic radiation will be enhanced, also charge transfer or complex formation between the molecule and the metal can happen [136,137]. The SMIP layer over this surface has been investigated extensively to enhance the selectivity of this type of sensor.

The SERS technique has been used for the detection of several antibiotics as a sensitive optical detection method, usually by using a confocal micro-Raman spectroscopy system integrated with SMIP for better selectivity. For example, enrofloxacin hydrochloride was detected in water samples with a linear range of 1-1000 μM and an LOD of 1 μM. In this study, a roughened membrane of poly (vinylidene fluoride) (PVDF) blended with flower-shaped vinyl-modified AgNPs using γ-methacryloxypropyl trimethoxy silane was fabricated. MIP polymerization was performed using the Ag/PVDF membrane as a substrate in a solution of enrofloxacin hydrochloride, EGDMA, AM, and AIBN in two steps. Precipitation polymerization was carried out at 50 ºC for 6 h followed by 60 ºC for 24 h, washing and drying [138]. Blending PVDF with graphene oxide/Ag composite could enhance the membrane hydrophilicity. Consequently, this change in the membrane provided better sensitivity with a lower LOD of 0.0078 nM selectively using the same polymerization technique for the same antibiotic [139]. The Raman signal could

be enhanced by incorporating magnetic nanoparticles and a magnetic field, which was used by He et al. [140] for the detection of ofloxacin. For this, AgNPs were added into silica coated Fe_3O_4 magnetic particles with a size of 250 nm, then an MIP layer of APTES as monomer, TEOS as a crosslinker, and ofloxacin as a template was fabricated for selective binding with ofloxacin. Besides the enhancement in the Raman signal when a magnetic field was applied, Fe_3O_4 could facilitate the separation of the MIP coated particles from the matrix by using external magnet. Using this method, ofloxacin was detected in commercial eye drops with a recovery of 96.9-106.9 % [140]. Rather than synthetic membranes, eggshell membrane (ESM) as an SERS substrate with good flexibility, different function groups, and high availability could be used. For example, spiramycin antibiotic was selectively detected using MIP on the surface of Ag/ESM with a linear range from 0.1-20 nM. The MIP layer was synthesized using acrylamide, EGDMA, AIBN, and spiramycin. The significance of this sensor was that it could be reused up to 10 times without a significant change in its peak intensity [141].

Despite the sensitivity and selectivity of these MIP-integrated methods for antibiotic detection, they still rely on using sophisticated laboratory-based instruments for optical detection. For further development and on-site detection, portable optical microfluidic sensors can be used, offering a miniaturized platform that can be low-cost and easy to use.

Table 1-2: Different types of SMIP-based optical sensors for antibiotic detection

Sensor	**MIP**						**Quantification technique**	**Sample**	**LOD**	**Linear range**	**Ref.**
	Monomer	Cross linker	Initiator/ Catalyst	Solvent	Template	Solid substrate					
$Eu(DBM)_3Phen$ @PS@MIP	methacrylic acid (MAA)	Ethylene glycol dimethacrylate (EGDMA)	Azobis(isobutryonitrile) (AIBN)	acetonitrile/methanol / triethylamine mixed solvent	ciprofloxacin	$Eu(DBM)_3$ Phen@PS	Spectrofluorometric (fluorescence quenching detection)	fish muscle	0.092 µg/L	0.5–100 µg/L	[102]
MIP–g/r-QD ratiometric fluorescence sensor	acrylamide (AM) OVDAC-modified g-QDs	EGDMA	AIBN	Acetonitrile	Tetracycline (TC)	KH-570-modified r-QD@SiO_2 nanoparticles		Milk	0.35 µM	10-160 µM	[104]
Mg,N-CDs@MIP	MAA	EGDMA	AIBN	Methanol/ water	TC	Mg,N-CDs		Milk Egg Pork	0.79 ng/mL	5–100 ng/mL	[106]
AuNCs@SiO2-MIPs	3-aminopropyltriethoxysilane (APTES)	Tetraethylorthosilicate (TEOS)	$NH_3 \cdot H_2O$	Phosphate buffer	Erythromycin	AuNCs		Human saliva Human urine	1.25×10^{-2} µM	0.1–11.9 µM	[114]
COOH@MWCNT-MIP-QDs optosensor	APTES	TEOS	$NH_3 \cdot H_2O$	Deionized water	ciprofloxacin	carboxylic acid functionalized multiwall carbon nanotubes and CdTe		Chicken muscles and milk samples	0.066 µg/L	0.10–1.0 µg/L and 1.0–100.0 µg/L	[116]

						quantum dots					
MIP-CdTe QDs	APTES		$NH_3 \cdot H_2O$	Cyclohexane, 1-hexanol and triton X-100	Norfloxacin	3-mercaptopropionic acid capped QDs@ SiO_2		Wastewater seawater	0.18 μM	0.5 - 28 μM	[117]
CDs@MIP	APTES	TEOS	NH_4F/ NH_4OH	Ethanol	ceftazidime	CDs		Urine	0.06 μg/L	0.18 - 1.27 μg/L	[118]
Y/B-CDs@MIPs	APTES	TEOS	NaOH	Ethanol/water	Penicillin G	B-CDs@SiO_2		Milk	0.34 nM	1–32 nM	[119]
Y/B-CDs@MIPs	APTES	TEOS	NaOH	Ethanol/water	Chloramphenicol	B-CDs@SiO_2		Milk	0.035 μg/L	0.1–3 μg/L	[120]
bCDs@SiO_2@aCDs@ZIF-8@MIP ratiometric fluorescence MOF sensor	APTES	TEOS	$NH_3 \cdot H_2O$	Ethanol/water	Thiamphenicol	bCDs@SiO_2@aCDs@ZIF-8		Fish, shrimp, beef and milk	0.9 nM	5.0 nM-26.0 μM	[121]

MOF@g-CdTe@r-CdTe@MIP ratiometric fluorescence MOF sensor	APTES	TEOS	$NH_3 \cdot H_2O$	Ethanol/water	Chloramphenicol	MOF@g-CdTe@r-CdTe		Meat, milk and honey	3.8 pM	10 pM–0.5 nM and 0.5 nM–4.5 nM	[122]
CDs@MIP	APTES	TEOS	$NH_3 \cdot H_2O$	Ethanol	TC	CDs-APTES		Honey	15.3 ng/mL	-	[123]
CDs@MIP	APTES	TEOS	$NH_3 \cdot H_2O$	Ethanol	TC	CDs		Milk	5.48nM	0.02-14 µM	[124]
GQDs@MIP	APTES	TEOS	$NH_3 \cdot H_2O$	Ethanol/ water	TC	GQDs		Milk	1 µg/L	1.0- 104 µg/L	[125]
MIP@QDs	3-Mercapto-propyltriethoxysilane (MPS)	TEOS	$NH_3 \cdot H_2O$	1-propanol/ 1,4-butanediol	TC	TGA-CdTe QDs		Bovine serum albumin Fetal bovine serum	0.45 µM	7.4 µM-0.37 mM	[126]
	APTES	TEOS	NH3·H2O						0.54 µM	7.4 µM-0.12 mM	
	Allyl mercaptan and MAA	EGDMA	AIBN						0.50 µM	7.4 µM-0.1 mM	
Fe/Zr-MOF@MIP r-CdTe@ZIF-67@MIP	APTES	TEOS	$NH_3 \cdot H_2O$	Ethanol/ water	Florfenicol Chloramphenicol	Fe/Zr-MOF	Smartphone	Lake water, chicken, fish and	7 nM 0.012 nM	$8.0–9 \times 10^2$ & $9 \times 10^2–7.4 \times 10^3$ nM	[127]

						r-CdTe@ZIF-67		human urine		0.015–0.12 & 0.12–17.22 nM	
MIP-SPR	Itaconic acid	EGDMA	benzophenone	ethanol and deionized water (ratio 7:3)	Ciprofloxacin	Au SPR chip	Surface plasmon resonance imaging (SPRi)	Deionized water	0.08 µg/L	10^{-11}–10^{-7} M	[130]
MIP-SPR	MAA and 2-hydroxyethylmethacrylate (HEMA)	EGDMA	Sodium bisulfite and ammonium persulfate	2 phases (DI water and Organic phase of monomers and cross linker)	Erythromycin	Au SPR chip	SPR	Aqueous solution	0.40 µM (0.29ppm or 0.29 µg/mL)	6.8–68.1 µM	[131]
MIP-SPR and QCM sensors	MAA HEMA	EGDMA	AIBN		Amoxicillin	allyl mercaptan modified SPR and QCM chips surface	SPR imager II QCM: RQCM	chicken egg	SPR: 0.0005 ng/mL QCM: 0.0023 ng/mL	0.1-10.0 ng/mL	[132]
MIP-SPR sensor	MAA HEMA	EGDMA	AIBN		Sulfamethoxazole	allyl mercaptan modified SPR chip surface	SPR imager II	Milk	0.0011 µg/L	0.025-253.2 µg/L	[133]

SPR-MIP sensor	HEMA & N-methacryloyl-(L)-glutamic acid (MAGA)	EGDMA	AIBN		Amoxicillin	allyl mercaptan modified SPR chip surface	SPR imager II	Milk	0.0012 ng/mL	0.1-200 ng/mL	[134]
LSPR/PDA-MIP sensor	Dopamine			Tris buffer	Enrofloxacin	AuNPs coated on glass chip	Localized SPR	chicken meat samples	61.1 ng/mL	25 to 1000 ng/mL	[135]
MIP-SERS sensor	Acrylamide (AM)	EGDMA	AIBN	Ethanol	Enrofloxacin hydrochloride	Ag NPs modified by γ-methacryloxypropyl trimethoxy on PVDF membrane	Confocal micro-Raman spectroscopy system	Water samples	1 μM	1-1000 μM	[138]
MIP-SERS sensor	AM	EGDMA	AIBN	Ethanol	Enrofloxacin hydrochloride	GO/Ag composites on PVDF membrane modified by γ-methacryloxypropyl trimethoxy silane	Confocal micro-Raman spectroscopy system	Aqueous solution	0.0078 nM	0.1-500 nM	[139]
MIP-SERS Sensor	APTES	TEOS	Ammonium hydroxide	Ethanol-acetonitrile (1:1)	Ofloxacin	Fe_3O_4@SiO_2@Ag	SERS	Eye drops		10^{-3}-10^{-8} M	[140]
MIP-SERS Sensor	AM	EGDMA	AIBN	Ethanol	Spiramycin	AgNPs/eggshell membrane (ESM)	Confocal micro-Raman	Aqueous solution		0.1-20 nM	[141]

							spectroscopy system				

Molecularly imprinted polymer (MIP); quantum dots (QDs); Quartz crystal microbalance (QCM); carboxylic functionalized multiwall carbon nanotubes (COOH@MWCNT); tris(dibenzoylmethane)(1,10-phenanthroline)europium(III) (Eu(DBM)3Phen); polystyrene microparticles (PS); molecularly imprinted polymer@carbon quantum dot-phase change microcapsules (MIP@CQD-PCM); thioglycolic acid CdTe quantum dots (TGA-CdTe QDs); octadecyl-4-vinylbenzyl dimethylammonium chloride (OVDAC); 3-(methacryloyloxy) propyl trimethoxy silane (KH-570); red-emitting quantum dots (r-QDs) and green-emitting quantum dots (g-QDs); metal-organic frameworks (MOF); combined zeolitic imidazolate (ZIF-8); 3-(2-aminoethylamino) propyl-dimethoxy methyl silane (AEAPMS); single-hole hollow molecularly imprinted polymers embedded carbon dots (HMIP@CD); localized surface plasmon resonance/polydopamine (LSPR/PDA); gold nanoparticles (AuNPs); graphene oxide- silver (GO/Ag); poly vinylidene fluoride (PVDF).

1.2.3. Optical MIP-based microfluidic sensors for antibiotics

Optical microfluidic sensors have emerged as a promising solution for antibiotic detection, offering low-cost, rapid, sensitive, and portable devices with less sample and chemical usage, and processing time compared to conventional analysis. Optical microfluidics devices used for antibiotic detection have been summarized in Table 1-3, covering different recognition elements, signal transducer and quantification techniques with some insights of the limitation and the required time of analysis. Different types of microfluidic devices have been investigated such as lateral flow immunoassay (LFIA) colorimetric devices [142], lab-on-paper, and lab-on-a-chip devices [46,143]. These devices have been widely used as point-of-care testing (POCT) for food and water quality monitoring, blood and urine analysis, and environmental monitoring, owing to their fast detection, portability, feasibility, high sensitivity, and low-cost analysis. In instance, LFIA overcomes the washing steps, time-consuming pipetting, and long incubation time of the conventional immunoassay techniques such as ELISA (Enzyme-linked immunosorbent assay). Herein, recognition elements which could be antibodies or aptamers (Aptamer is a synthetic single-strand DNA that has emerged recently as an alternative to antibodies as a recognition element for many types of molecules including antibiotics) were used for selective capturing of different antibiotics such as macrolide [144–149], sulfonamides [52,150], fluoroquinolone [48,151–153], tetracycline [48,154–156], chloramphenicol [155,157], aminoglycoside [158,159] antibiotics. In LFIA, nanoparticles play an important role as labeling materials for these receptors. Different types of nanoparticles can be used in LFIA such as magnetic nanoparticles, colored nanoparticles (e.g., gold and selenium nanoparticles), luminescent nanoparticles (e.g., quantum dots and dye-doped nanoparticles), and up-converting nanoparticles. The most widely used nanoparticles in antibiotics detection using LFIA are colloidal gold nanoparticles (AuNPs) owing to their stability, low toxicity, facile conjugation, and visual bright color which allows both qualitative detection of the analyte by the naked eye and quantitative detection by using an external strip scan reader. They have been used as colored label material in LFIA test strips for detection of trace macrolide antibiotics in different types of matrices such as Tap water, food products (Honey, milk, eggs, chicken muscles, pork, liver, and fish). These nanoparticles have a wine-red color which appears on the test strip lines after capturing. The color intensity can be affected by the size of the nanoparticles. Thus, choosing the best size of AuNPs is very important for visualizing the color of

the test lines. Increasing the *AuNPs* diameter size from 20 nm to 40 nm resulted in an increase in the color intensity from bright red to purple on the strip but did not affect the test sensitivity for detection of four macrolides [160]. Therefore, *AuNPs* with a 40 nm diameter are most used in LFIA for better visualization. Using LFIA allowed detection of several macrolides in ng/ml in just a few minutes with strip costs less than $1 . LFIA test strips mainly consists of a sample pad, conjugate or probe pad, a detection membrane (glass fiber or nitrocellulose membrane with different pore sizes are usually used), and an absorbent pad attached to polyvinyl chloride (PVC) sheet. Detection membrane characteristics are very important for optimizing the flow rate of the sample by the capillary action. On the membrane, there is a test line with a specific bioreceptor for capturing the labeled recognition element and a control line with goat anti-mouse IgG to ensure that the assay is working properly. However, the appearance of the color on the control line ensures the applicability of the test, the color of the test line can mean positive or negative results based on the used immunoassay technique. There are two used types of immunoassay techniques: (i) competitive immunoassay which is divided into the direct and indirect assay, and (ii) sandwich immunoassay. For the direct competitive immunoassay, both the analyte and the bioreceptor at the test line compete for binding to the labeled recognition element (primary antibody), in the presence of the analyte, it will bind to the labeled recognition element, and the binding at the test line will decrease, results in decreasing in the color intensity gradually by increasing the analyte concentration until certain concentration (cut off value), at which the color disappears. In the indirect competitive assay, there are two types of antibodies, primary and secondary antibodies. In the presence of the target, it will bind to the primary antibody which then binds to the secondary labeled antibody and causes no capturing by the coating antigen on the test line, and less color intensity. In the sandwich immunoassay, the analyte is captured between the labeled recognition element and the bioreceptor at the test line, resulting in the appearance of color, and the intensity increases with increasing the analyte's concentration. For antibiotics detection, a competitive assay has been usually used as it is suitable for analytes with low molecular size (<1 KDa) which cannot bind to two bioreceptors at the same time [161].

The main disadvantage in LFIA is the use of biological receptors which can be denatured under high temperature, pH change, or harsh chemical conditions. They also require a long time for preparation and experienced professionals [162]. In LFIA, the pretreatment process is based on the sample type, which sometimes is time-consuming and could affect the results if not done properly.

For instance, erythromycin was detected in spiked tap water samples without pretreatment [144]. Also, erythromycin, spiramycin, tylosin, tilmicosin, kitasamycin, and josamycin were detected in spiked raw milk samples using LFIA strips without any pretreatment [149,160]. However, sometimes researchers prefer simple pretreatment for milk samples to eliminate any background interference. Therefore, raw milk pretreatment was done for the detection of four macrolides (Erythromycin, clarithromycin, AZM, and roxithromycin) by centrifugation of the spiked sample at 6000 g for 10 minutes, then dilution of the middle emulsion layer 8-folds with phosphate buffered saline (PBS) [146]. Furthermore, kitasamycin, and josamycin were detected in spiked egg samples after homogenization and dilution with PBS [149]. In spiked honey samples, tylosin and tilmicosin were detected using test strips just after a 4-folds dilution of the spiked samples [163]. However, for further purification, pretreatment of tylosin spiked honey was done by dilution with water and then mixed with ethyl acetate for extraction. Then centrifugation at 5000 g was done for 10 minutes and finally, ethyl acetate supernatant was evaporated, and the residue was dissolved in PBS [147]. When it comes to solid and more complex samples, extraction would be essential. Thus, different macrolides can be extracted from the homogenized, buffered, centrifuged, and diluted solid samples by ethyl acetate or 50% acetonitrile in 0.02 M PB. Extraction was followed by centrifugation and evaporation of the supernatant, and then the residue was dissolved in buffer and used for analysis such as in case of tylosin and tilmicosin detection in egg samples [164], pork [148], liver, fish, and muscles [163]. Another disadvantage in LFIA sensing is that it is difficult to differentiate between structurally similar macrolide antibiotics if they are present in the same sample which means low detection selectivity within the same group. MIP as synthetic receptor with higher stability compared to the biological receptors could be also integrated with microfluidic optical detection of antibiotics such as chloramphenicol [165]. Herein, MIP was prepared inside microfluidic channels. After molecule capturing, reagent mixture was injected where chloramphenicol with its amide group can enhance the chemiluminescence of the reagent mixture. In all these sensors, optical detection relies on color, fluorescence, or chemiluminescence intensities which can be measured using smartphones, spectrophotometer, spectrofluorometer, fluorescence microscope, or portable reader, providing portable sensors that can be used for on-site detection.

Table 1-3: Different types of optical microfluidic sensors for antibiotic detection

Device type	Recognition element	Optical transducer	Quantification technique	Sample	Antibiotics	LOD	Linear range	Recovery %	Assay time	Drawback & limitations	Ref.
Paper based device		Colored metal complex formation	Visual or Smartphone image analysis	Pork	Oxytetracycline, Norfloxacin (NOR)	2.40, 2.25 µg/mL		60.1, 69.0			[48]
Paper-based device		carbonic anhydrase (CA) and 4-nitrophenyl acetate (enzyme inhibition)	Desktop scanner then analysis by photoshop	Milk	Sulfamethazine	2.80	2.5-40.0 µmol/L		15 min		[52]
					Sulfadimethoxine	2.70					
					Sulfathiazole	2.50 µmol/L					
Lateral flow aptasensor	Aptamer	Colloidal GNPs	Strip reader	Tap water	Erythromycin (ERY)	3 pM			50 min total	Require incubation & aptamer amplification, Aptamers synthesis is complicated	[144]
Latex based lateral flow immunoassay (LFIA)	Antibodies	Latex microparticles	By eye or using a portable scanner.	Breast milk	Clarithromycin (CLA), roxithromycin (ROX), ERY, dirithromycin, azithromycin (AZM), and oleandomycin	(Visual LOD)1, 1, 10, 10, 50, and 1000 ng/mL (instrumental LOD) 4.0, 2.5, 30, 42, 42 and 180 ng/mL	Visual:10–1000 ng/mL Instrumental: 2.5−180 ng/mL	71-110	10 min+ 20 min pretreatment	The pretreatment process is crucial and can impact the detection process	[145]
Paper based LFIA	Anti-clarithromycin (CLA) MAb	Colloidal GNPs	Portable Strip scan reader	Milk	CLA ERY	0.095 0.085	No linear range was	89.0-102.0 81.0-99.6	15 min	Required pretreatment and pH	[146]

					ROX AZM	0.055 0.175 ng /mL	mentioned but the assay has cutoff values of 2.5, 5, 5 and 10 ng/mL for CLA, ERY, ROX and AZM, respectively	92.0-98.4 91.2-102		adjustment beside antibodies complicated production process. low cutoff value above which the strip cannot be used for detection.	
LFIA	Anti-tylosin (TYL) MAb	Colloidal GNPs	Visual	Milk Honey Eggs	TYL Lincomycin	0.09 0.008 ng/mL	0.16–1.08 0.02–0.46 ng/mL	87.5-112.5			[147]
LFIA	Anti-TYL MAb	Colloidal gold (CG) Latex microspheres (LM)	Visualization by naked eye or fluorescence under UV	Milk Pork	TYL Tilmicosin (TLM)	Milk: (TYL:8 TLM:15 ng/mL), Pork: (TYL: 15 TLM:30 µg/kg) Milk: (TYL:4 TLM: 8 ng/mL),			5–8 min	Can not be used for higher concentration detection than the cut off values	[148]

						Pork (TYL:8 TLM:20 µg/kg)					
		Time-resolved fluorescent microsphere (TrFM)				Milk (TYL:2 TLM:4 ng/mL), Pork (TYL: 4 TLM:10 µg/kg)					
LFIA	Anti-kitasamycin (KIT) MAb	Colloidal GNPs		Milk Egg	Kitasamycin Josamycin	Milk: KIT:1.51 JOS:1.91 Egg: KIT:3.0 ng/g JOS:2.73 ng/g					[149]
Filter paper immunochromatographic assay (FP-ICA) with smartphone aid	Broad spectrum antibodies	Gold nanoparticles conjugated to antibodies	Smartphone and Photoshop software	Milk	Sulfadimethoxine	0.42-8.64 µg/L	2.42–7.74	88.2-116.9			[150]
					Sulfachloropyridazine		3.72-12.30				
					Sulfamethoxydiazine		3.42–10.80				
					Sulfapyridine		4.02–9.72				
					Sulfamonomethoxine		3.96–22.20				
					Sulfaquinoxaline		6.18–73.80				

					Sulfadiazine		14.94–97.10				
					Sulfaquinoxaline		2.22–24.42				
					Sulfaethoxypyridazine		1.02–20.40				
					Sulfamethazine		2.28–15.60				
					Sulfamethoxypyridazine		2.82–15.06				
					Sulfamerazine		2.52–18.84				
					Sulfanitran		2.16–8.88 µg/L				
Test stripes-fluorescence detection by smartphone reader	monoclonal antibody (MAb)	Quantum dot microsphere-monoclonal antibody (QDM-MAb)	Smartphone-based test strip reader	Fish meat	Ciprofloxacin	0.05 ng/mL	0.1 ng/mL to 100 ng/mL		15 min		[151]
Microchip capillary electrophoresis using UV LED and fluorescence PCB (printed circuit board)	For separation, microchip capillary electrophoresis was used		UV LED and fluorescence PCBs	Milk	Ciprofloxacin	0.19 mM				Prepartion:90 minutes for warming up the UV LED to stabilize the output, 15 minutes incubation with 1M NaOH, wash with citrate buffer, samplingpH 5.5	[152]
Paper based device	NOR-MAb	QDs labelled MAb	Fluorescence spectrophotometer	Milk	NOR	10 pg/mL	0.01 ng/mL to 2.56 ng/mL				[153]

Paper-based device (PAD)		Tetracyclines (TCs) fluorescence enhancement by field amplification stacking	fluorescent imaging which was induced by an UV light-emitting diode (UV LED) image with camera Fv5 software of smartphone in dark conditions	Milk, Environmental water	TCs	4.5 ng/mL	5–80 ng/mL	87- 112	5 min	Interference from negatively charged compounds such as vitamin B2	[154]
Colorimetric paper-based immunoassay sensor	Anti-TC MAb Anti-Chloramphenicol (CAP) MAb	Colorimetric enzymatic reaction (Horseradish peroxidase with 3,3′ ,5,5′ - tetramethylbenzidine (TMB)) inhibition	smartphone application with the functions of image recording	Milk Fish	TC CAP	TC: 0.5 ng/mL CAP: 0.05 ng/mL	1~103 ng/mL and 0.1~100 ng/mL			Wax printing and surface modification	[155]
Pump-free microfluidic chip		OVA-stabilized AuNCs (AuNCs@OVA)	Portable reader (LED, filter, optical lens, and photodiode)	chicken muscle	TC, chlortetracycline, oxytetracycline, doxycycline	0.09 μg/mL	0.09–1.56 and 6.25–100 μg/mL ranges	86.20-93.57	30 sec		[156]
Automated microfluidic immunoassay chip	anti-CAP antibody	fluorescein isothiocyanate	Fluorescence microscope	Milk	CAP	0.05 μg/L		91.3-105.5	<20 min		[157]
Ratiometric paper-based device with digital fluorescence	Aptamer	Graphitic carbon nitride nanosheets (g-C3N4 NSs)	Digital fluorescence detector	Milk, River water	Streptomycin Kanamycin Tobramycin	0.023 0.069 0.045 ng/mL	0.05−30 0.05−150	99.4−104.2	60 min	pH should be kept at 8, complicated fabrication	[158]

detector (RPD-DFD)							0.1−150 ng/mL				
A microflow Chemiluminescence (CL) sensor	MIP	Enhancing the CL from the reaction of tris(2, 2′-bipyridyl) ruthenium(II) with cerium(IV) sulphate in sulfuric acid	Custom built detector	Honey	CAP	7.46×10^{-6} µmol/L	1.55×10^{-4} to 3.09×10^{-3} µmol/L	78.07-104.2			[165]

Filter paper immunochromatographic assay (FP-ICA), ratiometric paper-based device with digital fluorescence detector (RPD-DFD), graphitic carbon nitride nanosheets (g-C3N4 NSs), quantum dot microsphere-monoclonal antibody (QDM-mAb), printed circuit board (PCB), pre-primer (PP), circular DNA template (CDT), aptamer (AP), lateral flow immunoassay (LFIA), clarithromycin (CLA), roxithromycin (ROX), erythromycin (ERY), dirithromycin, azithromycin (AZM), tylosin (TYL), kitasamycin (KIT), MIP-based microtiter chemiluminescence sensor (MIP-MCL), norfloxacin (NOR), carbonic anhydrase (CA), tetracycline (TC), chloramphenicol (CAP), tetramethylbenzidine (TMB), OVA-stabilized AuNCs (AuNCs@OVA), tilmicosin (TLM), colloidal gold (CG), latex microspheres (LM), time-resolved fluorescent microsphere (TrFM)

1.3. Proposed Research

1.3.1. Research gaps

1.3.1.1 Long reaction time, low sensitivity, and the need for chemical derivatization using harsh conditions with AZM optical detection techniques

Detection and monitoring of AZM concentration in environmental and biological samples is usually performed using conventional analytical techniques such as HPLC and LC-MS which are primarily conducted in a controlled environment, expensive, time demanding and require skilled operator. Therefore, several studies have been performed on developing new techniques to overcome these drawbacks. Optical detection of AZM has emerged as one of the sensitive, fast, and easily applied techniques. Methods such as spectrophotometric and spectrofluorometric techniques were developed for AZM detection in biological and pharmaceutical dosage form samples. State-of-the-art optical sensors for AZM could achieve LOD of 0.742 ng/mL, LOQ of 2.474 ng/mL with good sensitivity. However these developed optical techniques suffer from one or more disadvantages such as long reaction time between AZM and the used reagent from 5 to 30 minutes, pH adjustment, and some expensive and harsh chemicals sometimes required [32,35,37,44]. Moreover, some of these methods suffer from low sensitivity where the sensor's sensitivity (slope of the response-concentration curve) is very low and reaches 0.0009 [31] which means the differentiation between two AZM concentrations based on the optical response may be difficult and not accurate. Most of these studies have been using spectrophotometers for optical detection where light absorbance could be measured. Due to the poor optical characteristics of AZM where it does not emit any fluorescence when absorbing light, there were limited studies on its fluorescence-based detection. In these studies harsh acidic conditions using hydrochloric acid are sometimes required to produce a fluorescent product from AZM [34]. Moreover, several chemicals and multiple steps are sometimes required for developing certain reagents (such as nitrogen and sulfur co-doped carbon quantum dots) or for developing certain reactions with macrolide antibiotics (such as using malonic acid and acetic anhydride) to get a fluorescent product, which makes it not cost-effective and hard to be applied [31,32]. Moreover, all the previous studies have relied on using laboratory-based instruments which cannot be used for rapid on-site testing.

1.3.1.2 Optical microfluidic sensors for AZM detection mainly used antibodies as receptors for enhanced selectivity

The major problem with optical detection using different types of reagents is selectivity where the interaction between these reagents and the target compounds such as AZM, in our case, is mainly based on the presence of certain function groups in the compound which can be available in other compounds too. Therefore, receptors -specific for the target compound or group of structurally similar compounds- have been used for enhanced selectivity. For antibiotic optical detection, antibodies or aptamers have been extensively used, showing good selectivity but the preparation of these biological receptors is expensive, time-consuming and requires training. Moreover, the produced biological receptors can denature or degrade at high temperatures, extreme pH, and under harsh chemical conditions. Therefore, MIPs have already been used as excellent synthetic receptors with higher chemical, thermal, and physical stability compared to these biological receptors while still retaining the good specificity and selectivity. There are several studies on MIP-integrated electrochemical sensors for AZM detection but those require expensive instruments while there are no studies on its fluorescence-based detection using MIP as receptor. MIP has been used in solid phase extraction of AZM and other macrolide antibiotics where it was used as a stationary phase to extract the antibiotic [166,167]. After the extraction and elution of the antibiotic, it has been detected using separate detectors such as implementing MIP with HPLC or LC-MS technique as the stationary phase for the column. For this, MIP was prepared first using thermal polymerization at 60 °C for 24 h and then washed and treated to get fine powder which can be used to pack the column or the cartridge. There are two studies where AZM was detected in food samples using a microfluidic latex-based LFIA and paper-based LFIA devices [145,146] but with antibodies as receptors which has some disadvantages as mentioned. However, there is no study on developing SMIP inside a microfluidic device where photo-initiated polymerization, washing, extraction, and fluorescence-based detection of AZM on the same platform were performed and can be developed into a portable sensor for on-site monitoring of AZM.

1.3.2. Hypotheses

AZM as a weakly basic molecule owing to having 2 tertiary amine groups with pKa over 8 was found in our preliminary tests to increase the absorbance and the fluorescence intensity of FITC

which is an acidic fluorescent pH-sensitive dye. This can happen through electrostatic interaction between AZM and FITC through the formation of ion-pair complex and the optical response of FITC can increase by AZM concentration.

MIP using MAA as a monomer and a photo-initiator was found to be prepared within just 20 minutes on a treated glass surface using UV resulting in a porous white polymer. This can be used to capture AZM during its extraction from water sample inside a microfluidic device. This can provide a small platform for extraction and concentration enrichment of AZM inside the microfluidic channels. AZM bound to the MIP can be detected by using FITC as a reagent where the fluorescence intensity can be increased by the concentration of the extracted antibiotic.

1.3.3. Objectives

The overall objective of this research is *to develop an optical microfluidic sensor for AZM which can be used for its direct detection in different sample types including artificial urine and water samples*. In the pursuit of this objective, FITC has been chosen as an acidic dye which can interact with the weekly basic drug where an instant change in its light absorbance and green fluorescence intensity can be measured. For selective detection of AZM and portability, MIP using MAA as a monomer inside a microfluidic device has been chosen as a synthetic receptor owing to its physical, chemical, and thermal stability. To achieve the general objective, specific objectives have been identified as follows:

1. Development of direct optical detection techniques including spectrophotometric and fluorescence-based techniques for AZM using FITC.
2. Optimize the two developed methods to get the maximum optical response, followed by application on AZM detection in artificial urine.
3. Synthesis of MIP as synthetic receptor inside a glass- Polydimethylsiloxane (PDMS) microfluidic device.
4. Extraction and detection of AZM from aqueous solution using MIP integrated microfluidic device and FITC as a reagent for fluorescence-microscopic detection.

1.3.4. Novelty

Previous studies on optical detection of AZM suffer from long reaction time between AZM and the used reagent, sometimes chemical derivatization and pH adjustment needed, and low sensitivity [35,37,44]. We were able to develop new spectrophotometric and fluorescence-based microscopic methods for direct and instant detection of AZM in artificial urine samples using FITC as a reagent. After AZM liquid-liquid extraction from urine, FITC can be used as a reagent where the absorbance and the fluorescence intensity are directly related to the AZM concentration. An immediate response with a wide linear range 0-31.25 µg/mL and low detection limits of 0.41 and 0.82 µg/mL for the fluorescence-based and spectrophotometric methods were achieved, respectively. This proves that FITC can be an efficient reagent for immediate detection of AZM after its extraction and providing a sensitive fluorescence-based microscopic method with a calibration curve slope of 2.027, solving the drawbacks of other optical methods for AZM detection.

The latest papers on optical microfluidic detection of AZM were using antibodies as receptors which are less stable and harder to prepare compared to MIP [145,146]. In this study, we implemented MIP for AZM capturing into a microfluidic optical device aiming for portability and provides insights on different steps during device fabrication. Herein, oxygen plasma was used for glass treatment instead of harsh acidic or alkaline treatment solutions, providing a simple technique for glass treatment before functionalization for the first time in surface imprinting polymer on glass. Oxygen plasma was used for glass cleaning and to increase its hydrophilicity where oxygen ions and electrons can remove any grease and expose more hydroxyl groups on the glass surface. MIP for AZM was prepared on glass under UV was prepared just within 20 min compared to overnight preparation by heating. MIP preparation, washing, extraction, and detection was done on the device continuously and images were taken under a fluorescence microscope as a preliminary step for developing a portable sensor for on-site optical detection of antibiotics.

Chapter 2: Direct Fluorescence and Spectrophotometric-based Detection of Azithromycin Using Fluorescein Isothiocyanate: Method Development and Comparative Analysis[2]

2.1. Introduction

It is significant to monitor AZM concentration in treated urine samples to ensure its removal or degradation before being applied to the soil as shown in Figure 2-1A to avoid the development of anti-microbial resistant bacteria. The proposed methods in this research rely on the formation of an AZM-FITC ion-pair complex where AZM as a weakly basic compound can electrostatically interact with the FITC acidic dye resulting in an increase in absorbance and fluorescence intensity. Notably, these methods are characterized by their simplicity and the immediate recording of the response post mixing the reagent and analyte, eliminating the necessity for long reaction time. The study aims to provide a sensitive, direct, and straightforward analysis of AZM using fluorescence microscopy and spectrophotometry. Importantly, these methods are designed to eliminate the need for AZM derivatization, buffer utilization, or other chemical additions. The effectiveness of these methods has been demonstrated in the analysis of AZM in artificial urine samples following its extraction with dichloromethane and using FITC as a reagent as shown in Figure 2-1B. The fluorescence-based detection method has demonstrated better sensitivity and recovery compared to the spectrophotometric-based technique. This sensitivity is heightened compared to AZM detection using eosin-G [33], and usage of fewer chemicals and analysis time compared to those studies using N,S-CQDs [31] or malonic acid anhydride and acetic acid anhydride [32]. Overall, the study presents a novel and efficient approach for the optical detection of AZM, offering advantages such as simplicity, immediate response, and elimination of certain preparatory steps.

[2] *This chapter was published as "**Hasaneen, N.**, Pulicharla, R., Brar, S. K. & Rezai, P. Direct fluorescence and spectrophotometric-based detection of azithromycin using fluorescein isothiocyanate: Method development and comparative analysis. J. Environ. Chem. Eng. 12, 112803 (2024)".* [188]

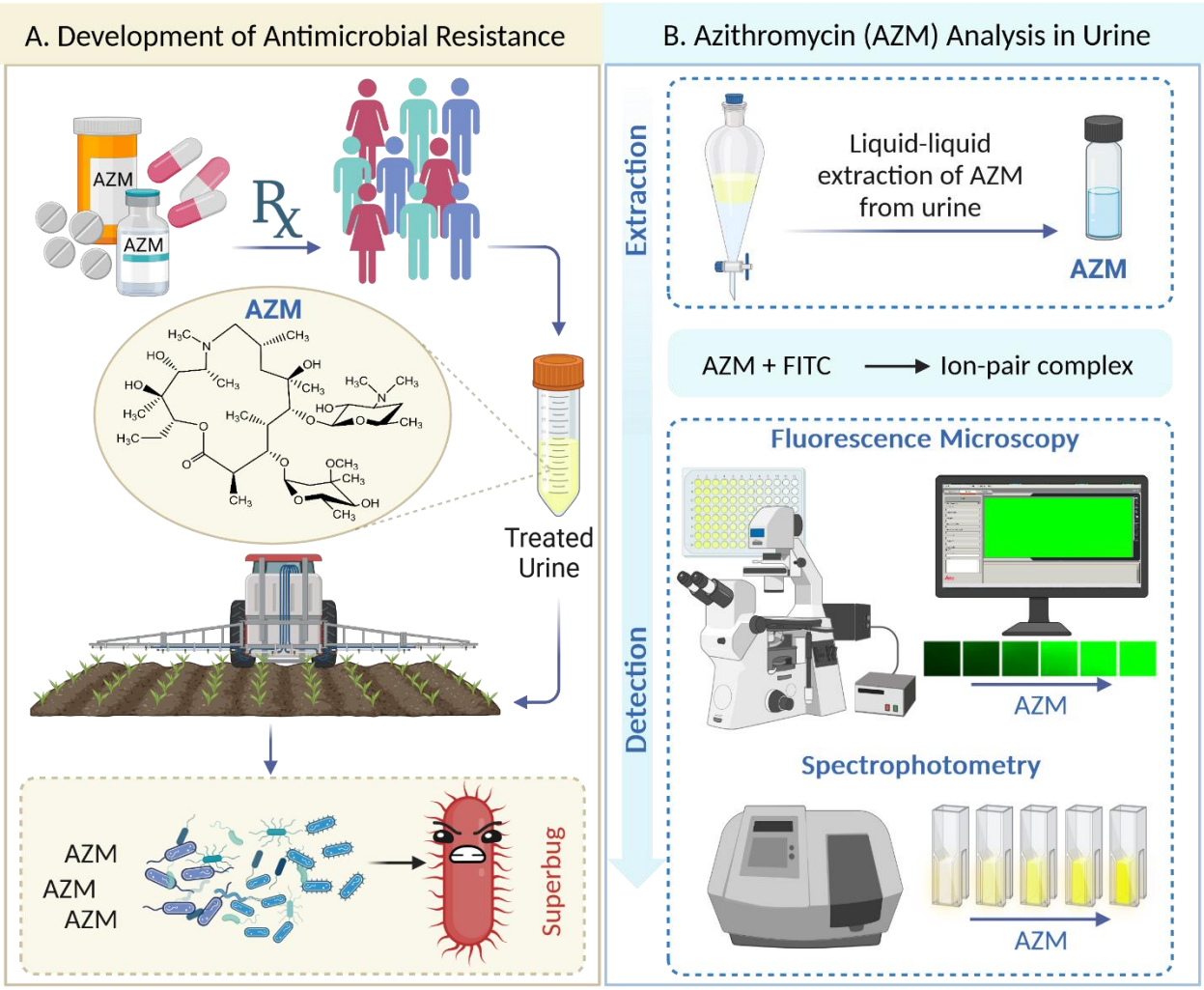

Figure 2-1: Schematic illustration of A. The antimicrobial resistance developed in the environment by AZM residues in treated urine (used as fertilizer) and B. The developed new simple and rapid methods for AZM detection in artificial urine using fluorescein isothiocyanate (FITC) as a reagent.

2.2. Materials and Methods

2.2.1. Chemicals and instruments

Azithromycin dihydrate (AZM), fluorescein isothiocyanate isomer l (FITC), methanol HPLC grade (≥ 99.9%), and acetonitrile anhydrous (99.8%) were purchased from Sigma-Aldrich,

Canada. Milli-Q water was obtained using a Milli-Q system (Millipore Ltd., Canada). Dichloromethane, environmental grade, 99.8%, stabilized with amylene was purchased from Fisher Scientific, Canada. Polystyrene 96 well plates with flat bases were used as the reaction vessels (Sarstedt). For fluorescence-based detection, a Leica inverted microscope (DMIL LED Inverted Routine Fluorescence Microscope, Leica, Germany) with green fluorescent protein (GFP) filter (Ex: 470/40, DC: 495, EM: 525/50) and a Leica MC170 HD color camera was used. For spectrophotometric detection, a UV-Vis spectrophotometer (DR6000, HACH, USA) with a 1mL quartz cuvette was used. pH was measured using a pH/conductivity benchtop meter (Fisher brand™ Accumet™ AB150, USA). Artificial Urine was purchased from BIOCHEMAZONE, Canada.

2.2.2. Fluorescence-based detection

AZM stock solution was freshly prepared at a concentration of 1000 µg/mL in methanol, from which serial dilutions were subsequently made. Simultaneously, 100 µg/mL FITC solution was prepared in methanol and stored at - 4°C, for later dilution and usage. The AZM and FITC were combined in a 1:1 v/v ratio in a 96-well plate. For building a calibration curve, serial dilutions of AZM in methanol, ranging from 500 to 1.95 µg /mL, were prepared, and mixed with 50 µg/mL FITC in methanol in a 1:1 v/v ratio. This experimental setup was replicated in triplicate under identical conditions. Finally, images were captured utilizing a Leica inverted microscope (DMIL LED Inverted Routine Fluorescence Microscope, Leica, Germany) with green fluorescent protein (GFP) filter (Excitation (Ex): 470/40, Dichroic (DC): 495, Emission (EM): 525/50) and a Leica MC170 HD color camera. Subsequently, fluorescence intensities were quantified using ImageJ software, wherein the mean gray value was measured for each image as shown in Figure 2-2. Different parameters were studied and optimized as follows:

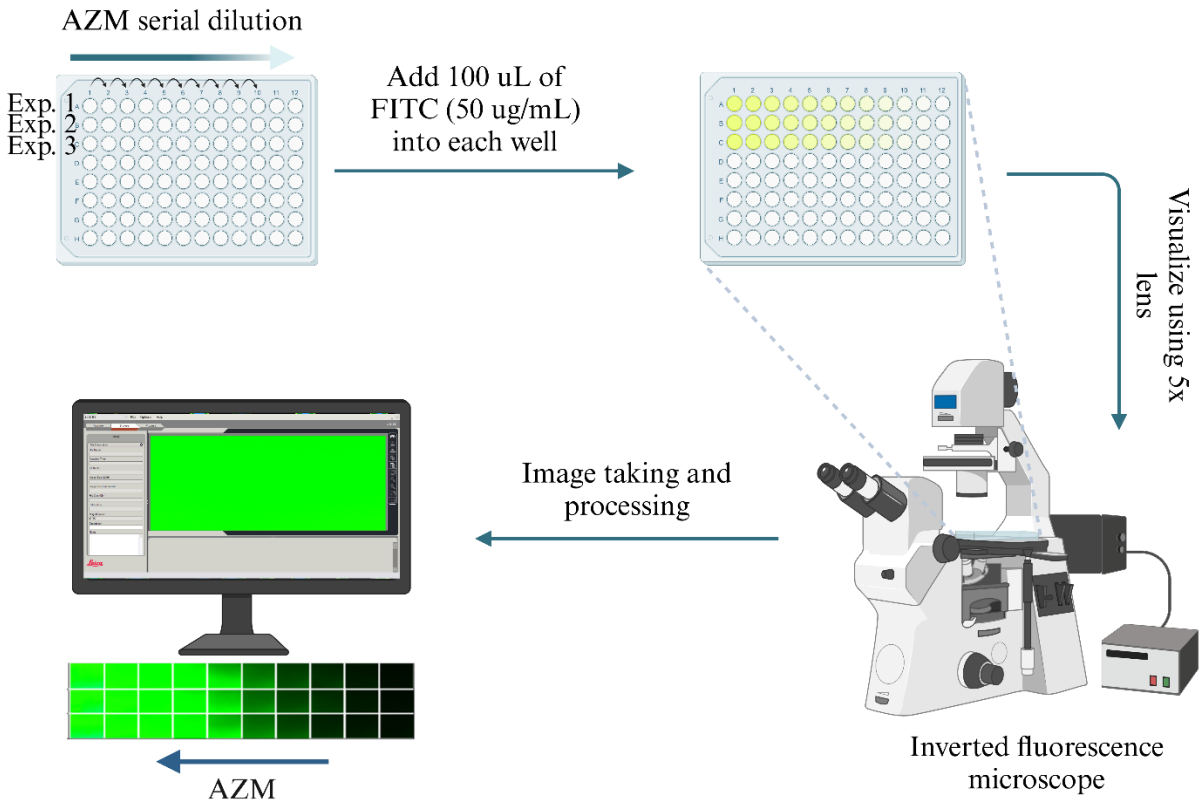

Figure 2-2: Schematic illustration of the fluorescence-based detection method where 100 µL of AZM dilutions from 500 to 1.95 µg /mL were mixed with 100 µL of FITC 50µg/mL in methanol in the 96 well plate.

2.2.2.1. Effect of reaction time

A solution of FITC at 50 µg/mL was combined with different AZM concentrations (2, 25, 50, and 100 µg /mL) all in methanol, covering the targeted range. The fluorescence intensity was measured for 10 minutes before adding AZM and for 20 minutes after the addition of AZM, utilizing an Inverted Leica Fluorescence microscope with a GFP filter. This experimental procedure was repeated three times to determine the optimal reaction time.

2.2.2.2. Effect of reagent concentration and stoichiometric ratio

In a 96-well plate, 100 µL of FITC at various concentrations ranging from 10 to 100 µg /mL was mixed with 100 µL of AZM (100 µg /mL), all dissolved in methanol. This experimental setup was replicated three times to ascertain the optimal FITC concentration. The stoichiometric ratio of the

ion-pair complex formed between AZM and FITC was determined using the molar ratio method, maintaining a constant AZM concentration of 1.3 mM while varying the FITC concentration accordingly. Images were captured with an inverted Leica fluorescence microscope equipped with a GFP filter and a colored camera and analyzed using ImageJ software to get the fluorescence intensity.

2.2.2.3. Effect of solvent

AZM, 1000 µg/mL stock solution was prepared in various solvent compositions, including methanol, acetonitrile, methanol/water 1:9, and methanol/water 1:1. Serial dilutions were then prepared from the 1000 µg/mL stock solution, utilizing the corresponding solvents. Simultaneously, 50 µg /mL FITC solution was prepared in acetonitrile to mix with corresponding AZM samples. Additionally, 50 µg /mL FITC solution in methanol was prepared to mix with AZM samples in methanol-containing solutions. Fluorescence-based detection was used to determine the fluorescence intensity of the formed ion-pair complex.

2.2.3. Statistical analysis

The statistical significance of the fluorescence intensity (FI) values of each two FITC concentrations to check the effect of reagent concentration or each two AZM concentrations to check the effect of solvent were ascertained using an Unpaired t-test. The level of significance difference was labeled with stars: * for p-value < 0.05, ** for p-value < 0.01, *** for p-value < 0.001, **** for p-value < 0.0001.

2.2.4. Spectrophotometric detection

AZM standard solution was freshly prepared in methanol at a concentration of 1000 µg/mL, and subsequent serial dilutions from 500 to 0.98 µg/mL were prepared. Each dilution was then mixed with FITC of 50 µg/mL in a 1:1 v/v ratio. The resulting mixture was transferred into a 1 ml quartz cuvette, and absorbance was measured using a UV-Vis spectrophotometer (DR6000, HACH, USA). This experiment was conducted in triplicate under consistent conditions, and a calibration curve was constructed based on the obtained results at maximum wavelength, λ_{max}, of 480 nm.

2.2.5. Artificial urine sample analysis

AZM was spiked into artificial urine samples to achieve final concentrations of 5, 15, and 25 µg /mL in 2 mL of artificial urine. Liquid-liquid extraction was employed to extract AZM from the artificial urine samples, using dichloromethane stabilized by amylene. This process was repeated three times, each time with 3 mL of dichloromethane. Subsequently, dichloromethane was evaporated under vacuum, and the residue was dissolved in 2 mL of methanol. For the analysis of the extracted AZM, fluorescence intensity and absorbance measurements were followed after mixing with 50 µg/mL FITC in methanol in a 1:1 v/v ratio.

2.2.6. Method validation

Different analytical parameters were studied to validate the proposed methods such as the LOD and LOQ as well as linear range, accuracy, and intra and inter-day precision as follows:

LOD, LOQ and linearity: LOD and LOQ were calculated using the following equations based on the ICH guidelines [168]:

$$\mathrm{LOD} = 3.3 \times \sigma/\mathrm{S} \qquad (eq\ 2-1)$$

$$\mathrm{LOQ} = 10 \times \sigma/\mathrm{S} \qquad (eq\ 2-2)$$

Where S is the slope of the concentration-response calibration curve and σ is the Standard deviation of 20 blank measurements. The linear range was determined based on the concentration-response range that provides the highest acceptable coefficient of determination (R^2).

Accuracy: Different concentrations of AZM (5, 15, and 25 µg /mL) within the linear range were prepared and analyzed in triplicate with the two developed detection techniques. Based on the response and using the calibration curve, the found concentrations were compared to the actual concentrations and the % Error was calculated, referring to the accuracy using the following formula:

$$\%\mathrm{Error} = \left[\frac{\mathrm{Found} - \mathrm{Actual}}{\mathrm{Actual}}\right] \times 100 \qquad (eq\ 2-3)$$

Precision: Precision was determined by evaluating intra-day and inter-day variations using 3 concentrations and replicate analysis (n=3). Analysis was done 3 times per day on 3 consecutive days for each concentration. Relative standard deviation (%RSD) was used to show the precision using the following formula:

$$\%\text{RSD} = \sigma/\mu \times 100 \qquad (eq\ 2-4)$$

Where σ and μ are the standard deviations and the mean of the determined concentrations of 3 measurements, respectively.

2.3. Results and Discussion

2.3.1. Fluorescence-based detection

FITC has a weak fluorescence intensity when dissolved in methanol while by adding AZM, the fluorescence intensity increased. By increasing the AZM concentration using 50 µg/mL FITC, the green fluorescence intensity increased using AZM concentrations from 1.95 to 500 µg/mL in a triplicate experiment as shown in the microscopic images of Figure 2-3A and the concentration-response curves in Figure 2-3B. AZM, as a weak alkaline organic compound can form an ion-pair complex with FITC which is an acidic dye in methanol where both are predominantly ionized and can electrostatically interact. The formation of an ion-pair complex between AZM and other dyes was previously investigated such as its complex with eosin-G where an increase in the fluorescence intensity of the dye was detected using the spectrofluorometer [33]. In this study, fluorescence microscopy was used to detect the increase in the fluorescence intensity of the FITC dye upon the formation of the ion-pair complex with AZM within a wide linear range of 0-31.25 µg/mL. Compared to using the spectrofluorometer in other studies, fluorescence microscopy in this study offers a detection technique which is simple, easily operated, time and chemical saving, and suitable for developing portable and miniaturized optical sensors.

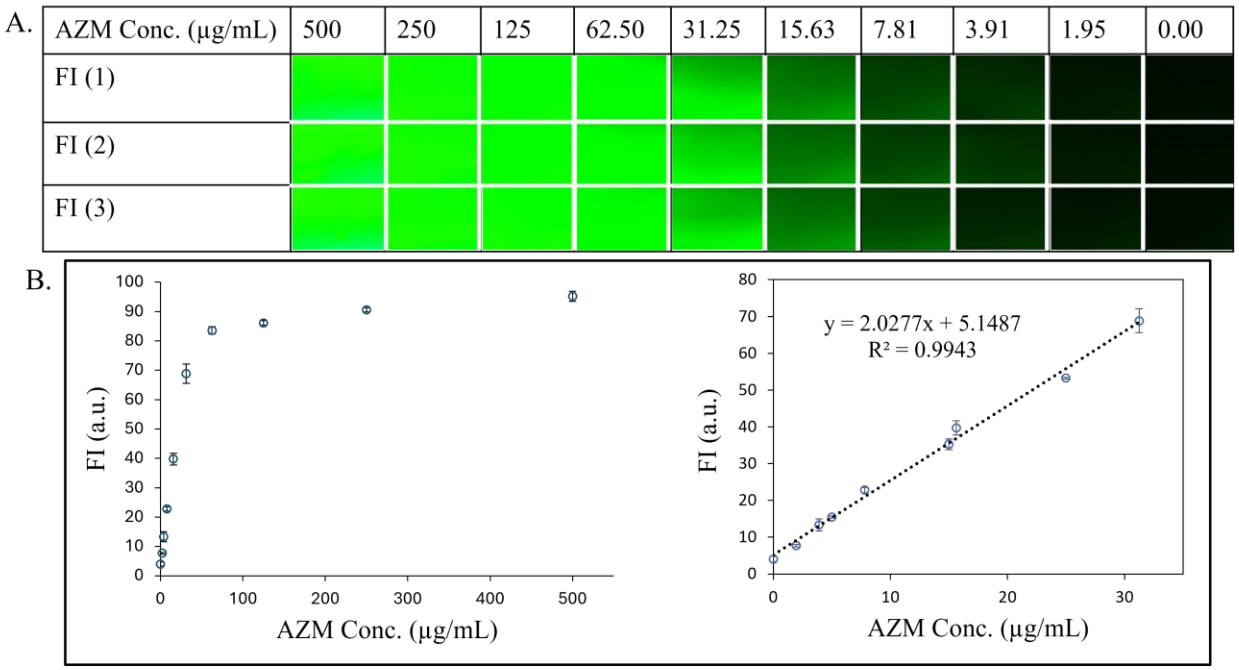

Figure 2-3: A. Microscopic images showing the effect of AZM different concentrations on the fluorescence intensity (FI) of FITC (50 µg/mL) in methanol in triplicate experiments; B. Concentration-response curve and the calibration curve of the fluorescence-based detection technique where FI is the fluorescence intensity.

Different experimental parameters were studied and optimized as follows:

2.3.1.1. Effect of reaction time

An immediate increase in the fluorescence intensity was observed after mixing AZM with 50 µg/mL FITC, using four different concentrations of AZM (2, 25, 50, and 100 µg/mL), covering the targeted studied concentration range, as depicted in Figure 2-4. During the first 10 min where there was no AZM and only FITC was present in methanol, the fluorescence intensity remained stable with no significant change. However, after AZM addition by different concentrations covering the targeted concentration range, a significant increase in the fluorescence intensity was observed due to the immediate formation of the ion-pair complex. Importantly, the analysis method exhibited an instantaneous response, eliminating the need for long reaction time compared to other previous studies for optical detection of AZM. For instance, a reaction time of 5, 15, or 30 min is required while detecting AZM using quinalizarin [35], bromophenol [37], or haematoxylin [44] as

a reagent, respectively. Having a more time-efficient detection method is crucial for applicability of the analysis technique especially for the real-time applications which require immediate results.

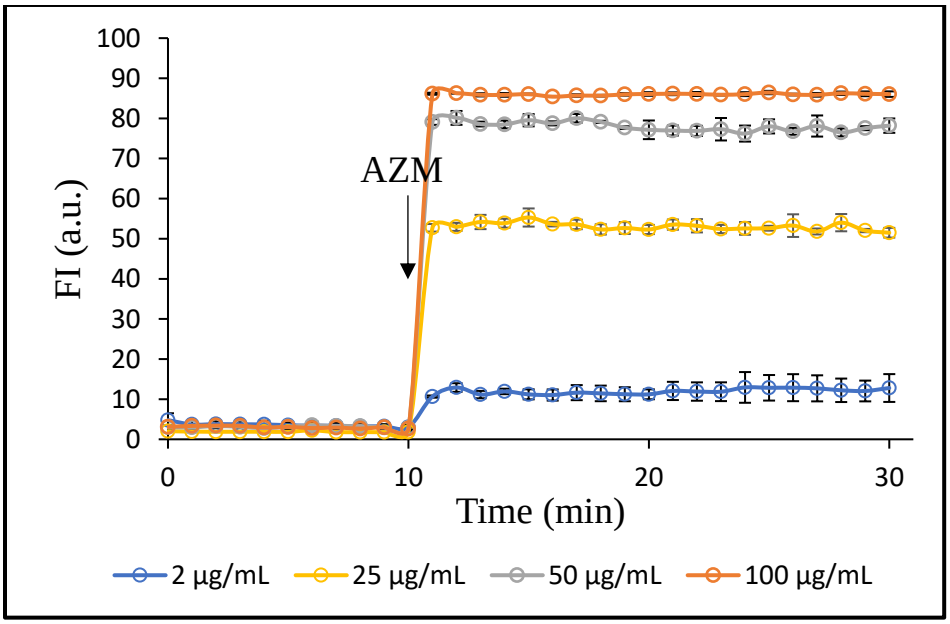

Figure 2-4: Immediate formation of AZM-FITC ion-pair complex and effect of reaction time on AZM-FITC ion-pair complex fluorescence intensity, AZM was mixed at min 10 using four different concentrations of 2 , 25, 50, and 100 µg/mL with 50 µg/mL FITC.

2.3.1.2. Effect of reagent concentration

Finding out the optimum reagent concentration is critical for detection and can vary based on the detection methods, experimental conditions, and the applications. In this instance, increasing the FITC concentration from 10 to 100 µg/mL and keeping the concentration of AZM (100 µg/mL) constant, at 1:1 v/v ratio, resulted in increasing the fluorescence intensity until 50 µg/mL, after which the fluorescence intensity remained stable with no significant difference as shown in Figure 2-5. As a result, 50 µg/mL FITC was used as the optimum reagent concentration to build the calibration curve where FITC can be found in excess.

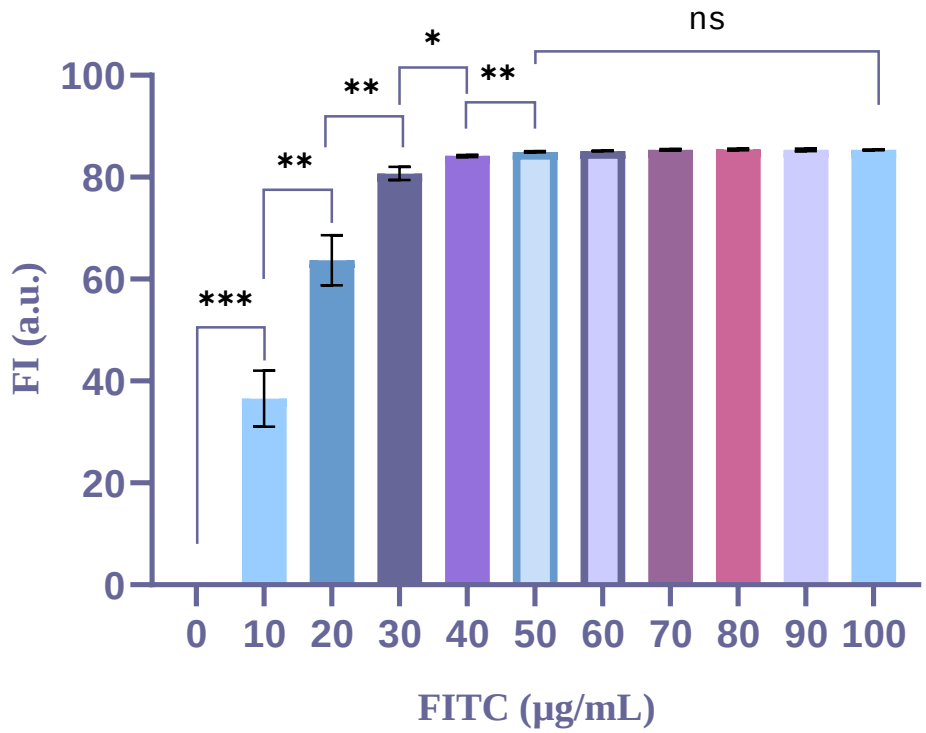

*Figure 2-5: Effect of FITC concentrations from 10 to 100 µg/mL on the fluorescence intensity using 100 µg/mL AZM in methanol in ratio 1:1 v/v AZM:FITC. Significance difference was calculated using p<0.05, ns: no significant difference, * for p-value < 0.05, ** for p-value < 0.01, *** for p-value < 0.001, **** for p-value < 0.0001.*

2.3.1.3. Effect of solvent

Different solvent compositions were used to dissolve AZM before mixing with FITC and the solvent effect on the fluorescence intensity measurements was investigated. As shown in Figure 2-6, methanol and a 1:1 mixture of methanol/Milli-Q water exhibited superior sensitivity where the response was significantly different between each 2 AZM concentrations even at low concentrations with p-values < 0.01, < 0.001, or < 0.0001. In contrast, using 1:9 methanol/Milli-Q water or acetonitrile as solvents did not provide a sensitive response at low AZM concentrations. This can be related to the low solubility of both AZM and FITC in water with large partition coefficients (log P) of 4.02 and 5.25, respectively, and also the lower solubility of FITC in acetonitrile than in methanol [169,170]. As a result, methanol was selected as a solvent for analysis due to its enhanced solubility for both AZM and FITC, along with its simplicity in analysis. Images

were captured under experimental conditions, revealing negligible fluorescence for the FITC alone in methanol and higher fluorescence for the complex, increasing proportionally with the AZM concentration, up to the measured 500 µg/mL.

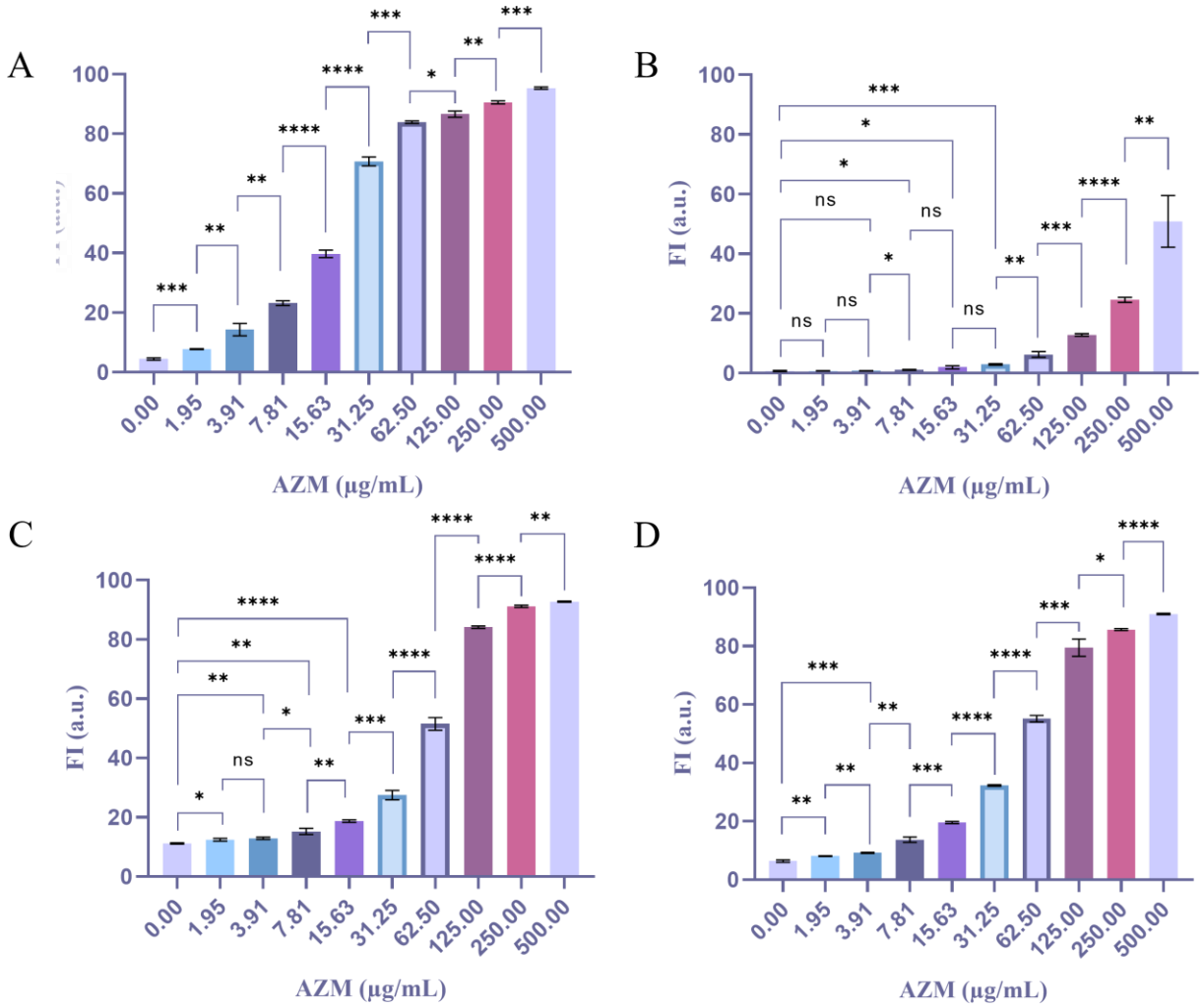

*Figure 2-6: Effect of solvent on the fluorescence intensity, significance difference was calculated using p<0.05, ns: no significant difference, * for p-value < 0.05, ** for p-value < 0.01, *** for p-value < 0.001, **** for p-value < 0.0001. A: AZM and FITC in methanol, B: AZM and FITC in acetonitrile, C: AZM in 1:9 methanol/Milli-Q water and FITC in methanol, D: AZM in 1:1 methanol/Milli-Q water and FITC in methanol.*

2.3.1.4. Composition of AZM-FITC ion-pair complex

The molar ratio analysis where 0.13 mM AZM was mixed with varied concentrations of FITC was performed in methanol in a 96-well plate and images were taken under the fluorescent microscope

and analyzed for the fluorescence intensity. As a result, at equimolar AZM-FITC concentration, AZM was completely consumed with no significant increase in fluorescence intensity even with higher reagent concentrations as shown in Figure 2-7. This outcome can be elucidated by examining the chemistry of AZM and FITC. AZM contains tertiary amine groups that can be protonated at a pH lower than its pKa (8.1-9.5) [22]. FITC, behaving similarly to fluorescein, exhibited different forms in aqueous solution, cationic, neutral, monoanionic, and dianionic based on the surrounding environment with pKa values of 2.05 ± 0.03 (cation-neutral), 4.35 ± 0.02 (neutral-monoanion), and 6.62 ± 0.01 (monoanion-dianion) [171]. FITC was found to exist predominantly in its monoanionic form at pH above 5 and in its dianionic form at pH above 7.0 [172]. This finding was corroborated by measuring the pH of the ion-pair mixture solutions, ranging from 5.5 to 6.5 based on the AZM concentration using pH/conductivity benchtop meter (Fisher brand™ Accumet™ AB150, USA). The absorbance spectrum comparison of the FITC-AZM complex (at AZM concentrations from 0-31.25 µg/mL) with different fluorescein forms studied by Robert SjÖback et al. [173] indicates that the major form in these solutions is the monoanion. Hence, AZM can electrostatically interact with FITC forming an ion-pair complex of 1:1 molar ratio.

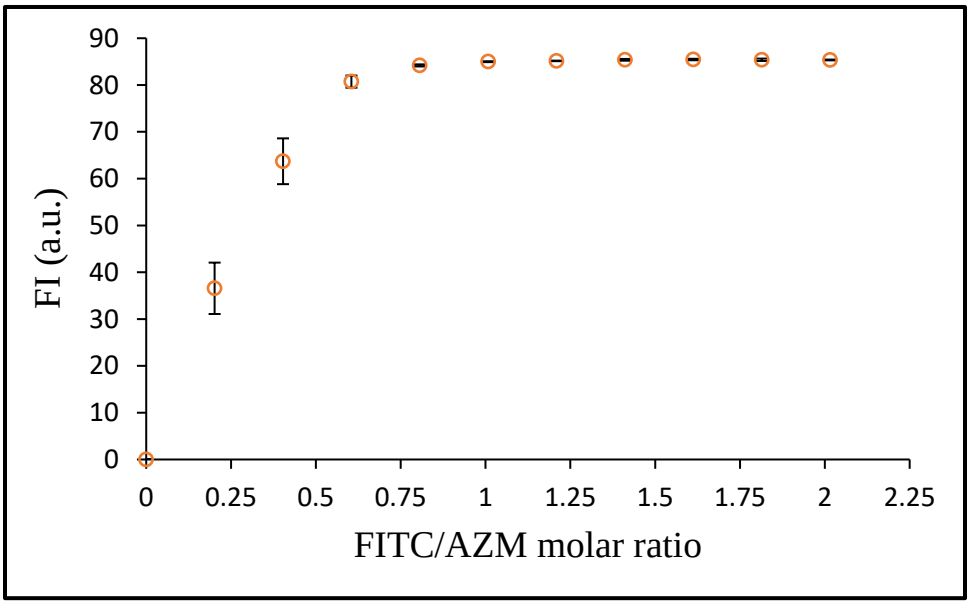

Figure 2-7: Molar ratio plots for the ion-pair complexes using 0.13 mM of AZM with various concentrations of FITC in methanol.

2.3.2. Spectrophotometric detection

FITC has very low absorbance when dissolved in methanol. Mixing different concentrations of AZM with 50 µg/mL FITC in a 1:1 v/v ratio in methanol resulted in increasing the absorbance at a wavelength of 480 nm due to the formation of the ion-pair complex between AZM and FITC as shown in Figure 2-8A. With AZM concentration over 125 µg/mL, the shape of the peak changed showing a redshift owing to the formation of the FITC dianion form following the same peak shape of fluorescein studied by Robert SjÖback et al. [173]. A calibration curve with linear response was established using concentrations from 0 to 31.25 µg/mL of AZM where AZM formed an ion-pair complex with the monoanion FITC form as shown in Figure 2-8B. Increasing the absorbance upon forming an ion-pair complex between AZM and other dyes such as bromophenol blue, bromothymol blue, bromocresol green, and bromocresol purple were studied [37,38]. However, in this study, a wider linear range was achieved with instant response after mixing AZM with FITC with no need for long reaction time compared to other studies.

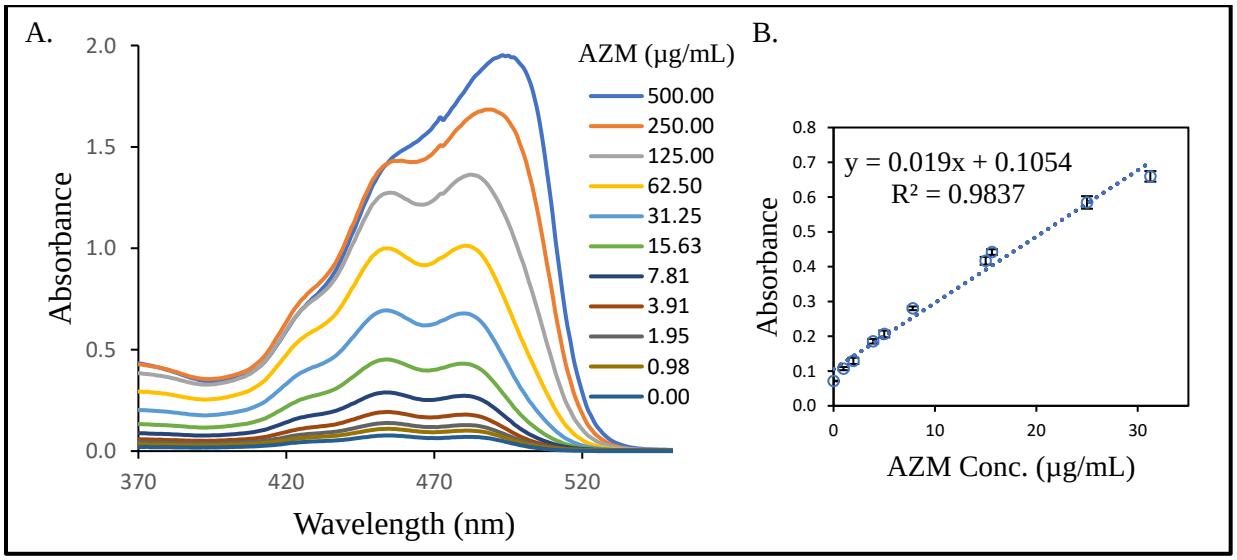

Figure 2-8: A. Absorbance graph showing the effect of AZM different concentrations on the FITC absorbance using 50 µg/mL FITC in methanol and the calibration curve; B. Absorbance-concentration calibration curve showing the linear range at λ_{max} of 480 nm.

2.3.3. Comparison between the two developed methods for AZM detection

2.3.3.1. Performance and sensitivity

An LOD of 0.41 µg/mL and an LOQ of 1.23 µg/mL were calculated for the fluorescence-based method, and an LOD of 0.82 µg/mL and an LOQ of 2.49 µg/mL were calculated in the case of the spectrophotometric detection method. The fluorescence-based method demonstrated lower LOD and LOQ compared to the spectrophotometric method with a larger slope obtained from the calibration curve. This indicated that the fluorescence-based method was more sensitive and could be used for detecting and quantifying lower concentrations of AZM. Both methods showed high linearity within the specified linear range (0-31.25 µg/mL). The fluorescence-based method exhibited a higher coefficient of determination (R^2) of 0.9943 compared to the spectrophotometric method (R^2 of 0.9837) as shown in Table 2-1. The higher R^2 for the fluorescence-based method suggested a stronger correlation between concentration and response, indicating a more reliable linear relationship. Table 2-2 illustrates a comparison between the proposed methods and the methods reported in the literature. The former exhibits a broader linear range when applied to artificial urine in contrast to the latter with an immediate response. Even though the proposed methods have higher LOD and LOQ compared to most of the reported studies, they remain within the acceptable range for AZM concentration in human urine. This was particularly relevant if 6-14% of the 250 or 500 mg AZM oral dose is excreted unchanged in urine, resulting in concentrations exceeding 5 µg/mL. Using FITC as a reagent enabled the detection of AZM using two different techniques, offering a versatile detection approach. Compared to most of the reported methods, the proposed fluorescence-based method with a higher slope of 2.0277 indicated a more sensitive technique in terms of analytical sensitivity. The sensitivity measured how well a method can distinguish between two analyte concentrations that were extremely close to one another [174].

Table 2-1: Quantitative and statistical parameters for the proposed methods

Parameters	Fluorescence-based Method	Spectrophotometric Method
LOD[a] (µg/mL)	0.41	0.82
LOQ[b] (µg/mL)	1.23	2.49
Linear range (µg/mL)	0-31.25	
Linear regression equation		
Intercept	5.17	0.1054
Slope	2.0277	0.019
Coefficient of determination (R^2)	0.9943	0.9837

[a] Limit of detection
[b] Limit of quantification

Table 2-2: Comparison between the reported studies for AZM optical detection and this study

Reagent used	**Detection method**	**Linear range (µg/mL)**	**LOD (µg/mL)**	**LOQ (µg/mL)**	**Slope**	**Application**	**Ref.**
nitrogen and sulfur co-doped carbon quantum dots	Spectrofluorometry	1.87–24.19 and 27.86–82.39	0.57	_	0.000896 and 0.00196	Tablets, cells	[31]
malonic acid/acetic anhydride	Spectrofluorometry	0.003-0.04	0.742×10^{-3}	2.474×10^{-3}	5.75	Tablets, capsules, oral suspension, spiked human urine and plasma	[32]
Eosin-G	Spectrofluorometry	0.04-0.2	0.0114	0.038	0.0158	Tablets, oral suspension	[33]
Quinalizarin	Spectrophotometry	4-20	0.35	1.2	0.0134	Tablets	[35]
Methyl orange	Spectrophotometry	10-50	1.1	5.7	0.001	Tablets	[36]
Bromophenol blue	Spectrophotometry	0-50	0.1	0.35	0.0178	Tablets, capsules, oral suspension	[37]
bromocresol green	Spectrophotometry	2-20	0.15	0.50	0.0425	Tablets, capsules	[38]
bromocresol purple		2-18	0.23	0.77	0.0338		
bromophenol blue		2-12	0.14	0.47	0.0541		
bromothymol blue		2-14	0.16	0.53	0.0345		
Eosin-Y	Spectrophotometry	1-10	0.153	0.514	0.111	Tablets, capsules, oral suspension,	[39]

						spiked human urine and plasma	
Haematoxylin/boric acid	Spectrophotometry	0.3-6	0.0561	0.187	0.1550	Tablets, oral suspension	[44]
Rose bengal copper	Spectrophotometry	4-20	0.31	0.95	0.0617	Tablets, capsules, oral suspension	[45]
Fluorescein isothiocyanate	Spectrophotometry Fluorescence microscopy	0-31.25	0.82 0.41	2.49 1.23	0.019 2.0277	Artificial urine	This study

2.3.3.2. Accuracy and precision

Both methods revealed good accuracy, with % Error values less than 10% and %Recovery values close to 100% for the three analyzed concentrations as shown in Table 2-3 with the fluorescence-based method generally demonstrating slightly better accuracy. This indicated that both methods provided reliable quantitative measurements of different AZM concentrations within the linear range. The fluorescence-based method demonstrated lower %RSD values, reflecting better precision in both intra and inter-day analyses compared to the spectrophotometric method. The analytical results of accuracy and precision indicated that the proposed methods have good repeatability and reproducibility as shown in Table 2-3.

Table 2-3: Accuracy and precision studies

Fluorescence-based Method									
Intra-day (n=3)					Inter-day (n=3)				
Actual (µg/mL)	Found[a] (µg/mL)	%Recovery ± SD	Precision (%RSD)	Accuracy (%Error)	Actual (µg/mL)	Found[a] (µg/mL)	%Recovery ± SD	Precision (%RSD)	Accuracy (%Error)
5	4.86	97.2 ± 5.3	5.46	-2.8	5	5.08	101.6 ± 3.1	3.05	1.6
15	15.66	104.4 ± 4.7	4.54	4.4	15	14.85	99.0 ± 4.7	4.76	-1.0
25	23.72	94.9 ± 1.8	1.93	-5.1	25	23.73	94.9 ± 0.5	0.48	-5.1
Spectrophotometric Method									
Intra-day (n=3)					Inter-day (n=3)				
Actual (µg/mL)	Found[a] (µg/mL)	%Recovery ± SD	Precision (%RSD)	Accuracy (%Error)	Actual (µg/mL)	Found[a] (µg/mL)	%Recovery ± SD	Precision (%RSD)	Accuracy (%Error)
5	5.00	99.9 ± 6.7	6.68	-0.1	5	5.39	107.9 ± 7.1	6.56	7.9
15	16.07	107.1 ± 2.4	2.27	7.1	15	16.48	109.9 ± 0.4	0.35	9.9
25	24.79	99.1 ± 2.6	2.61	-0.9	25	24.87	99.5 ± 1.0	1.04	-0.5

[a] Average of 3 determinations

SD: Standard deviation

%RSD: Relative standard deviation

2.3.3.3. Application of the proposed methods on AZM analysis in artificial urine

Percent recovery was calculated for 3 different concentrations of AZM (5, 15, and 25 µg/mL) in spiked artificial urine samples. A recovery of 93.1-101.3% was obtained when the detection was conducted using the fluorescence-based method in a triplicate experiment. The same was done using the spectrophotometric method and a recovery of 85.8-112.2% was obtained as shown in Table 2-4. The narrower recovery range in the fluorescence-based method indicates higher precision, as all values fall within a more confined interval compared to the spectrophotometric method. As artificial urine, designed to mimic real urine, introduces a complex matrix, it can impact the accuracy of the analytical methods. The fluorescence-based method appears to be less affected, as evidenced by the narrower percent recovery range. However, the spectrophotometric method might be more susceptible to interference from components in the artificial urine matrix, leading to a wider range of recovery values. Based on the results, the fluorescence-based method appeared more robust in this study, offering potential advantages for the accurate determination of AZM in artificial urine. Compared to the optical detection of AZM in urine based on ion-pair complex formation with eosin-Y and eosin-G [33,39], the proposed methods can be used for analysis of a wider AZM concentration range (0-31.25 µg/mL) providing an acceptable %recovery and a faster analysis with less chemical to be used.

Table 2-4: Recovery studies from artificial urine

Fluorescence-based Method			**Spectrophotometric Method**		
Concentration (µg/mL)	Found[a] (µg/mL)	%Recovery ± SD	Concentration (µg/mL)	Found[a] (µg/mL)	%Recovery ± SD
5	5.06	101.3 ± 4.3	5	5.61	112.2 ± 6.2
15	14.71	98.0 ± 3.3	15	12.87	85.8 ± 4.8
25	23.27	93.1 ± 1.4	25	21.94	87.8 ± 1.2

[a] Average of 3 determinations

SD: Standard deviation

2.4. Conclusion

This research systematically investigated novel approaches for analyzing AZM in artificial urine samples by using FITC as a reagent. The developed fluorescence and spectrophotometric-based methods provide simple, rapid, and sensitive assays for the detection of AZM instantly after being mixed with FITC with LOD of 0.41 and 0.82 µg/mL and LOQ of 1.23 and 2.34 µg/mL, respectively. The identified 1:1 molar ratio of the AZM-FITC ion-pair complex revealed instantaneous response kinetics, eliminating the need for long reaction time. Validation of the two methods involved analyzing three different AZM concentrations in both intra and inter-day analyses. The fluorescence-based method showed slightly higher accuracy and lower %RSD values, demonstrating repeatability and reproducibility. Overall, the proposed methods provide sensitive, direct, and reliable means for AZM analysis, showcasing potential applications in complex matrices such as artificial urine with a %recovery of >93% using the fluorescence-based method and >85% using the spectrophotometric method. In summary, these methods provide valuable insights offering efficient alternatives for AZM detection without the complexities associated with conventional methods that contribute to environmental protection and public health.

Chapter 3: Integrating Molecularly Imprinted Polymer into Microfluidics for Azithromycin Fluorescence-based Detection

3.1. Introduction

MIP could offer a solid phase extraction stationary phase before AZM detection. Only one study has mentioned the preparation of AZM-MIP on a gold chip for a surface plasmon resonance sensor which is a type of optical sensor without any details about the linear range or the detection limit [130]. Other studies have prepared MIP for AZM as a solid phase extraction technique to concentrate and extract AZM prior to its detection by electrochemical sensors [17,65–71], HPLC or LC-MS [166,167] which are costly and necessitate individuals with specialized knowledge. Moreover, microfluidic paper or latex-based LFIA devices were developed for AZM optical detection but they used biological receptors which are expensive and less stable compared to MIP [145,146]. To the best of our knowledge, no studies have been conducted on AZM detection using MIPs as receptors integrated with fluorescence-based microfluidic sensor.

Herein, MIP was prepared inside a glass-PDMS microfluidic device by photo-initiated polymerization where the polymerization could be accomplished within 20 minutes compared to thermal polymerization that requires 24 hours. AZM, MAA, EGDMA were used in a ratio of 1:4:12 as a template, monomer, and cross linker, respectively. Using a microfluidic device with multiple channels and chambers could provide a platform where multiple experiments could be achieved at once. During device fabrication, glass treatment is the most critical step to ensure the attachment of the MIP to the glass after polymerization without being peeled off easily. To ensure the proper treatment, contact angle can be measured before and after the treatment to get an idea about the change in the glass hydrophilicity by the treatment. After polymerization, template should be removed to leave complementary cavities for molecule capturing during the extraction step. This can be accelerated by using ultrasonication with the washing solution. Another way to remove the template molecules is by continuous washing inside the device using a syringe pump. In this study, both techniques were tested and their effect on the polymer and further experiments for detection were studied. After molecule capturing, FITC can be used as a reagent for microscopic fluorescence-based detection. The all process using the 2 different approaches for template removal is summarized as shown in Figure 3-1. Overall, this study presents a novel

approach for AZM optical detection aiming to have a portable device that can be used for on-site detection. Moreover, it presents an investigation of critical steps during the MIP preparation inside a microfluidic device using photopolymerization and its applicability for AZM detection.

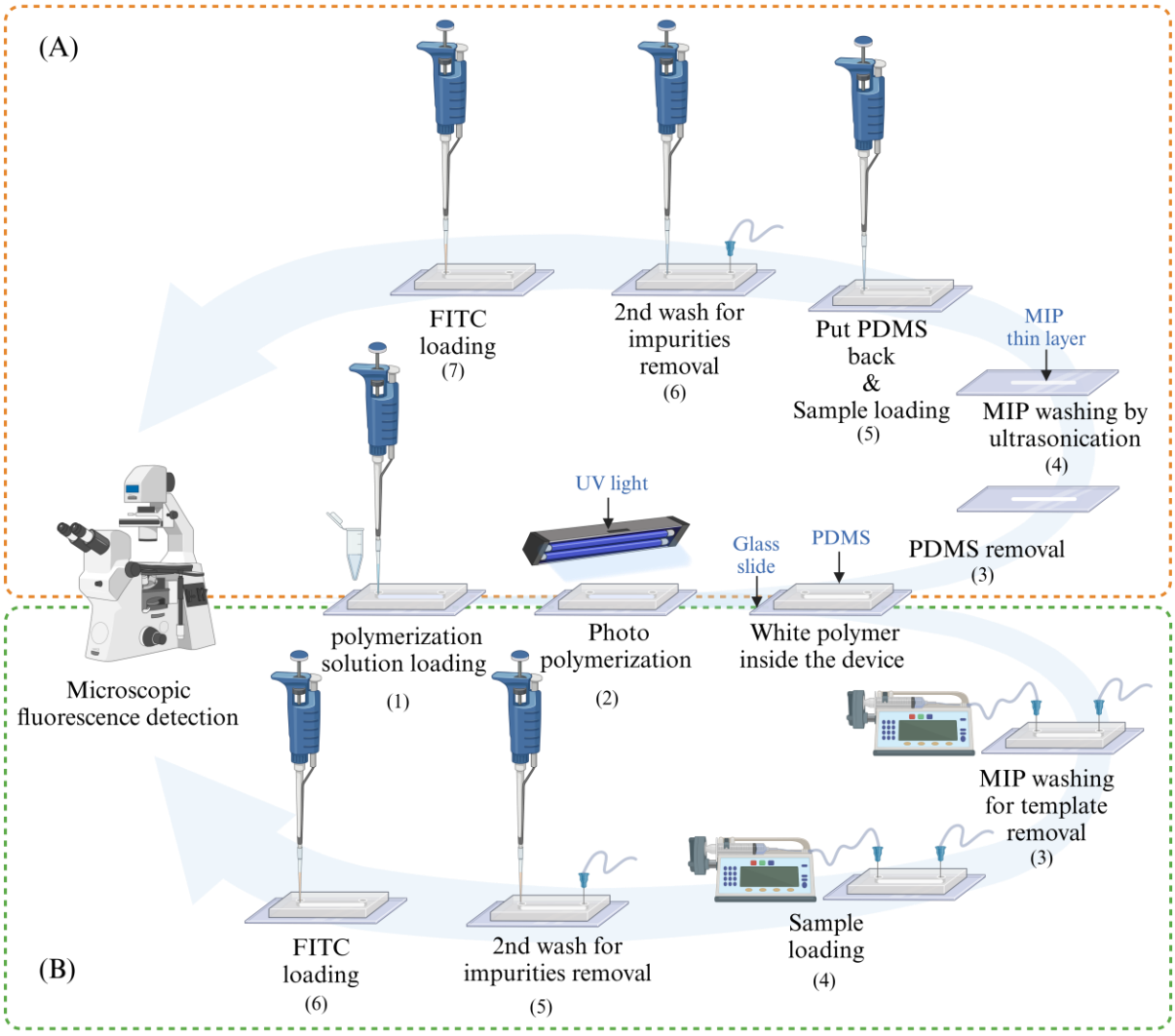

Figure 3-1: Schematic illustration of MIP-integrated microfluidic device fabrication followed by fluorescence-based detection where (A) is the experiment where MIP was washed with aid of ultrasonication and (B) is the experiment where MIP was washed inside the device using a syringe pump.

3.2. Materials and Methods

3.2.1. Chemicals and instruments

AZM, FITC, methanol HPLC grade (≥ 99.9%), ethanol (100%), toluene (≥ 99.5%), acetonitrile anhydrous (99.8%), glacial acetic acid (≥99%), MAA, EGDMA, 3-(trimethoxysilyl) propyl methacrylate, and 2-propanol were purchased from Sigma-Aldrich, Canada. Ammonium hydroxide solution (5.0 M) was purchased from Honeywell Fluka. Formic acid laboratory grade (88%) was purchased from Fisher Chemical. Milli-Q water was obtained using a Milli-Q system (Millipore Ltd., Canada). PDMS was purchased from Dow Corning Corporation.

For contact angle measurements, a drop shape analyzer (Kruss DSA100E) was used. For fluorescence-based detection, a Leica inverted microscope (DMIL LED Inverted Routine Fluorescence Microscope, Leica, Germany) with green fluorescent protein (GFP) filter (Ex: 470/40, DC: 495, EM: 525/50) and a Leica MC170 HD color camera was used. pH was measured using a pH/conductivity benchtop meter (Fisher brand™ Accumet™ AB150, USA). For absorbance measurements, GENESYS 50 UV-Vis spectrophotometer was used (Thermo Scientific, Canada).

3.2.2. MIP-integrated microfluidic device fabrication

Two microfluidic devices were fabricated for two different experiments where glass was the base and a PDMS replica containing channels was attached into the surface, each channel has inlet and outlet as shown in Figure 3-2. The first device had 2 parallel channels while the second one had seven parallel channels with hexagon chambers in the middle. Fabrication consisted of two main steps: 1) glass slide treatment and 2) 3D printed mold and PDMS replica attachment to the glass substrate as follows:

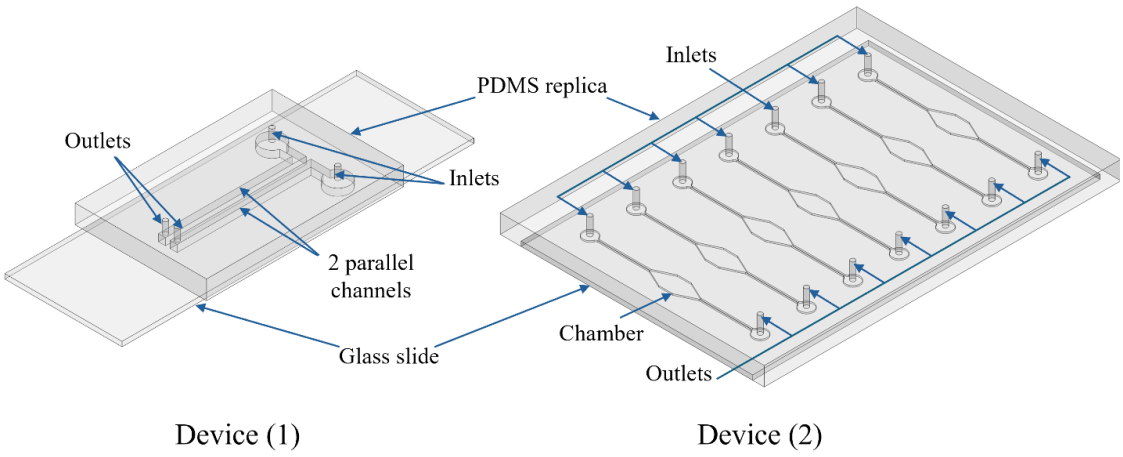

Figure 3-2: A scheme of the used microfluidic devices.

3.2.2.1. Glass slide treatment

Glass treatment is an essential step to ensure the attachment of the MIP onto the glass surface without being peeled off. Glass slides were treated in three steps. First, glass was washed with acetone for 1 min, 2-propanol for 1 min, deionized water for 2 min, then dried on a hot plate for 10 min at 110 °C. Second, cleaned slides were treated with oxygen plasma for different times (30, 60, 90, and 120 seconds) under 600 mTorr pressure and 30 W (PDC-001-HP Harrick Plasma, USA) to expose more hydroxyl groups on the glass surface before being treated in the next step. Third, glass was treated with a treatment solution to provide vinyl groups on the glass surface which can interact with the MIP. Two treatment solutions were popularly used in literature for treating glass. The first solution is a slightly acidic ethanol solution (40 mL ethanol and 1.2 mL 10:1 water/acetic acid) of 20% v/v 3-(trimethoxysilyl) propyl methacrylate [175]. The second solution was 2% v/v 3-(trimethoxysilyl) propyl methacrylate in toluene [176]. Glass slides exposed to plasma were shaken inside the different solutions overnight, then washed with ethanol in the case of using the first treatment solution while with methanol in the case of the second treatment solution. Contact angle was measured for the dried glass slides after each step during the treatment to check the hydrophilic/hydrophobic characteristics of the glass slides using a drop shape analyzer (Kruss DSA100E). Glass slide was put on the stage and 2 µL MilliQ water was pipetted on it then image was taken by the camera and contact angle was measured using the ADVANCE software.

3.2.2.2. Mold and PDMS replica fabrication

Two 3D printed molds as shown in Figure 3-3 were fabricated using a 3D printer. The molds were designed using Solid Works 2023 software. Then, they were washed with water and soap, isopropyl alcohol, dried using pressurized air, and put under UV 395 nm light for complete curing for 1 hour. This was followed by 5 cycles of heating in oven at 80 °C for 1 h each cycle and washing with water, soap, and isopropyl alcohol in between until they are fully cured.

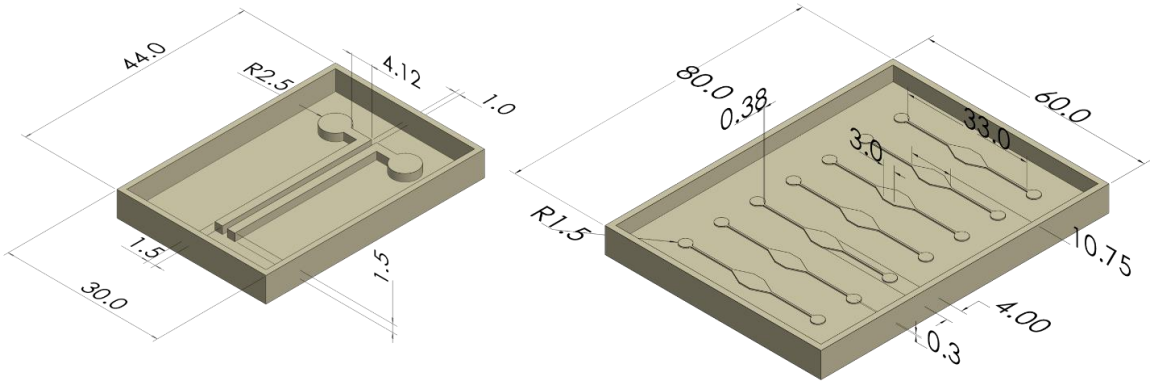

Figure 3-3: A scheme of the used 3D printed molds with dimensions in mm to be used during the PDMS replica preparation.

To fabricate the microfluidic device, a 10:1 mixture of PDMS elastomer and curing agent was prepared and air bubbles were removed under vacuum using a desiccator for 20 min. Then the PDMS prepolymer was poured over the master mold and left to cure in the oven at 70 °C for 3 h. After the complete curing of the PDMS, it was peeled off and inlets and outlets were punctured in the PDMS replica using a 1 mm Miltex® biopsy punch with a plunger as shown in Figure 3-4.

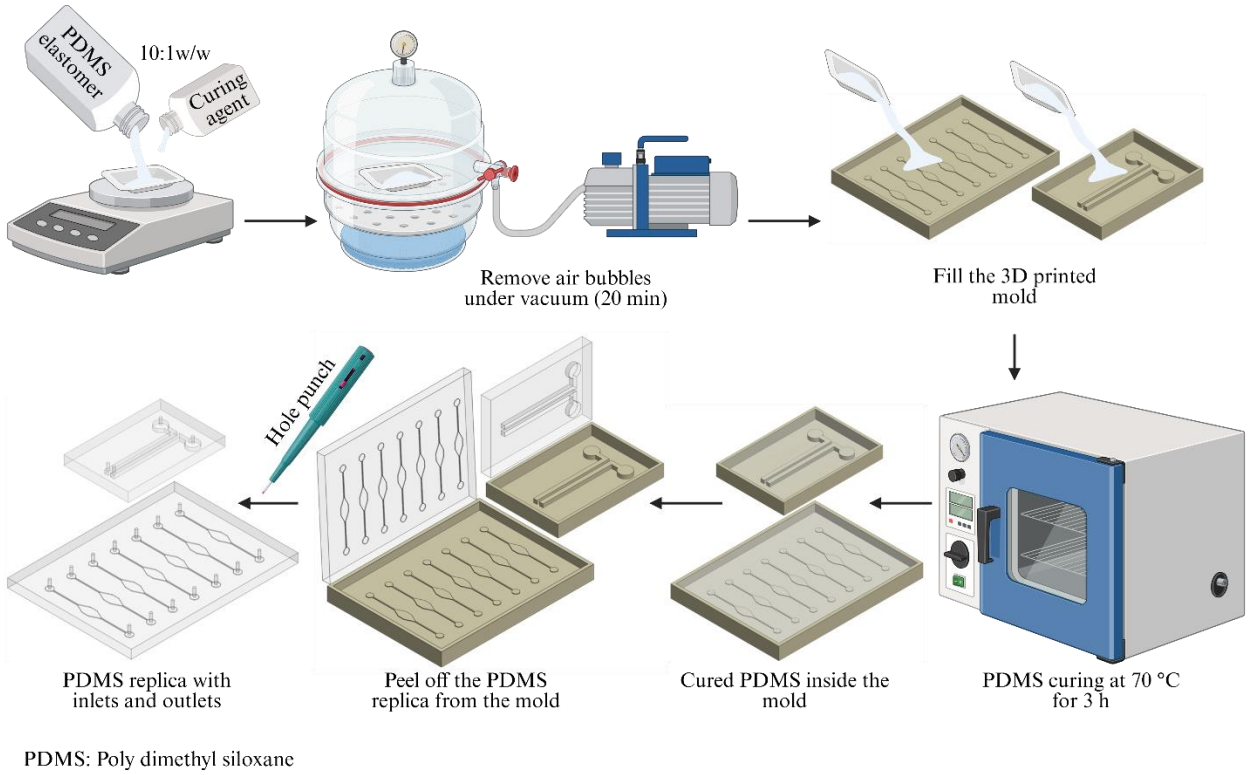

Figure 3-4: Schematic illustration of PDMS replica preparation.

A PDMS replica with double L shape channels of 1.5 mm height and width, inlet, and outlet (Device 1) was used for the first experiment. It was bound temporarily on the fully treated glass slide by physical pressing for the first experiment where PDMS was removed after MIP polymerization. For the second experiment, the PDMS replica with 7 channels with chambers (Device 2) was irreversibly bound to a washed and dried glass slide as a substrate (7.5 × 5 cm^2) using oxygen plasma at 600 mTorr and 30 W for 32 s (PDC-001-HP Harrick Plasma, USA). Then, the glass treatment solution was injected into the channels and kept overnight in a dark place as shown in Figure 3-5. Finally, the channels were washed with ethanol and kept in a dark place for further use in the MIP polymerization step. The channels height was optimized to get a chamber filled with the polymer after the polymerization step. A mold with channels with different heights was 3D printed and used to get a PDMS replica with channels of 700, 600, 500, 400, 300, 200, and 100 μm which was used for height optimization.

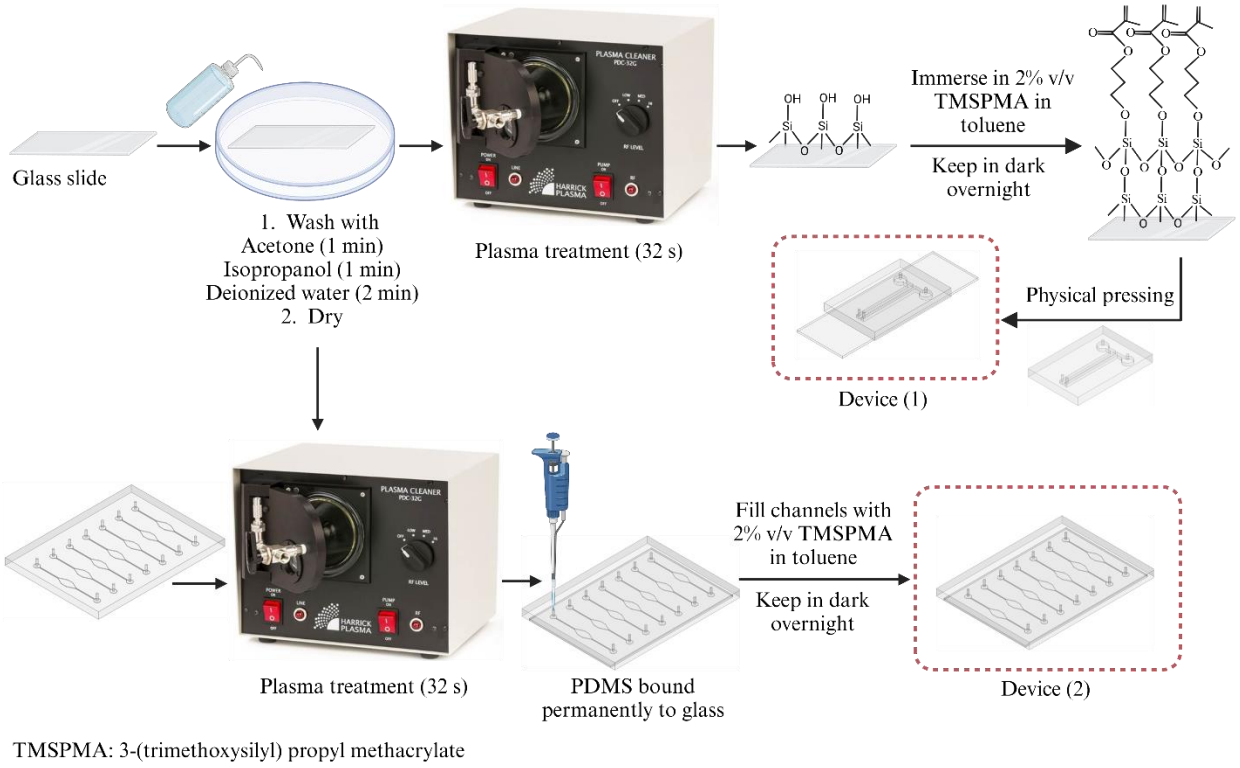

Figure 3-5: Schematic illustration of glass treatment and full device fabrication to be used in experiment 1 and 2.

3.2.3. MIP and NIP synthesis

AZM dihydrate at 0.0157 g as a template molecule was mixed with 6.7 µL MAA as a monomer in acetonitrile 400 µL as a solvent for 4 hours at room temperature. Then, 45.2 µL ethyleneglycol dimethacrylate as a cross linker and 2 mg 2,2-Dimethoxy-2-phenylacetophenone as a photo initiator were added. The solution was ultrasonicated for 1 min and purged with nitrogen for 2 min to remove any oxygen from the polymerization solution. NIP solution was prepared by the same method but without adding AZM as a control.

The above prepolymer solutions were used to fill the microfluidic channels, inlet and outlet were temporarily sealed with thick tape, and the whole device was exposed to the UV radiation using Everbeam US-395NM50W UV lamp (BC, CA) for 20 min. MIP was synthesized inside the channels using a pre-polymerization mixture with a molar ratio of 1:4:12 template:monomer:cross linker which was shown by Sheybani et al. [177] to have the highest binding capacity to AZM compared to other investigated ratios. Herein, a photo initiator has replaced the thermal initiator,

and polymerization was conducted under UV 395 nm for 20 min instead of heating at 60 °C for 24 h.

3.2.4. Template removal

In the first experiment, the formed polymeric layer was washed with the aid of ultrasonication in acetic acid/methanol 1:9 v/v for 20 minutes followed by methanol two times for 5 minutes each, to remove the template molecule and provide complementary cavities for AZM molecules. The remaining thin layers of MIP and NIP were then dried with pressurized air and over the hot plate 60 °C for 5 min.

For the second experiment, the polymer was washed using a syringe pump using 5 mL of 1:9 v/v acetic acid/methanol followed by 10 mL methanol at room temperature and over a hotplate with 65 °C. Different flow rates (1, 0.5, 0.2, 0.05 mL/min) were tested to choose the optimal flow rate to remove AZM from the polymer. Each 1 mL effluent was collected separately, and their light absorbance was measured using UV/Vis spectrophotometer at a wavelength of 210 nm. Moreover, three different washing solution compositions were tested using a flow rate of 0.01 mL/min including: 1 % formic acid in acetonitrile, 1 % formic acid in 70% ethanol, and 5% ammonium hydroxide in methanol. The effluent was collected at 3 points of washing; after 10-, 15-, and 25-mL washing, then AZM concentration was measured using LC-MS. To minimize the washing time, three different flow rates (1, 0.1, 0.01 mL/min) were tested for the chosen solution (1 % formic acid in 70% ethanol). For each flow rate test, 10 mL of washing solution were injected and the entire 10 mL effluent were collected, the AZM concentration was then checked using LC-MS. Afterwards, the remaining acid was washed with 20 mL water (0.2 mL/min) and the water effluent's pH was measured using a pH/conductivity benchtop meter (Fisher brand™ Accumet™ AB150, USA) to ensure the total removal of the used acid. Finally, 1 mL of acetonitrile was injected inside the channel for conditioning the stationary phase before use.

3.2.5. AZM-MIP and NIP characterization

The thickness of MIP and NIP thin layers was measured using optical profilometer (Contour GT-X8 3D Microscope, Arizona, USA) and the morphology of the two layers was characterized by scanning electron microscopy (SEM EM-30AX plus, Coxem, Daejeon, South Corea) after the washing and the drying steps using 1500, 5000, and 35000 x magnification.

3.2.6. AZM extraction and detection procedure

3.2.6.1. Detection on MIP washed by the aid of ultrasonication (Experiment 1)

About 50 µL of AZM at 10, 100, 1000 µg/mL in 1:9 methanol:MilliQ was injected into the washed MIP, while 50 µL of AZM at 1000 µg/mL was injected on the washed NIP and incubated for 10 min. Then a 2nd wash using 200 µL methanol was done and followed by injecting 50 µL of FITC 100 µg/mL in methanol. MIP and NIP controls were tested where only 50 µL solvent (1:9 methanol/MilliQ) was incubated on them followed by 2nd wash and FITC application. Methanol was used to improve the solubility of AZM in water. Images were taken using the inverted Leica fluorescence microscope and analyzed using ImageJ software.

3.2.6.2. Detection on MIP washed using a syringe pump (Experiment 2)

One milliliter of three different AZM concentrations (1, 10, and 100 µg/mL) in 1:9 acetonitrile/MilliQ water was injected into the MIP-containing chambers with flow rate of 0.05 mL/min and 1 mL of the 100 µg/mL AZM was injected into the NIP-containing chambers. A control experiment was conducted where 1 mL of the solvent only was injected into the MIP. Then, each channel was flushed by 40 µL acetonitrile/MilliQ water to remove any impurities that can dissolve in water followed by 200 µL acetonitrile to remove the remaining water. Finally, 20 µL of 50 µg/mL FITC was injected into the channel then images were taken after 2 minutes using the inverted Leica fluorescence microscope and analyzed using ImageJ software.

3.3. Results and Discussion

3.3.1. Glass treatment

Before MIP polymerization on glass slides, glass treatment should be performed to ensure the binding of the polymer into the glass surface. Different methods have been used for glass treatment to clean it and expose hydroxyl groups on its surface prior to treating it with acrylic monomers. Soaking the glass in strong acidic or basic solutions is one of the most used techniques to clean the glass and enhance its hydrophilicity [175,176,178–181]. On the other hand, exposing the glass to oxygen plasma can perform similarly while avoiding usage of caustic chemicals and their etching effect on the used material [182]. The change in the glass hydrophilicity can be concluded by measuring the contact angle between a water droplet and the glass surface after each step during

the cleaning and the treatment processes. Washed glass slides were exposed to oxygen plasma for different time periods (30, 60, 90, and 120 s). The contact angle was found to be the least (less than 3° and could not be detected) after 60 s of exposure as shown in **Error! Reference source not found.** and Figure 3-6. However, to bind the PDMS replica to the glass, both must be treated with plasma for only 32 s which was found to be optimal for their permanent binding in the second experiment to avoid any leakage during the experiment. Decrease in the contact angle means that the surface became more hydrophilic and more hydroxyl groups were exposed on the surface. Having more hydroxyl groups on the glass surface is essential for the next treatment process where the 3-(trimethoxysilyl) propyl methacrylate monomer can bind efficiently to the glass and functionalize the glass surface with vinyl groups that can bind to the MIP by the end.

Table 3-1: Contact angle measurements on glass after plasma treatment for different time periods.

Treatment type	Washed	Washed + 30 s plasma	Washed + 60 s plasma	Washed + 90 s plasma	Washed + 120 s plasma
Contact angle for 2µL water in 3 replicate experiments	14.3	4	<3	4.9	5.9
	14.1	4.2	<3	5.7	4.3
	14.4	4.9	<3	5.7	5.9
Mean	14.26	4.36	<3	5.43	5.36
SD	0.12	0.39	-	0.38	0.75

SD: Standard deviation

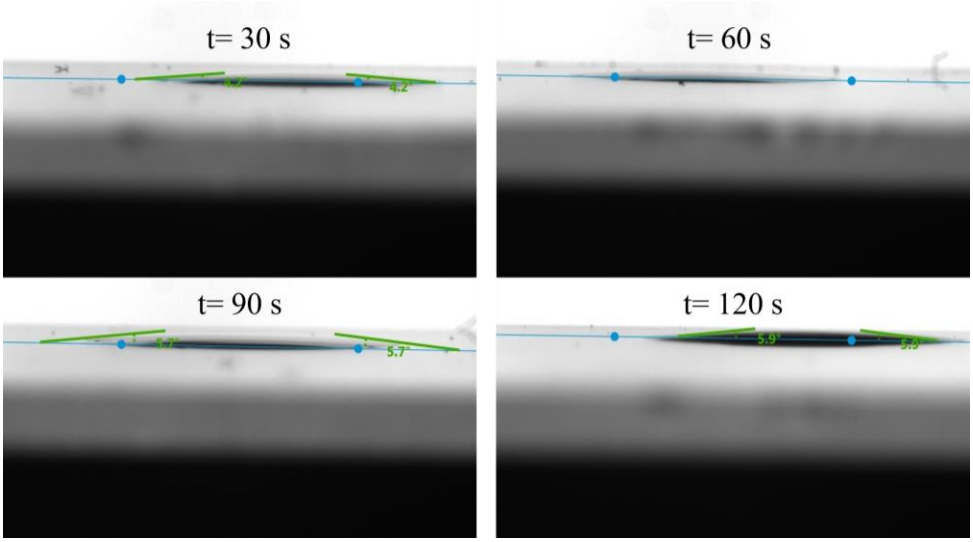

Figure 3-6: Images for contact angle of water droplet on glass treated with plasma for different time periods (30, 60, 90, and 120 s).

Plasma treated glass slides were immersed in the treatment solution overnight. When the silica monomer (3-(trimethoxysilyl) propyl methacrylate) was mixed with toluene in 2% v/v and used as a treatment solution, the contact angle of water droplet to the glass was higher than that mixed with acidic ethanol as shown in

Table *3-2* and Figure 3-7. This means that the glass became less hydrophilic and silica monomers were bound to the glass. This increase in the contact angle after the treatment with the silica monomer agrees with the results for the glass treatment done by Korzhikova-Vlakh et al. [175]. Therefore, the treatment using 2% v/v 3-(trimethoxysilyl) propyl methacrylate in toluene was used to add vinyl groups on the glass surface which can bind to the MIP and NIP during polymerization and keep the polymer bound to the glass.

Table 3-2: Contact angle measurements on glass after and before the two different treatments.

Treatment type	Washed	Washed + 60s plasma	After overnight toluene/monomer treatment	After overnight acidic ethanol/monomer treatment
Contact angle for 2µL water in 3 replicate experiments	14.3	<3	68.8	42
	14.1	<3	67.6	41.4
	14.4	<3	67.4	43.3
Mean	14.26	<3	67.9	42.2
SD	0.12	-	0.62	0.79

SD: Standard deviation

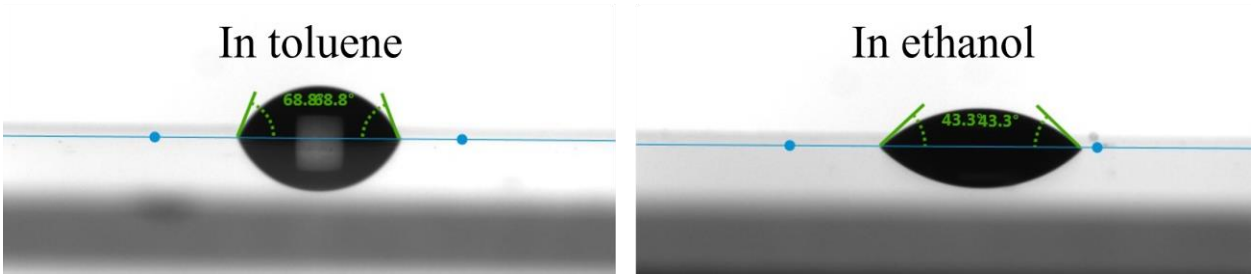

Figure 3-7: Images for contact angle of water droplet on glass after the two different treatments.

3.3.2. MIP integration with microfluidics

In general, MIP can be synthesized by thermal or photo-initiated polymerization. However, thermal polymerization takes long time up to 24 hours. On the other hand, photopolymerization

has been known for being a fast method for polymerization [183]. Therefore, Device 1 in Figure 3-2 was used to investigate the applicability of injecting and curing the MIP within a microfluidic channel. In this regard, only 20 minutes were enough for complete polymerization of the NIP and MIP polymeric solution where a photo initiator and UV light were used. As a result, white porous polymeric layers were successfully prepared inside the channels as shown in Figure 3-8A without any cracks. Template removal after polymerization is the hardest and the most time and solvent consuming step in the MIP preparation process. Challenges and some solutions regarding this step have been summarized by Lorenzo et al. [184]. It is usually done by using the Soxhlet apparatus for several hours (6-24 h) with a large solvent amount which can reach 300 mL. Another way is by shaking or stirring the polymer in the washing solution and doing repetitive washing. One way to accelerate the washing process is by applying ultrasonic waves while immersing the glass slide with the polymer in the washing solution. Results are shown in Figure 3-8B.

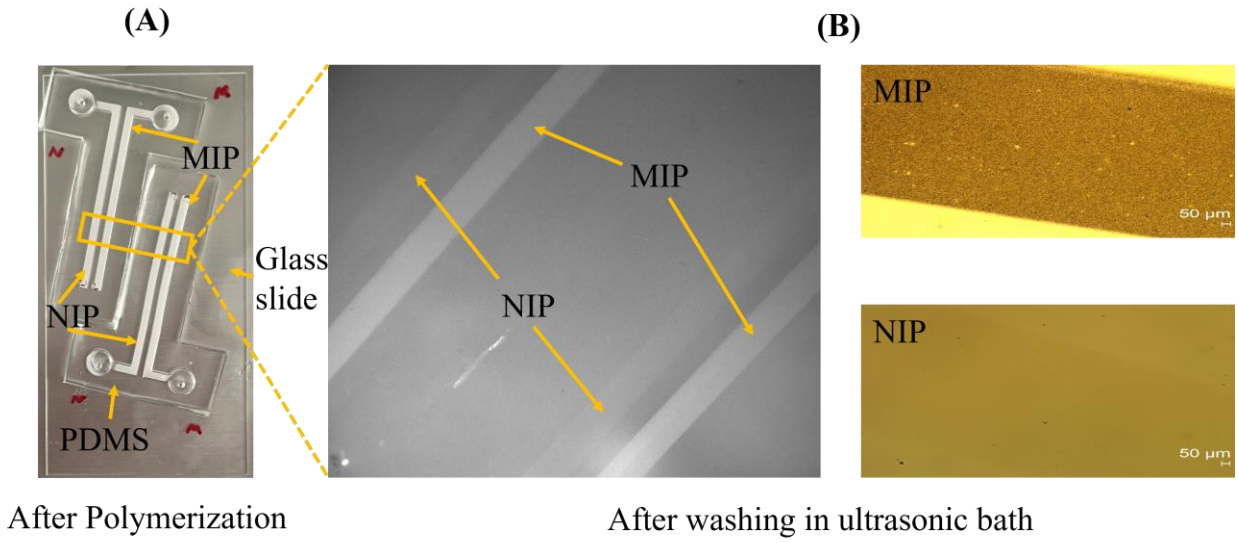

Figure 3-8: Fabricated NIP and MIP in experiment 1 before and after washing where (A) shows NIP and MIP white polymers inside the channels just after polymerization and (B) shows NIP and MIP images after washing with aid of ultrasonication with thicker polymer of MIP compared to that of NIP.

As seen in the figure, all the formed polymer was removed after washing and just a very thin layer of the polymer that was attached to the glass was left where the MIP layer was thicker than the NIP layer. Optical profilometer was used to check the thickness of both layers where MIP was

found to be thicker with highest thickness of ~3 µm and rougher surface compared to the NIP layer with highest thickness of ~1 µm as shown in Figure 3-9. Moreover, SEM images using 3 magnifications 1,500x, 5,000x, and 35,000x were taken for both NIP and MIP thin layers showing that NIP and MIP are both formed of porous layer with smaller features in the NIP than in the MIP as shown in Figure 3-10. This could be due to the presence of the template molecules in the MIP pre-polymerization solution that affect the polymer configuration and leave cavities in the polymer structure after their removal by the washing solution.

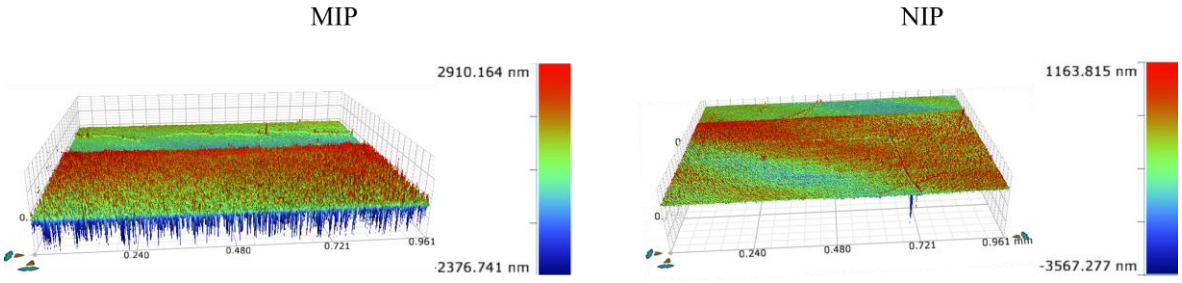

Figure 3-9: Optical profilometer images for MIP and NIP thin layers after being washed with acetic acid/methanol 1:9 v/v and methanol using ultrasonic bath showing the thickness of each layer.

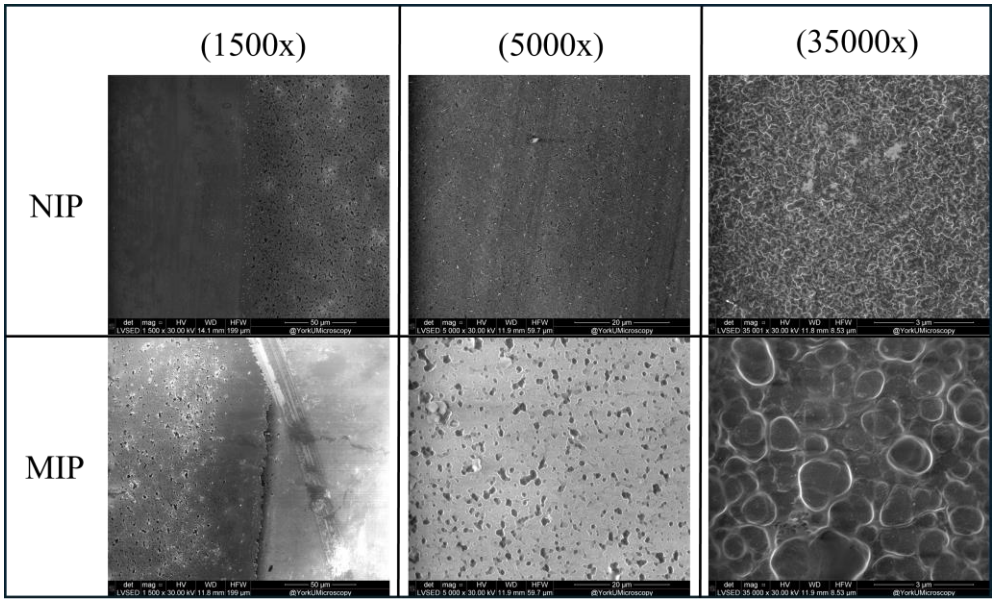

Figure 3-10: SEM images for NIP and MIP thin layers after being washed with acetic acid/methanol 1:9 v/v and methanol using ultrasonic bath using three different magnifying power.

The main challenge with the used device is the solution leakage from the channels because only physical bonding by pressing was used to stick the PDMS to the glass slide. Moreover, after polymerization and ultrasonication, the resulting thin layer of the polymer - which was almost transparent in the case of the NIP - could result in low extraction efficiency and affect the detection. For this, a second experiment was performed where all the porous polymer was kept inside the device, in which PDMS is permanently bound to the glass, and washed using a syringe pump to avoid: 1) the leakage problem, and 2) the effect of ultrasonication on the polymer. Another challenge was the difficulty to control the polymer formation inside a certain length of the channel even after using a photo mask. Therefore, for the second experiment, thin channels with wide chambers in the middle were used where the polymerization can be focused in the chambers.

In the second experiment, a 3D printed mold containing multiple straight channels with middle hexagon chambers (with a width of 4 mm and a height of 300 µm in the middle) was fabricated as shown in Figure 3-3. The design was chosen based on the view area of the fluorescence microscope where fluorescence can be measured for the whole chamber using a 5X magnification lens, minimizing the fluorescence intensity variations, and providing a larger surface area for molecule capturing compared to straight channels. Moreover, having the polymer focused inside the chamber could prevent the polymer dispersion to adjacent channels during next processes. NIP solution was injected inside the channels and polymerized under UV as discussed in the method section. The effect of the chambers' height using a mold with different chambers heights from 100 to 700 µm, as shown in Figure 3-11A, was investigated aiming to get a uniform polymer with minimum height. A Uniform polymeric layer filling the whole chamber was formed in chambers with heights over 200 µm as shown in Figure 3-11B. Therefore, mold design with height of 300 µm was chosen for further experiments. In this experiment, PDMS was permanently bound to the glass and template removal from the polymer could be enhanced by testing the washing flow rate, temperature, and the washing solution composition.

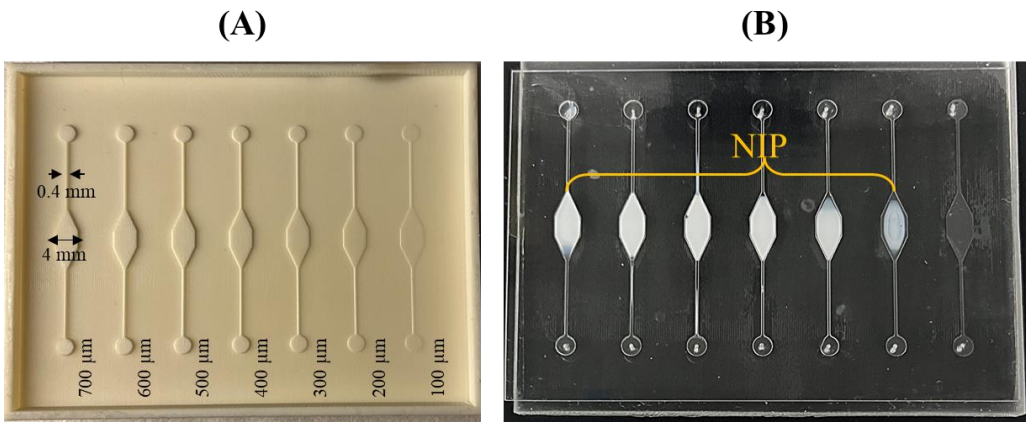

Figure 3-11:Images of (A) 3D printed mold with chambers height from 100-700 µm and (B) NIP white polymer after photopolymerization inside the device where PDMS replica with the 7 chambers, inlets, and outlets was bound to the treated glass slide.

3.3.3. Effect of flow rate, temperature, and washing solution composition on template removal

Parameters such as the flow rate, temperature, and washing solution composition could affect the removal efficiency of the template molecules from the polymer. MIP inside the chambers was washed for template removal at room temperature and at 65 °C using a hot plate and the effect of the flow rate was tested. Different flow rates were used (0.05, 0.2, 0.5, and 1 mL/min) using 5 mL acetic acid/methanol 1:9 as the most used washing solution for MIP's template removal [65,69,177,185], followed by 20 mL methanol. Washing solution was injected into the inlet using a syringe pump and each 1 mL of effluent was collected and measured for absorbance using a 1 mL quartz cuvette and UV-Vis spectrophotometer at 210 nm as shown in Figure 3-12. For the first 5 mL (i.e. the acetic acid/methanol solution), the absorbance of all measurements was almost the same which could be due to the presence of excess acetic acid in the effluent, that can absorb light at the same wavelength for AZM. Methanol was used to remove the excess acid and continue the template removal. Decreasing the flow rate resulted in an increase in the absorbance, meaning that more molecules were washed out from the MIP compared to the higher flow rates as shown in Figure 3-12. Therefore, a flow rate of 0.01 mL/min which is lower than the tested 0.05 mL/min and can be more effective for template removal was used for the next experiment. The effect of

heat when washing at the tested flow rates was found to be insignificant. Therefore, template removal was done at room temperature in the next experiment to choose the best washing solution.

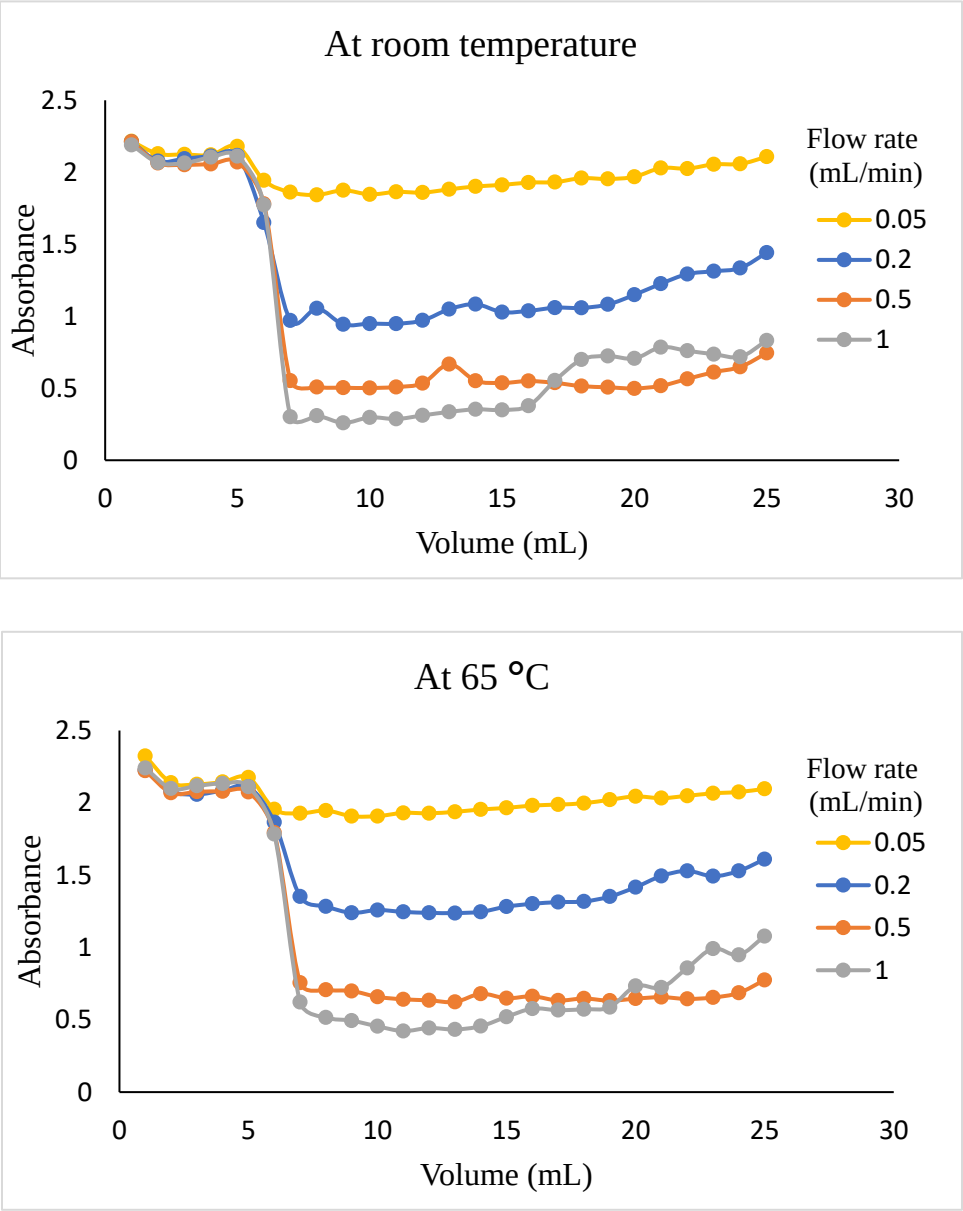

Figure 3-12: Effect of flow rate and temperature on the absorbance of the washing effluent at wavelength of 210 nm during AZM (template) removal step from the MIP after polymerization in the microfluidic device.

For optimal template (AZM) removal from the MIP, different washing solutions were tested including, 5% ammonium hydroxide in methanol, 1% formic acid in acetonitrile, and 1%formic

acid in 70% ethanol using a flow rate of 0.01 mL/min. These solvents aim to disturb the pH inside the chambers and weaken the interaction between the template molecules and the monomers. Although acetic acid/methanol 1:9 v/v was extensively used in literature for MIP washing step, it was found that alkaline methanol using 5% ammonium hydroxide/methanol revealed better elution of AZM and other macrolides from the MIP during the recovery experiments done by Song et al. [16]. Therefore, 5% ammonium hydroxide/methanol was chosen as an alkaline washing solution to be tried. Moreover, in LC-MS and HPLC analysis of AZM and other macrolides, formic acid/acetonitrile was the most used eluent with excellent recovery percentage. Therefore, 1% formic acid in acetonitrile and the same in 70% ethanol (AZM solubility in ethanol is 16 mg/mL) were tried as acidic washing solutions. 40 mL of the three solutions were injected into three MIP-containing channels, then a 1 mL effluent sample was collected at three points of washing (i.e. 10, 25, and 40 mL) to check the AZM removal effect over time, which was measured by LC-MS as shown in Table 3-3.

Table 3-3: Effect of washing solution composition on AZM (template) removal

Washing solution	**AZM Conc. (µg/mL) at**		
	10 mL	**25 mL**	**40 mL**
5% ammonium hydroxide/methanol	1.33	0.07	0.28
1% formic acid/acetonitrile	2.20	0.08	0.10
1% formic acid/70%ethanol	0.42	0.02	0.03

After testing the three washing solutions, the lowest AZM concentration after 10 mL washing was found to result from using the 1% formic acid/70% ethanol solution. No further increase was observed with further washing. This means that almost all AZM was removed within the first 10 mL washing and only minute, trace amounts are observed with further washing. This could be due to the better solubility of AZM in ethanol compared to methanol, and to acetonitrile where the formic acid lowers the pH and results in weakening the interaction of AZM with the monomers. Ethanol and acetonitrile have lower polarity compared to methanol, which is better for dissolving AZM [186]. However, ethanol is a protic solvent and can form hydrogen bond with AZM compared to acetonitrile which is an aprotic solvent and cannot form hydrogen bonds. The only

challenge here is the long time needed for washing as by using 0.01 mL/min flow rate it takes 16 h 40 min for 10 mL washing.

For further optimization, 3 channels containing MIP were washed with 10 mL of 1% formic acid/70% ethanol each but using 3 different flow rates (0.01, 0.1, and 1 mL/min) and all the 10 mL effluent was collected in a 15 mL Falcon tube to be analyzed for AZM concentration by LC-MS. The results shown in Table 3-4 revealed that by increasing the flow rate from 0.01 mL/min to 0.1 mL/min, improved AZM removal was observed, means better washing. However, by further increase of the flow rate to 1 mL/min, the washing efficiency decreased.

Table 3-4: Investigating the flow rate effect for template removal using 1% formic acid/70% ethanol

Flow rate (mL/min)	0.01	0.1	1
AZM Conc. (µg/mL)	73.52	79.82	55.83

This can be explained by having two main factors affecting the washing step. Firstly, the contact time between the solvent and the polymer that is required for the solvent to get through the polymer structure to disturb the interaction between AZM and the monomers. Hence, increasing the contact time -means decreasing the flow rate- could be required. Secondly, the shear force that can increase by increasing the flow rate as we have a gap between the polymer's top surface and the PDMS allowing the solvent to pass over the polymer. Thus, by decreasing the flow rate to 0.01 mL/min, the shear force was decreased but the contact time was increased and vice versa when the flow rate was increased to 1 mL/min, proving that at a middle flow rate 0.1 mL/min both factors could be in equilibrium to remove the template molecules from the polymer. As a result, 1% formic acid/70%ethanol at room temperature and a flow rate of 0.1 mL/min was chosen for the template removal experiments.

3.3.4. AZM detection in MIP-integrated microfluidic device

3.3.4.1. Detection on MIP washed by aid of ultrasonication (Experiment 1)

To capture AZM by the polymer, monomers should have function groups that can bind to AZM. MAA as an acidic monomer can bind to AZM through electrostatic and hydrogen bonding based on the reaction condition. As shown in Figure 3-13 AZM has many hydroxyl groups which can

form hydrogen bonds with the MAA carboxylic groups, it also has two tertiary amine groups which can electrostatically interact with the carboxylic groups of the monomers.

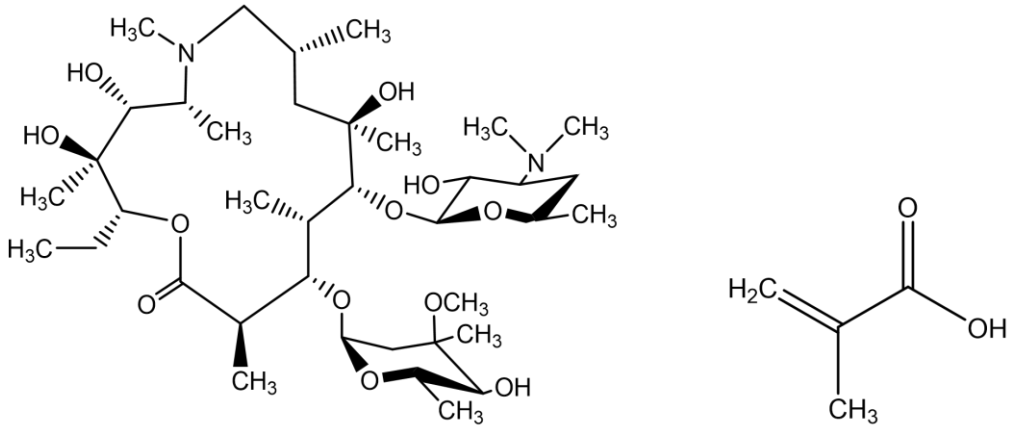

Figure 3-13: Chemical structures of Azithromycin (AZM) and methacrylic acid (MAA).

For template removal after polymerization, ultrasonication was used to facilitate and accelerate the bond breakage between AZM and the monomers. This resulted in very thin layers of both NIP and MIP which were then used for AZM capturing. By injecting 50 µL of AZM (1000 µg/mL) inside the channels over the MIP and the NIP thin layers, AZM was supposed to bind to its complementary cavities in the MIP and a very little amount to be adsorbed on the NIP. This captured AZM could form an ion-pair complex with FITC when 50 µL of FITC (100 µg/mL) was applied into the channels. With the MIP, a significant increase in the fluorescence intensity was observed compared to that with the NIP as shown in Figure 3-14. This increase in the fluorescence intensity when 1000 µg/mL AZM was applied on the NIP can be due to the non-specific adsorption on the polymer. By increasing the concentration of AZM samples applied on the MIP from 0 to 1000 µg/mL, the fluorescence intensity increased. This could be due to the increased numbers of the captured AZM molecules which resulted in increasing the medium pH and the fluorescence intensity of the FITC in methanol, consequently. Challenges with this method came from the difference in the polymeric layer thickness between the NIP and MIP which makes the comparison between them unreliable. NIP was almost a transparent layer while MIP was a thin white layer after washing while before washing, both NIP and MIP channels had a thick white porous polymer.

Moreover, leaking sometimes happened for AZM and FITC solutions after physical rebinding of the PDMS to the glass slide after the ultrasonication bath. This makes a permanent bonding essential for a more controlled experiment.

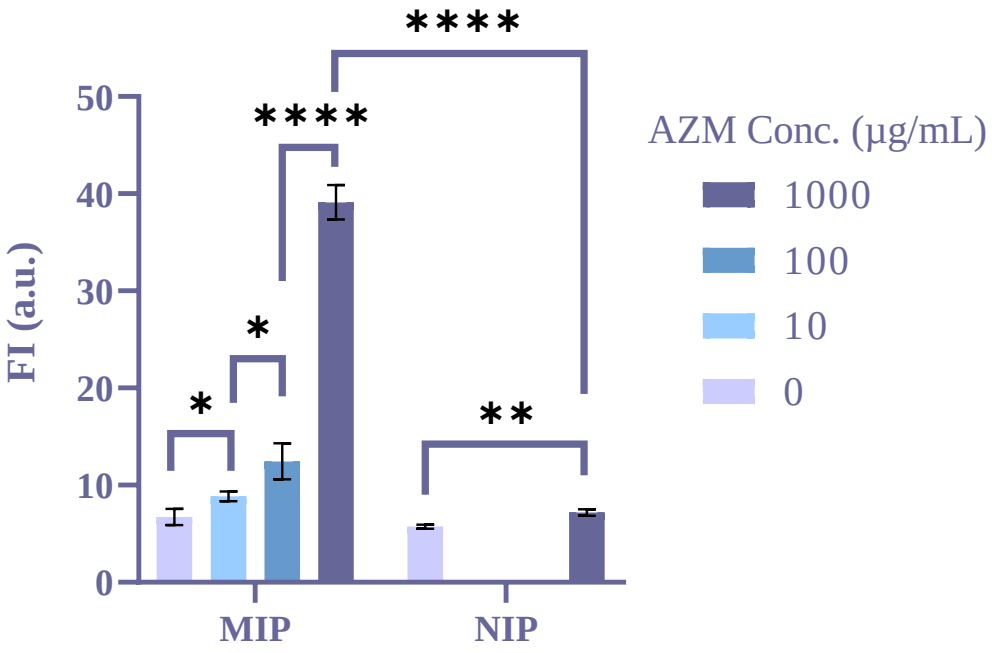

*Figure 3-14: AZM detection using MIP- and NIP-integrated microfluidic devices where MIP was washed by aid of ultrasonication. Significance difference was calculated using $p<0.05$, * for p-value < 0.05, ** for p-value < 0.01, **** for p-value < 0.0001.*

3.3.4.2. Detection on MIP washed using a syringe pump (Experiment 2)

Template removal from MIP inside the microfluidic chambers using continuous flow by a syringe pump resulted in a thick, porous polymer inside the chambers. This could capture AZM and result in concentration enrichment of AZM inside the device which then be detected by using FITC as a fluorescent reagent. By injecting 3 different concentrations of AZM (100, 10, and 1µg/mL) followed by 2nd wash, and FITC application, an increase in the fluorescence intensity of the FITC was observed by increasing the AZM concentration on both MIP and NIP as shown in the microscopic images in Figure 3-15A. However, the fluorescence intensity on NIP when 100 µg/mL AZM was applied was very high. Due to having two different surface qualities, fluorescence intensity was normalized to the highest intensity of the NIP and MIP to compare the

results of detection on both as shown in Figure 3-15B. MIP was found to have higher fluorescence intensity compared to NIP when low concentrations of AZM was used (1 and 10 µg/mL) however it is also higher when only solvent was used for the control experiment. This could be the effect of AZM traces that might be still embedded in the polymer after the template removal, giving a background effect. NIP was found to have higher level of significant difference between 1 and 10 µg/mL, and 10 and 100 µg/mL of AZM samples with no significant difference in the fluorescence intensity between the control and 1 µg/mL AZM sample in both cases which might be due to the effect of surface morphology and porosity which requires more studies to be performed.

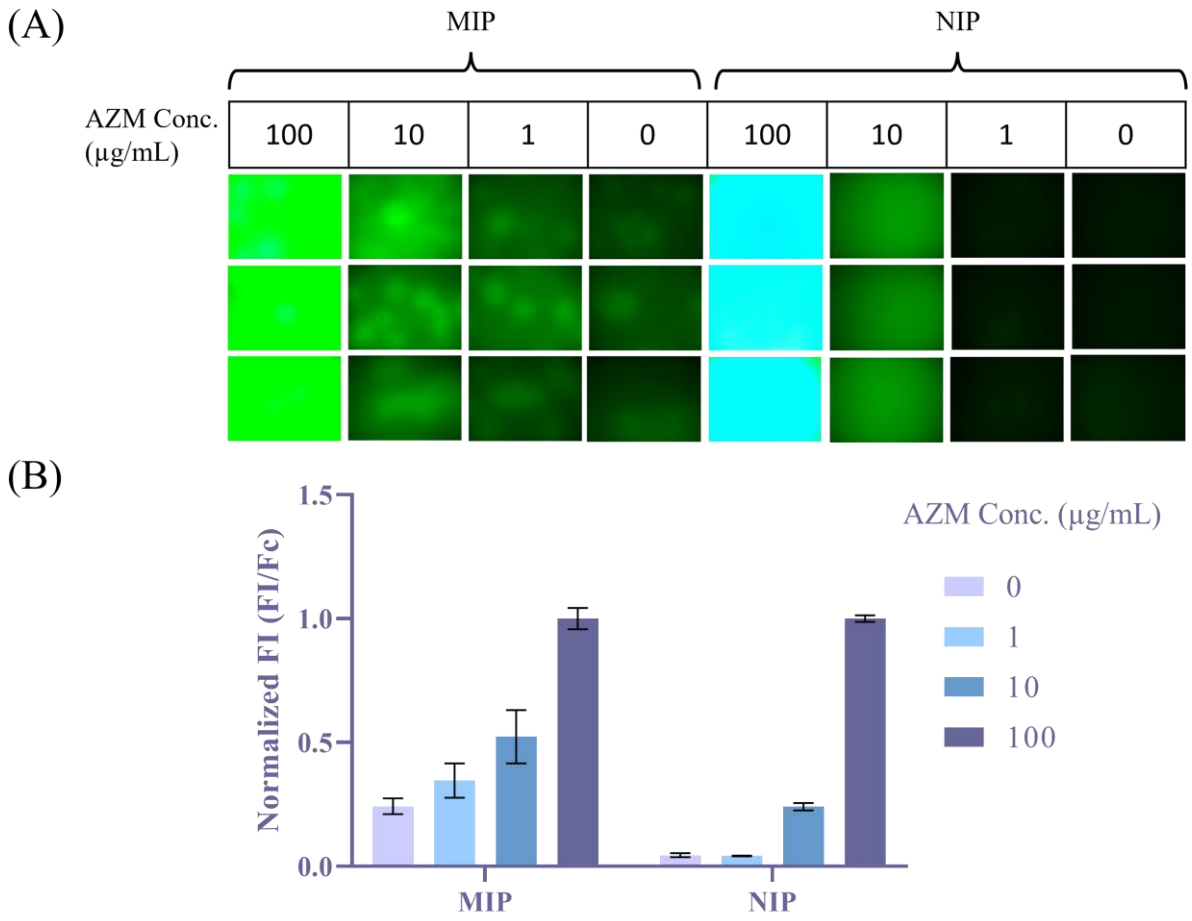

Figure 3-15: AZM detection using MIP-integrated microfluidic device where MIP was washed using syringe pump including A) Images of triplicate experiment and B) The normalized fluorescence intensity graph.

3.4. Conclusion

This study investigated the ability of facile and fast preparation of MIP inside a microfluidic device within 20 min using MAA and EGDMA in acetonitrile as a monomer and a cross linker, respectively. A white polymeric layer can be formed inside channels and chambers of a treated glass-PDMS microfluidic device with no cracking or peeling off problems after polymer fabrication and washing. Contact angle measurement was used to check the increase of the glass hydrophilicity after plasma treatment which offered a greener technique for glass treatment away from using piranha solution or strong alkaline solutions. 2% v/v 3-(trimethoxysilyl) propyl methacrylate in toluene was found to be efficient in treating the cleaned glass to provide better adhesion of the prepared polymer on the glass without peeling off problem. After MIP preparation, template removal was found to be the most time-consuming step, and to facilitate the washing, ultrasonication was used which provided unequal thickness of NIP and MIP to be used for capturing and detection. To overcome the problems with this method, washing inside the microfluidic device was used where 1% formic acid in 70% ethanol was found to be efficient for template removal using a flow rate of 0.1 mL/min. After AZM capturing and FITC application, NIP provided high fluorescence intensities which can be due to the roughness and the large surface area of the NIP, contradicting the expectation of having low absorption on NIP due to the lack of cavities. More investigation is required to compare the results of this study where photopolymerization was used to that if thermal polymerization is used for polymer preparation inside the same microfluidic device. Moreover, optimization of the 2^{nd} washing step should be performed which may solve any problems related to the non-specific absorption effect on detection.

Chapter 4: Thesis Summary and Future Recommendations

4.1. Thesis Summary

The presence of antibiotics in environmental matrices such as wastewater effluent and influent has gained an intense concern due to the hazard of development of antimicrobial resistant genes and bacteria. This can affect the ecosystem as well as human health. AZM as one of the most used antibiotics and essential in some cases such as respiratory tract infections and sexually transmitted diseases was detected in the Canadian wastewater. Nowadays, treated urine is used as fertilizers as an alternative to synthetic fertilizers which raises a concern of soil and environment contamination by the pharmaceuticals that may still be present in the that urine. 6-14 % of AZM dose is excreted unchanged in urine and with lack of rapid and direct monitoring and removal of the drug from that urine, it can contaminate the environment. Therefore, in this thesis a study was conducted to solve some problems with AZM analysis to overcome the challenges with conventional analytical techniques.

This chapter summarizes the findings of this thesis along with future recommendations where two main objectives were studied. Firstly, developing an optical, simple, fast, and direct detection method for AZM to overcome the limitations with the other developed optical techniques for its detection was studied in Chapter 2. FITC was found to be an ideal reagent for instant and sensitive spectrophotometric and fluorescence microscopic-based analysis of AZM. AZM was found to raise the absorbance and the fluorescence intensity of FITC when mixed in methanol in a ratio of 1:1 v/v. A wide linear range from 0-31.25 µg/ mL with LOD of 0.41 µg/mL 0.82 µg/mL and LOQ of 1.23 µg/mL and 2.49 µg/mL were achieved for the fluorescence-based and the spectrophotometric analysis, respectively. Application of these techniques on AZM detection in spiked artificial urine samples was successfully performed where %recovery of >93% and >85% were achieved when using the fluorescence-based and the spectrophotometric methods, respectively. The main challenge with this method is the selectivity where the method can be used for selective detection of AZM over other existing ones. Therefore, the second objective was to use receptors specific for AZM to extract it prior to its detection. In Chapter 3, MIP was used as a synthetic receptor to capture AZM from water samples. A study was conducted on integrating MIP with microfluidics as a step in developing a portable device where both extraction and detection

of AZM in liquid samples can be held on the same platform. MIP and NIP were successfully prepared inside a portable device using photopolymerization in just 20 min compared to thermal polymerization which may take 24 hours. Polymer peeling off problem from the glass was solved by the correct treatment of the glass slide using oxygen plasma for 32 seconds and 2% v/v (3-(trimethoxysilyl) propyl methacrylate) in toluene. For efficient removal of the template molecules from the MIP after polymerization, two methods for washing were tried using ultrasonication and syringe pumps. Despite using ultrasonication for washing is very effective and takes short time, it removes almost all the polymer from the glass and just leaves very thin layer with thickness of ~3µm in MIP and ~1µm in NIP and suffers from a leakage problem due to the temporary binding of the glass to the PDMS replica that contains the channels. Therefore, a device with permanent bonding between the PDMS and the glass was used and the polymer was prepared inside it and syringe pumps were used to inject the washing solution into the channels to remove the template molecules. Different washing solutions and flow rates were tested where 10 mL 1% formic acid in 70%ethanol was found to effectively remove the template when a flow rate of 0.1 mL/min. The device was used to capture AZM from spiked water samples followed by the application of FITC in methanol for detection. Both MIP and NIP could capture AZM and higher fluorescence intensity was obtained when higher concentration of AZM was used and decreased by decreasing the concentration. This confirms the applicability of using the same platform for extraction and detection of AZM in water samples. However, more studies are required to optimize the polymer preparation step and the extraction step where the 2^{nd} washing is essential to remove any non-specific adsorption which can affect the results obtained for detection on NIP and MIP.

4.2. Future Recommendations

Throughout the extraction of AZM from artificial urine or water sample prior to its simple detection using FITC, a liquid-liquid extraction was required to extract AZM from the liquid sample. A separating funnel was used with organic solvents multiple times to extract the compound from its solution. In this regard, using a portable microfluidic device inside which liquid-liquid extraction can be accomplished instead of the separating funnel could decrease the volume of solvents needed for extraction and save time and effort. Sensor selectivity is one of the main characteristics which can be accomplished by integrating receptors into the sensor. AS MIP was found to have higher chemical, physical, and thermal stability compared to the biological receptors

and the lack of studies on optical detection of AZM where MIP was used as receptors, more studies should be done on integrating MIP into the optical portable sensors. This requires a comprehensive comparison between different polymerization techniques such as thermal and photo-initiated polymerization to prepare MIP for AZM. Thermal polymerization of MIP specific for AZM has been studied before showing a better capturing on MIP compared to the NIP however when photopolymerization was used in our case, it showed the opposite which can be due to the effect of UV on the template molecules or on the polymer structure. Additionally, optimization of the 2nd washing step during solid phase extraction where different solvent compositions, flow rates can be tested would lower the effect of the non-specific adsorption of AZM to the polymer in the detection step. Moreover, a comparison between using a pre-prepared polymer outside the microfluidic device then packing it into the microfluidic channels and its preparation directly inside the channels would grasp a deeper understanding of the sensor feasibility and the cost-effectiveness. Investigating the effect of other existing compounds on the detection of AZM and the response of the sensor to other compound could give an idea about the sensor selectivity and specificity. Moreover, other materials instead of PDMS and glass which are transparent can be tested for ease device fabrication and to lower the cost and minimize the amount of chemicals required for the fabrication. Multiplexing where different MIP can be prepared inside different microfluidic channels on the same device could help in detecting multiple targets using the same device where the MIP will be specific for each targeted compound. Furthermore, using a portable fluorescent microscope which is easier to use and cheaper than the regular laboratory microscopes could facilitate the on-site detection and the portability of the sensor. Another approach for enhanced portability can be by using smartphones for image taking and analysis and LED of specific wavelength as an excitation light source.

Bibliography

[1] Canada PHA of. Canadian Antimicrobial Resistance Surveillance System - Update 2020. 2020.

[2] Martin TMP, Esculier F, Levavasseur F, Houot S. Human urine-based fertilizers: A review. Crit Rev Environ Sci Technol 2022;52:890–936. doi:10.1080/10643389.2020.1838214.

[3] Zhou X, Cuasquer GJP, Li Z, Mang HP, Lv Y. Occurrence of typical antibiotics, representative antibiotic-resistant bacteria, and genes in fresh and stored source-separated human urine. Environ Int 2021;146:106280. doi:10.1016/j.envint.2020.106280.

[4] Özel Duygan BD, Udert KM, Remmele A, McArdell CS. Removal of pharmaceuticals from human urine during storage, aerobic biological treatment, and activated carbon adsorption to produce a safe fertilizer. Resour Conserv Recycl 2021;166. doi:10.1016/j.resconrec.2020.105341.

[5] Rodvold KA, Piscitelli SC. New Oral Macrolide and Fluoroquinolone Antibiotics : An Overview of Pharmacokinetics , Interactions , and Safety Author (s): Keith A . Rodvold and Stephen C . Piscitelli Source : Clinical Infectious Diseases , Vol . 17 , Supplement 1 . The Changing Role 2018;17.

[6] Page RL, Ruscin JM, Fish D, Lapointe M. Possible interaction between intravenous Azithromycin and oral Cyclosporine. Pharmacotherapy 2001;21:1436–43. doi:10.1592/phco.21.17.1436.34434.

[7] Lode H. 10 807 Eur. J Clin Microbiol Infect Dis 1991;10:807–12.

[8] Yang ZY, Wang L, Tang X. Determination of azithromycin by ion-pair HPLC with UV detection. J Pharm Biomed Anal 2009;49:811–5. doi:10.1016/J.JPBA.2008.12.018.

[9] Al-Rimawi F, Kharoaf M. Analysis of Azithromycin and Its Related Compounds by RP-HPLC with UV Detection. J Chromatogr Sci 2010;48:86–90. doi:10.1093/CHROMSCI/48.2.86.

[10] Habibi B, Ghorbel-Abid I, Lahsini R, Chehimi Ben Hassen D, Trabelsi-Ayadi M. Development and validation of a rapid HPLC method for multiresidue determination of erythromycin, clarithromycin, and azithromycin in aquaculture fish muscles. Acta Chromatogr 2019;31:109–12. doi:10.1556/1326.2017.00376.

[11] Bahrami G, Mirzaeei S, Kiani A. High performance liquid chromatographic determination of azithromycin in serum using fluorescence detection and its application in human pharmacokinetic studies. J Chromatogr B 2005;820:277–81. doi:10.1016/J.JCHROMB.2005.03.042.

[12] Paul P, Duchateau T, Sänger-van de Griend C, Adams E, Van Schepdael A. Capillary electrophoresis with capacitively coupled contactless conductivity detection method development and validation for the determination of azithromycin, clarithromycin, and clindamycin. J Sep Sci 2017;40:3535–44. doi:10.1002/JSSC.201700560.

[13] Sharma K, Mullangi R. A concise review of HPLC, LC-MS and LC-MS/MS methods for determination of azithromycin in various biological matrices. Biomed Chromatogr 2013;27:1243–58. doi:10.1002/BMC.2898.

[14] Song X, Zhou T, Li J, Su Y, Xie J, He L. Determination of macrolide antibiotics residues in pork using molecularly imprinted dispersive solid-phase extraction coupled with LC–MS/MS. J Sep Sci 2018;41:1138–48. doi:10.1002/JSSC.201700973.

[15] Lan C, Yin D, Yang Z, Zhao W, Chen Y, Zhang W, et al. Determination of Six Macrolide Antibiotics in Chicken Sample by Liquid Chromatography-Tandem Mass Spectrometry Based on Solid Phase Extraction. J Anal Methods Chem 2019;2019. doi:10.1155/2019/6849457.

[16] Song X, Zhou T, Li J, Zhang M, Xie J, He L. Determination of Ten Macrolide Drugs in Environmental Water Using Molecularly Imprinted Solid-Phase Extraction Coupled with Liquid Chromatography-Tandem Mass Spectrometry. Mol 2018, Vol 23, Page 1172 2018;23:1172. doi:10.3390/MOLECULES23051172.

[17] Rebelo P, Pacheco JG, Cordeiro MNDS, Melo A, Delerue-Matos C. Azithromycin electrochemical detection using a molecularly imprinted polymer prepared on a disposable screen-printed electrode. Anal Methods 2020;12:1486–94. doi:10.1039/C9AY02566A.

[18] Veloso WB, Almeida AT de FO, Ribeiro LK, de Assis M, Longo E, Garcia MAS, et al. Rapid and sensitivity determination of macrolides antibiotics using disposable electrochemical sensor based on Super P carbon black and chitosan composite. Microchem J 2022;172:106939. doi:10.1016/J.MICROC.2021.106939.

[19] Mater Mahnashi H, Mahmoud AM, Saad Alkahtani A, El-Wekil MM. Simultaneous electrochemical detection of azithromycin and hydroxychloroquine based on VS2 QDs embedded N, S @graphene aerogel/cCNTs 3D nanostructure. Microchem J 2021;163:105925. doi:10.1016/J.MICROC.2021.105925.

[20] Nigović B, Šimunić B. Voltammetric assay of azithromycin in pharmaceutical dosage forms. J Pharm Biomed Anal 2003;32:197–202. doi:10.1016/S0731-7085(03)00060-8.

[21] Ensafi AA, Allafchian AR, Rezaei B. A sensitive and selective voltammetric sensor based on multiwall carbon nanotubes decorated with MgCr2O4 for the determination of azithromycin. Colloids Surfaces B Biointerfaces 2013;103:468–74. doi:10.1016/J.COLSURFB.2012.11.021.

[22] Vajdle O, Guzsvány V, Škorić D, Csanádi J, Petković M, Avramov-Ivić M, et al. Voltammetric behavior and determination of the macrolide antibiotics azithromycin, clarithromycin and roxithromycin at a renewable silver – amalgam film electrode. Electrochim Acta 2017;229:334–44. doi:10.1016/J.ELECTACTA.2017.01.146.

[23] Li M, Jia L, Chen X, Li Y, Zhao D, Zhang L, et al. Web system-assisted ratiometric fluorescent probe embedded with machine learning for intelligent detection of pefloxacin. Sensors Actuators B Chem 2024;407:135491. doi:10.1016/j.snb.2024.135491.

[24] Xu J, Li R, Chen X, Zhang L, Li Y, Huang Y, et al. A multi-color fluorescent sensing system integrated with color recognition, liquid crystal display, and voice output module

for intelligent detection of two targets. Appl Surf Sci 2024;653:159436. doi:10.1016/j.apsusc.2024.159436.

[25] Xu J, Wang J, Li Y, Zhang L, Bi N, Gou J, et al. A wearable gloved sensor based on fluorescent Ag nanoparticles and europium complexes for visualized assessment of tetracycline in food samples. Food Chem 2023;424:136376. doi:10.1016/j.foodchem.2023.136376.

[26] Li C, Zhang X, Wen S, Xiang R, Han Y, Tang W, et al. Interface engineering of zeolite imidazolate framework−8 on two-dimensional Al−metal−organic framework nanoplates enhancing performance for simultaneous capture and sensing tetracyclines. J Hazard Mater 2020;395:122615. doi:10.1016/J.JHAZMAT.2020.122615.

[27] Lamaoui A, Karrat A, Amine A. Molecularly imprinted polymer integrated into paper-based analytical device for smartphone-based detection: Application for sulfamethoxazole. Sensors Actuators B Chem 2022;368:132122. doi:10.1016/j.snb.2022.132122.

[28] Shen Y, Wei Y, Chen H, Wu Z, Ye Y, Han DM. Liposome-encapsulated aggregation-induced emission fluorogen assisted with portable smartphone for dynamically on-site imaging of residual tetracycline. Sensors Actuators B Chem 2022;350:130871. doi:10.1016/J.SNB.2021.130871.

[29] Xu J, Guo S, Jia L, Zhu T, Chen X, Zhao T. A smartphone-integrated method for visual detection of tetracycline. Chem Eng J 2021;416:127741. doi:10.1016/j.cej.2020.127741.

[30] Wang T, Mei Q, Tao Z, Wu H, Zhao M, Wang S, et al. A smartphone-integrated ratiometric fluorescence sensing platform for visual and quantitative point-of-care testing of tetracycline. Biosens Bioelectron 2020;148:111791. doi:10.1016/J.BIOS.2019.111791.

[31] Guo X, Liu Y, Dong W, Hu Q, Li Y, Shuang S, et al. Azithromycin detection in cells and tablets by N,S co-doped carbon quantum dots. Spectrochim Acta - Part A Mol Biomol Spectrosc 2021;252:119506. doi:10.1016/j.saa.2021.119506.

[32] El-Rabbat N, Askal HF, Khashaba PY, Attia NN. A validated spectrofluorometric assay for the determination of certain macrolide antibiotics in pharmaceutical formulations and spiked biological fluids. J AOAC Int 2006;89:1276–87. doi:10.1093/jaoac/89.5.1276.

[33] Abdelmageed O, Kashaba P, Darwish I. Spectrofluorimetric Determination of Macrolide Antibiotics Using Eosin-G Dye. Bull Pharm Sci Assiut 2006;29:338–409. doi:10.21608/bfsa.2006.65217.

[34] Almeida VGK, Braga VSM, Pacheco WF, Cassella RJ. Fluorescence determination of azithromycin in pharmaceutical formulations by using the synchronous scanning approach after its acid derivatization. J Fluoresc 2013;23:31–9. doi:10.1007/s10895-012-1111-8.

[35] De Paula CER, Almeida VGK, Cassella RJ. Novel spectrophotometric method for the determination of azithromycin in pharmaceutical formulations based on its charge transfer reaction with quinalizarin. J Braz Chem Soc 2010;21:1664–71. doi:10.1590/S0103-50532010000900010.

[36] Ajima U, Onah JO, Onyekwelu JU. Quantitative determination of azithromycin by

extractive ion-pair spectrophotometry using methyl orange as ion pairing agent. Der Pharma Chem 2015;7:160–7.

[37] Mrudul Keskar RJ. Spectrophotometric Determination of Some Antibiotics Using Bromophenol Blue as Ion Pair Reagent. Pharm Anal Acta 2015;06. doi:10.4172/2153-2435.1000380.

[38] Abdullah JH, Yahya TAA, Alkaf AG, Alghorafi MA, Yassin SH. Selective spectrophotometric methods for the determination of azithromycin in pharmaceutical formulation. J Chem Pharm Res 2014;6:202–8.

[39] Walash MI, Rizk MS, Eid MI, Fathy ME. Spectrophotometric determination of four macrolide antibiotics in pharmaceutical formulations and biological fluids via binary complex formation with eosin and spectrophotometry. J AOAC Int 2007;90:1579–87.

[40] Adam AMA, Saad HA, Alsuhaibani AM, Refat MS, Hegab MS. Charge-transfer chemistry of azithromycin, the antibiotic used worldwide to treat the coronavirus disease (COVID-19). Part I: Complexation with iodine in different solvents. J Mol Liq 2021;325:115187. doi:10.1016/j.molliq.2020.115187.

[41] Adam AMA, Saad HA, Alsuhaibani AM, Refat MS, Hegab MS. Charge-transfer chemistry of azithromycin, the antibiotic used worldwide to treat the coronavirus disease (COVID-19). Part II: Complexation with several π-acceptors (PA, CLA, CHL). J Mol Liq 2021;325:115121. doi:10.1016/j.molliq.2020.115121.

[42] Adam AMA, Refat MS, Altalhi TA, Alsuhaibani KS. Charge-transfer complexation of TCNE with azithromycin, the antibiotic used worldwide to treat the coronavirus disease (COVID-19). Part IV: A comparison between solid and liquid interactions. J Mol Liq 2021;340:117224. doi:10.1016/j.molliq.2021.117224.

[43] Adam AMA, Saad HA, Alsuhaibani AM, Refat MS, Hegab MS. Charge-transfer chemistry of azithromycin, the antibiotic used worldwide to treat the coronavirus disease (COVID-19). Part III: A green protocol for facile synthesis of complexes with TCNQ, DDQ, and TFQ acceptors. J Mol Liq 2021;335:116250. doi:10.1016/J.MOLLIQ.2021.116250.

[44] Gouda AA, El-Sheikh R, Khalil KM. Spectrophotometric Determination of Certain Macrolide Antibiotics in Pharmaceutical Preparations. Int J TechnoChem Res 2015;01:11–24.

[45] Sayed RA, Hassan WS, El-Mammli MY, Shalaby A. New spectrophotometric and conductometric methods for macrolide antibiotics determination in pure and pharmaceutical dosage forms using rose Bengal. J Spectrosc 2013;1. doi:10.1155/2013/214270.

[46] Ng HY, Lee WC, Kung C Te, Li LC, Lee C Te, Fu LM. Recent Advances in Microfluidic Devices for Contamination Detection and Quality Inspection of Milk. Micromachines 2021, Vol 12, Page 558 2021;12:558. doi:10.3390/MI12050558.

[47] Sun Y, Zhao J, Liang L. Recent development of antibiotic detection in food and environment: the combination of sensors and nanomaterials. Microchim Acta 2021 1881

2021;188:1–22. doi:10.1007/S00604-020-04671-3.

[48] Nilghaz A, Lu X. Detection of antibiotic residues in pork using paper-based microfluidic device coupled with filtration and concentration. Anal Chim Acta 2019;1046:163–9. doi:10.1016/J.ACA.2018.09.041.

[49] Cui P, Wang S. Application of microfluidic chip technology in pharmaceutical analysis: A review. J Pharm Anal 2019;9:238–47. doi:10.1016/J.JPHA.2018.12.001.

[50] Al-Hetlani E. Forensic drug analysis and microfluidics. Electrophoresis 2013;34:1262–72. doi:10.1002/ELPS.201200637.

[51] Mesquita P, Gong L, Lin Y. Low-cost microfluidics: Towards affordable environmental monitoring and assessment. Front Lab a Chip Technol 2022;1:1074009. doi:10.3389/FRLCT.2022.1074009.

[52] Carolina Rafanhin Sousa A, Nascimento Makara C, Canniatti Brazaca L, Carrilho E. A colorimetric microfluidic paper-based analytical device for sulfonamides in cow milk using enzymatic inhibition. Food Chem 2021;356:129692. doi:10.1016/j.foodchem.2021.129692.

[53] Liao Z, Zhang Y, Li Y, Miao Y, Gao S, Lin F, et al. Microfluidic chip coupled with optical biosensors for simultaneous detection of multiple analytes: A review. Biosens Bioelectron 2019;126:697–706. doi:10.1016/J.BIOS.2018.11.032.

[54] Liu J, Zhang Y, Jiang M, Tian L, Sun S, Zhao N, et al. Electrochemical microfluidic chip based on molecular imprinting technique applied for therapeutic drug monitoring. Biosens Bioelectron 2017;91:714–20. doi:10.1016/J.BIOS.2017.01.037.

[55] Zhao Y, Tang M, Liu F, Li H, Wang H, Xu D. Highly integrated microfluidic chip coupled to mass spectrometry for on-line analysis of residual quinolones in milk. Anal Chem 2019. doi:10.1021/ACS.ANALCHEM.9B01844/SUPPL_FILE/AC9B01844_SI_001.PDF.

[56] Sharma N, Barstis T, Giri B. Advances in paper-analytical methods for pharmaceutical analysis. Eur J Pharm Sci 2018;111:46–56. doi:10.1016/J.EJPS.2017.09.031.

[57] Pollap A, Kochana J. Electrochemical Immunosensors for Antibiotic Detection. Biosens 2019, Vol 9, Page 61 2019;9:61. doi:10.3390/BIOS9020061.

[58] Aghamirzaei M, Khiabani MS, Hamishehkar H, Mokarram RR, Amjadi M. Plasmonic Sensor for Detection of β-Lactam Antibiotics based on the Conjugated Antibody with Gold Nanoparticles. J Appl Spectrosc 2021;88:233–41. doi:10.1007/S10812-021-01162-Y/METRICS.

[59] Yue F, Li F, Kong Q, Guo Y, Sun X. Recent advances in aptamer-based sensors for aminoglycoside antibiotics detection and their applications. Sci Total Environ 2021;762:143129. doi:10.1016/J.SCITOTENV.2020.143129.

[60] Liu Y, Deng Y, Li S, Wang-Ngai Chow F, Liu M, He N. Monitoring and detection of antibiotic residues in animal derived foods: Solutions using aptamers. Trends Food Sci Technol 2022;125:200–35. doi:10.1016/J.TIFS.2022.04.008.

[61] Nag P, Sadani K, Mohapatra S, Mukherji S, Mukherji S. Evanescent Wave Optical Fiber Sensors Using Enzymatic Hydrolysis on Nanostructured Polyaniline for Detection of β-Lactam Antibiotics in Food and Environment. Anal Chem 2021;93:2299–308. doi:10.1021/ACS.ANALCHEM.0C04169/SUPPL_FILE/AC0C04169_SI_001.PDF.

[62] Zhao G, Zhang Y, Sun D, Yan S, Wen Y, Wang Y, et al. Recent Advances in Molecularly Imprinted Polymers for Antibiotic Analysis. Mol 2023, Vol 28, Page 335 2023;28:335. doi:10.3390/MOLECULES28010335.

[63] Banan K, Hatamabadi D, Afsharara H, Mostafiz B, Sadeghi H, Rashidi S, et al. MIP-based extraction techniques for the determination of antibiotic residues in edible meat samples: Design, performance & recent developments. Trends Food Sci Technol 2022;119:164–78. doi:10.1016/J.TIFS.2021.11.022.

[64] Guan G, Liu B, Wang Z, Zhang Z. Imprinting of Molecular Recognition Sites on Nanostructures and Its Applications in Chemosensors. Sensors 2008, Vol 8, Pages 8291-8320 2008;8:8291–320. doi:10.3390/S8128291.

[65] Pan Y, Shan D, Ding L, Yang X, Xu K, Huang H, et al. Developing a generally applicable electrochemical sensor for detecting macrolides in water with thiophene-based molecularly imprinted polymers. Water Res 2021;205:117670. doi:10.1016/j.watres.2021.117670.

[66] Stoian IA, Iacob BC, Dudaș CL, Barbu-Tudoran L, Bogdan D, Marian IO, et al. Biomimetic electrochemical sensor for the highly selective detection of azithromycin in biological samples. Biosens Bioelectron 2020;155:112098. doi:10.1016/j.bios.2020.112098.

[67] Jafari S, Dehghani M, Nasirizadeh N, Azimzadeh M. An azithromycin electrochemical sensor based on an aniline MIP film electropolymerized on a gold nano urchins/graphene oxide modified glassy carbon electrode. J Electroanal Chem 2018;829:27–34. doi:10.1016/J.JELECHEM.2018.09.053.

[68] Abu-Dalo MA, Nassory NS, Abdulla NI, Al-Mheidat IR. Azithromycin-molecularly imprinted polymer based on PVC membrane for Azithromycin determination in drugs using coated graphite electrode. J Electroanal Chem 2015;751:75–9. doi:10.1016/J.JELECHEM.2015.05.030.

[69] Hu L, Zhou T, Feng J, Jin H, Tao Y, Luo D, et al. A rapid and sensitive molecularly imprinted electrochemiluminescence sensor for Azithromycin determination in biological samples. J Electroanal Chem 2018;813:1–8. doi:10.1016/J.JELECHEM.2018.02.010.

[70] Zhou T, Yang H, Jin Z, Liu Q, Song X, He L, et al. Determination of azithromycin residue in pork using a molecularly imprinted monolithic microcolumn coupled to liquid chromatography with tandem mass spectrometry. J Sep Sci 2016;39:1339–46. doi:10.1002/JSSC.201501249.

[71] Bizina E V., Efrosinina A V., Farafonova O V., Zolotareva NI, Grazhulene SS, Ermolaeva TN. Nanocomposites Based on Multi-Walled Carbon Nanotubes, Magnetite Nanoparticles, and Core–Shell Molecularly Imprinted Polymers in Piezoelectric Sensors for the Determination of Macrolide Antibiotics. J Anal Chem 2023;78:1566–74.

doi:10.1134/S1061934823110035.

[72] Klugerman MR. Chemical and Physical Variables Affecting the Properties of Fluorescein Isothiocyanate and Its Protein Conjugates. J Immunol 1965;95:1165–73. doi:10.4049/jimmunol.95.6.1165.

[73] Boutoille D, Marechal X, Pichenot M, Chemani C, Guery B, Faure K. FItc-albumin as a marker for assessment of endothelial permeability in Mice: Comparison with125i-albumin. Exp Lung Res 2009;35:263–71. doi:10.1080/01902140802632290.

[74] Chaganti LK, Venkatakrishnan N, Bose K. An efficient method for FITC labelling of proteins using tandem affinity purification. Biosci Rep 2018;38:1–8. doi:10.1042/BSR20181764.

[75] Trott DJ, Turnidge J, Kovac JH, Simjee S, Wilson D, Watts J. Comparative macrolide use in humans and animals: should macrolides be moved off the World Health Organisation's critically important antimicrobial list? J Antimicrob Chemother 2021;76:1955–61. doi:10.1093/JAC/DKAB120.

[76] Pyörälä S, Baptiste KE, Catry B, van Duijkeren E, Greko C, Moreno MA, et al. Macrolides and lincosamides in cattle and pigs: Use and development of antimicrobial resistance. Vet J 2014;200:230–9. doi:10.1016/J.TVJL.2014.02.028.

[77] Hasaneen N, Khurana P, Pulicharla R, Rezai P, Brar SK. Nanomaterial-Based Sensors for Macrolide Sensing BT - Nanoscale Matter and Principles for Sensing and Labeling Applications. In: Mohanta D, Chakraborty P, editors., Singapore: Springer Nature Singapore; 2024, p. 513–35. doi:10.1007/978-981-99-7848-9_25.

[78] Guerra P, Kim M, Shah A, Alaee M, Smyth SA. Occurrence and fate of antibiotic, analgesic/anti-inflammatory, and antifungal compounds in five wastewater treatment processes. Sci Total Environ 2014;473–474:235–43. doi:10.1016/J.SCITOTENV.2013.12.008.

[79] List of Maximum Residue Limits (MRLs) for Veterinary Drugs in Foods - Canada.ca n.d. https://www.canada.ca/en/health-canada/services/drugs-health-products/veterinary-drugs/maximum-residue-limits-mrls/list-maximum-residue-limits-mrls-veterinary-drugs-foods.html (accessed November 26, 2021).

[80] Amelin VG, Bol'shakov DS. Sample Preparation, Identification, and Determination of Twelve Macrolides in Raw Food Materials and Food Products Using High-Resolution Mass Spectrometry. Moscow Univ Chem Bull 2019 742 2019;74:63–9. doi:10.3103/S0027131419020032.

[81] Thangadurai S. Gas chromatographic–mass spectrometric determination of azithromycin in biological fluids. J Anal Sci Technol 2015;6:1–6. doi:10.1186/S40543-015-0059-0/FIGURES/4.

[82] Hu C, Zhang Y, Zhou Y, Liu Z fei, Meng Q, Feng X song. A review of pretreatment and analysis of macrolides in food (Update Since 2010). J Chromatogr A 2020;1634:461662. doi:10.1016/J.CHROMA.2020.461662.

[83] Choemunng A, Na-Bangchang K. AN ALTERNATIVE LIQUID

CHROMATOGRAPHY-MASS SPECTROMETRIC METHOD FOR THE DETERMINATION OF AZITHROMYCIN IN HUMAN PLASMA AND ITS APPLICATION TO PHARMACOKINETIC STUDY. Http://DxDoiOrg/101080/108260762010489009 2010;33:1516–28. doi:10.1080/10826076.2010.489009.

[84] Liao QG, Wen Z Da, Guang LL, Dan ZXC. Ultrasonic-assisted dispersive liquid–liquid microextraction based on a simple and green deep eutectic solvent for preconcentration of macrolides from swine urine samples. Sep Sci Plus 2020;3:22–7. doi:10.1002/SSCP.201900064.

[85] Dong C, Shi H, Han Y, Yang Y, Wang R, Men J. Molecularly imprinted polymers by the surface imprinting technique. Eur Polym J 2021;145:110231. doi:10.1016/j.eurpolymj.2020.110231.

[86] Włoch M, Datta J. Synthesis and polymerisation techniques of molecularly imprinted polymers. Compr Anal Chem 2019;86:17–40. doi:10.1016/BS.COAC.2019.05.011.

[87] Belbruno JJ. Molecularly Imprinted Polymers. Chem Rev 2019;119:94–119. doi:10.1021/acs.chemrev.8b00171.

[88] Dong X, Zhang C, Du X, Zhang Z. Recent Advances of Nanomaterials-Based Molecularly Imprinted Electrochemical Sensors. Nanomaterials 2022;12. doi:10.3390/NANO12111913.

[89] Dolati S, Ramezani M, Nabavinia MS, Soheili V, Abnous K, Taghdisi SM. Selection of specific aptamer against enrofloxacin and fabrication of graphene oxide based label-free fluorescent assay. Anal Biochem 2018;549:124–9. doi:10.1016/J.AB.2018.03.021.

[90] Liu X, Su L, Zhu L, Gao X, Wang Y, Bai F, et al. Hybrid material for enrofloxacin sensing based on aptamer-functionalized magnetic nanoparticle conjugated with upconversion nanoprobes. Sensors Actuators B Chem 2016;233:394–401. doi:10.1016/J.SNB.2016.04.096.

[91] Hong KY, de Albuquerque CDL, Poppi RJ, Brolo AG. Determination of aqueous antibiotic solutions using SERS nanogratings. Anal Chim Acta 2017;982:148–55. doi:10.1016/J.ACA.2017.05.025.

[92] Lavaee P, Danesh NM, Ramezani M, Abnous K, Taghdisi SM. Colorimetric aptamer based assay for the determination of fluoroquinolones by triggering the reduction-catalyzing activity of gold nanoparticles. Microchim Acta 2017;184:2039–45. doi:10.1007/S00604-017-2213-4/FIGURES/2.

[93] Liu X, Huang D, Lai C, Zeng G, Qin L, Zhang C, et al. Recent advances in sensors for tetracycline antibiotics and their applications. TrAC Trends Anal Chem 2018;109:260–74. doi:10.1016/J.TRAC.2018.10.011.

[94] Greene NT, Shimizu KD. Colorimetric molecularly imprinted polymer sensor array using dye displacement. J Am Chem Soc 2005;127:5695–700. doi:10.1021/ja0468022.

[95] Lowdon JW, Diliën H, van Grinsven B, Eersels K, Cleij TJ. Colorimetric sensing of amoxicillin facilitated by molecularly imprinted polymers. Polymers (Basel) 2021;13.

doi:10.3390/polym13132221.

[96] Lowdon JW, Eersels K, Rogosic R, Heidt B, Diliën H, Redeker ES, et al. Substrate displacement colorimetry for the detection of diarylethylamines. Sensors Actuators, B Chem 2019;282:137–44. doi:10.1016/j.snb.2018.11.053.

[97] Sharma A, Majdinasab M, Khan R, Li Z, Hayat A, Marty JL. Nanomaterials in fluorescence-based biosensors: Defining key roles. Nano-Structures & Nano-Objects 2021;27:100774. doi:10.1016/J.NANOSO.2021.100774.

[98] Patel S, Jamunkar R, Sinha D, Monisha, Patle TK, Kant T, et al. Recent development in nanomaterials fabricated paper-based colorimetric and fluorescent sensors: A review. Trends Environ Anal Chem 2021;31:e00136. doi:10.1016/J.TEAC.2021.E00136.

[99] Croce R, Cinà F, Lombardo A, Crispeyn G, Cappelli CI, Vian M, et al. Aquatic toxicity of several textile dye formulations: Acute and chronic assays with Daphnia magna and Raphidocelis subcapitata. Ecotoxicol Environ Saf 2017;144:79–87. doi:10.1016/J.ECOENV.2017.05.046.

[100] Novotný Č, Dias N, Kapanen A, Malachová K, Vándrovcová M, Itävaara M, et al. Comparative use of bacterial, algal and protozoan tests to study toxicity of azo- and anthraquinone dyes. Chemosphere 2006;63:1436–42. doi:10.1016/J.CHEMOSPHERE.2005.10.002.

[101] Güngördü A, Birhanli A, Ozmen M. Biochemical response to exposure to six textile dyes in early developmental stages of Xenopus laevis. Environ Sci Pollut Res 2013;20:452–60. doi:10.1007/S11356-012-1063-1/TABLES/3.

[102] Li Z, Cui Z, Tang Y, Liu X, Zhang X, Liu B, et al. Fluorometric determination of ciprofloxacin using molecularly imprinted polymer and polystyrene microparticles doped with europium(III)(DBM) 3 phen. Microchim Acta 2019;186:1–10. doi:10.1007/S00604-019-3448-Z/TABLES/2.

[103] Liang H, Zheng Z, Zhang Q, Ming H, Chen B, Xu J, et al. Radiative properties of Eu(DBM)3Phen-doped poly(methyl methacrylate). J Mater Res 2003;18:1895–9. doi:10.1557/JMR.2003.0265.

[104] Wei X, Chen H. Ratiometric fluorescence molecularly imprinted sensor based on dual-emission quantum dots hybrid for determination of tetracycline. Anal Bioanal Chem 2019;411:5809–16. doi:10.1007/s00216-019-01963-3.

[105] Badıllı U, Mollarasouli F, Bakirhan NK, Ozkan Y, Ozkan SA. Role of quantum dots in pharmaceutical and biomedical analysis, and its application in drug delivery. TrAC Trends Anal Chem 2020;131:116013. doi:10.1016/J.TRAC.2020.116013.

[106] Hu X, Zhao Y, Dong J, Liu C, Qi Y, Fang G, et al. A strong blue fluorescent nanoprobe based on Mg/N co-doped carbon dots coupled with molecularly imprinted polymer for ultrasensitive and highly selective detection of tetracycline in animal-derived foods. Sensors Actuators B Chem 2021;338:129809. doi:10.1016/J.SNB.2021.129809.

[107] Satarug S, Moore MR. Adverse health effects of chronic exposure to low-level cadmium in foodstuffs and cigarette smoke. Environ Health Perspect 2004;112:1099–103.

doi:10.1289/EHP.6751.

[108] Modlitbová P, Pořízka P, Novotný K, Drbohlavová J, Chamradová I, Farka Z, et al. Short-term assessment of cadmium toxicity and uptake from different types of Cd-based Quantum Dots in the model plant Allium cepa L. Ecotoxicol Environ Saf 2018;153:23–31. doi:10.1016/J.ECOENV.2018.01.044.

[109] Zabihihesari A, Parand S, Coulthard AB, Molnar A, Hilliker AJ, Rezai P. An in-vivo microfluidic assay reveals cardiac toxicity of heavy metals and the protective effect of metal responsive transcription factor (MTF-1) in Drosophila model. 3 Biotech 2022;12:1–15. doi:10.1007/S13205-022-03336-7/FIGURES/7.

[110] Sharma N, Yun K. Dual sensing of tetracycline and l-Lysine using green synthesized carbon dots from Nigella sativa seeds. Dye Pigment 2020;182:108640. doi:10.1016/J.DYEPIG.2020.108640.

[111] Chauhan P, Chaudhary S. One step production of Se doped carbon dots for rapid sensing of tetracycline in real water sample. Opt Mater (Amst) 2021;121:111638. doi:10.1016/J.OPTMAT.2021.111638.

[112] Yan F, Sun Z, Pang J, Jiang Y, Zheng W. Functionalized carbon dots of thiazole derivatives based on inner filter effect for tetracyclines detection. Dye Pigment 2020;183:108673. doi:10.1016/J.DYEPIG.2020.108673.

[113] Danks AE, Hall SR, Schnepp Z. The evolution of 'sol–gel' chemistry as a technique for materials synthesis. Mater Horizons 2016;3:91–112. doi:10.1039/C5MH00260E.

[114] Zhang Y, Zhou Z, Zheng J, Li H, Cui J, Liu S, et al. SiO2-MIP core-shell nanoparticles containing gold nanoclusters for sensitive fluorescence detection of the antibiotic erythromycin. Microchim Acta 2017;184:2241–8. doi:10.1007/S00604-017-2216-1/TABLES/2.

[115] Zheng J, Nicovich PR, Dickson RM. Highly Fluorescent Noble-Metal Quantum Dots. Https://DoiOrg/101146/AnnurevPhyschem58032806104546 2007;58:409–31. doi:10.1146/ANNUREV.PHYSCHEM.58.032806.104546.

[116] Yuphintharakun N, Nurerk P, Chullasat K, Kanatharana P, Davis F, Sooksawat D, et al. A nanocomposite optosensor containing carboxylic functionalized multiwall carbon nanotubes and quantum dots incorporated into a molecularly imprinted polymer for highly selective and sensitive detection of ciprofloxacin. Spectrochim Acta - Part A Mol Biomol Spectrosc 2018;201:382–91. doi:10.1016/j.saa.2018.05.034.

[117] Shi T, Fu H, Tan L, Wang J. CdTe quantum dots coated with a molecularly imprinted polymer for fluorometric determination of norfloxacin in seawater. Microchim Acta 2019;186:1–8. doi:10.1007/S00604-019-3440-7/TABLES/2.

[118] Amiri A, Faridbod F, Zoughi S. An optical nanosensor fabricated by carbon dots embedded in silica molecularly imprinted polymer for sensitive detection of ceftazidime antibiotic. J Photochem Photobiol A Chem 2021;408:113111. doi:10.1016/J.JPHOTOCHEM.2020.113111.

[119] Jalili R, Khataee A, Rashidi MR, Razmjou A. Detection of penicillin G residues in milk

based on dual-emission carbon dots and molecularly imprinted polymers. Food Chem 2020;314:126172. doi:10.1016/J.FOODCHEM.2020.126172.

[120] Jalili R, Khataee A. Application of molecularly imprinted polymers and dual-emission carbon dots hybrid for ratiometric determination of chloramphenicol in milk. Food Chem Toxicol 2020;146:111806. doi:10.1016/J.FCT.2020.111806.

[121] Fu J, Zhou S, Wu X, Tang S, Zhao P, Tang K, et al. Down/up-conversion dual-mode ratiometric fluorescence imprinted sensor embedded with metal-organic frameworks for dual-channel multi-emission multiplexed visual detection of thiamphenicol. Environ Pollut 2022;309. doi:10.1016/j.envpol.2022.119762.

[122] Wu X, Tang S, Zhao P, Tang K, Chen Y, Fu J, et al. One-pot synthesis of ternary-emission molecularly imprinted fluorescence sensor based on metal–organic framework for visual detection of chloramphenicol. Food Chem 2023;402:2–10. doi:10.1016/j.foodchem.2022.134256.

[123] Liu H, Ding L, Chen L, Chen Y, Zhou T, Li H, et al. A facile, green synthesis of biomass carbon dots coupled with molecularly imprinted polymers for highly selective detection of oxytetracycline. J Ind Eng Chem 2019;69:455–63. doi:10.1016/J.JIEC.2018.10.007.

[124] Hou J, Li H, Wang L, Zhang P, Zhou T, Ding H, et al. Rapid microwave-assisted synthesis of molecularly imprinted polymers on carbon quantum dots for fluorescent sensing of tetracycline in milk. Talanta 2016;146:34–40. doi:10.1016/j.talanta.2015.08.024.

[125] Zhou T, Halder A, Sun Y. Fluorescent Nanosensor Based on Molecularly Imprinted Polymers Coated on Graphene Quantum Dots for Fast Detection of Antibiotics. Biosens 2018, Vol 8, Page 82 2018;8:82. doi:10.3390/BIOS8030082.

[126] Chao MR, Hu CW, Chen JL. Comparative syntheses of tetracycline-imprinted polymeric silicate and acrylate on CdTe quantum dots as fluorescent sensors. Biosens Bioelectron 2014;61:471–7. doi:10.1016/j.bios.2014.05.058.

[127] Tang K, Chen Y, Wang X, Zhou Q, Lei H, Yang Z, et al. Smartphone-integrated tri-color fluorescence sensing platform based on acid-sensitive fluorescence imprinted polymers for dual-mode visual intelligent detection of ibuprofen, chloramphenicol and florfenicol. Anal Chim Acta 2023;1260:341174. doi:10.1016/J.ACA.2023.341174.

[128] Nguyen HH, Park J, Kang S, Kim M. Surface Plasmon Resonance: A Versatile Technique for Biosensor Applications. Sensors 2015, Vol 15, Pages 10481-10510 2015;15:10481–510. doi:10.3390/S150510481.

[129] Jung LS, Campbell CT, Chinowsky TM, Mar MN, Yee SS. Quantitative interpretation of the response of surface plasmon resonance sensors to adsorbed films. Langmuir 1998;14:5636–48. doi:10.1021/LA971228B/ASSET/IMAGES/LARGE/LA971228BF00013.JPEG.

[130] Luo Q, Yu N, Shi C, Wang X, Wu J. Surface plasmon resonance sensor for antibiotics detection based on photo-initiated polymerization molecularly imprinted array. Talanta 2016;161:797–803. doi:10.1016/J.TALANTA.2016.09.049.

[131] Sari E, Üzek R, Duman M, Denizli A. Fabrication of surface plasmon resonance nanosensor for the selective determination of erythromycin via molecular imprinted nanoparticles. Talanta 2016;150:607–14. doi:10.1016/J.TALANTA.2015.12.043.

[132] Bereli N, Çimen D, Hüseynli S, Denizli A. Detection of amoxicillin residues in egg extract with a molecularly imprinted polymer on gold microchip using surface plasmon resonance and quartz crystal microbalance methods. J Food Sci 2020;85:4152–60. doi:10.1111/1750-3841.15529.

[133] Kurç Ö, Türkmen D. Molecularly Imprinted Polymers Based Surface Plasmon Resonance Sensor for Sulfamethoxazole Detection. Photonic Sensors 2022;12. doi:10.1007/s13320-022-0658-5.

[134] Faalnouri S, Çimen D, Bereli N, Denizli A. Surface Plasmon Resonance Nanosensors for Detecting Amoxicillin in Milk Samples with Amoxicillin Imprinted Poly(hydroxyethyl methacrylate-N-methacryloyl-(L)- glutamic acid). ChemistrySelect 2020;5:4761–9. doi:10.1002/slct.202000621.

[135] Wang W, Wang R, Liao M, Kidd MT, Li Y. Rapid detection of enrofloxacin using a localized surface plasmon resonance sensor based on polydopamine molecular imprinted recognition polymer. J Food Meas Charact 2021;15:3376–86. doi:10.1007/s11694-021-00913-x.

[136] Pérez-Jiménez AI, Lyu D, Lu Z, Liu G, Ren B. Surface-enhanced Raman spectroscopy: benefits, trade-offs and future developments. Chem Sci 2020;11:4563–77. doi:10.1039/D0SC00809E.

[137] Moskovits M. Surface-enhanced Raman spectroscopy: a brief retrospective. J Raman Spectrosc 2005;36:485–96. doi:10.1002/JRS.1362.

[138] Wang M, Wang Y, Qiao Y, Wei M, Gao L, Wang L, et al. High-sensitive imprinted membranes based on surface-enhanced Raman scattering for selective detection of antibiotics in water. Spectrochim Acta Part A Mol Biomol Spectrosc 2019;222:117116. doi:10.1016/J.SAA.2019.05.021.

[139] Li H, Zhang J, Wang D, Wang J, Jiang W, Zhou T, et al. Synthesization of flexible SERS imprinted sensor based on Ag/GO composites and selective detection of antibiotic in aqueous sample. Adv Powder Technol 2021;32:3405–11. doi:10.1016/J.APT.2021.07.014.

[140] He Y, Li L, Li X, Zhang J. Preparation of Magnetic Molecularly Imprinted Polymer Fe3O4@SiO2@Ag-MIPs and Its Identification and SERS Detection of Ofloxacin. Https://DoiOrg/101246/Cl200145 2020;49:713–6. doi:10.1246/CL.200145.

[141] Sui G, Yang X, Li H, Li Y, Li L, Shao J, et al. Synthesis of SERS imprinted membrane based on Ag/ESM with different morphologies for selective detection of antibiotics in aqueous sample. Opt Mater (Amst) 2021;121:111581. doi:10.1016/J.OPTMAT.2021.111581.

[142] Di Nardo F, Chiarello M, Cavalera S, Baggiani C, Anfossi L. Ten Years of Lateral Flow Immunoassay Technique Applications: Trends, Challenges and Future Perspectives. Sensors 2021, Vol 21, Page 5185 2021;21:5185. doi:10.3390/S21155185.

[143] Sun J, Warden AR, Ding X. Recent advances in microfluidics for drug screening. Biomicrofluidics 2019;13:061503. doi:10.1063/1.5121200.

[144] Du Y, Liu D, Wang M, Guo F, Lin JS. Preparation of DNA aptamer and development of lateral flow aptasensor combining recombinase polymerase amplification for detection of erythromycin. Biosens Bioelectron 2021;181:113157. doi:10.1016/J.BIOS.2021.113157.

[145] Raysyan A, Galvidis IA, Schneider RJ, Eremin SA, Burkin MA. Development of a latex particles-based lateral flow immunoassay for group determination of macrolide antibiotics in breast milk. J Pharm Biomed Anal 2020;189:113450. doi:10.1016/J.JPBA.2020.113450.

[146] Zeng L, Liu L, Kuang H, Cui G, Xu C. A paper-based colorimetric assay for rapid detection of four macrolides in milk. Mater Chem Front 2019;3:2175–83. doi:10.1039/C9QM00429G.

[147] Hendrickson OD, Zvereva EA, Zherdev A V., Godjevargova T, Xu C, Dzantiev BB. Development of a double immunochromatographic test system for simultaneous determination of lincomycin and tylosin antibiotics in foodstuffs. Food Chem 2020;318:126510. doi:10.1016/J.FOODCHEM.2020.126510.

[148] Li X, Wu X, Wang J, Hua Q, Wu J, Shen X, et al. Three lateral flow immunochromatographic assays based on different nanoparticle probes for on-site detection of tylosin and tilmicosin in milk and pork. Sensors Actuators B Chem 2019;301:127059. doi:10.1016/J.SNB.2019.127059.

[149] Guo L, Liu L, Cui G, Ma S, Wu X, Kuang H. Gold immunochromatographic assay for kitasamycin and josamycin residues screening in milk and egg samples. Https://DoiOrg/101080/0954010520191677567 2019;30:1189–201. doi:10.1080/09540105.2019.1677567.

[150] Zeng Y, Liang D, Zheng P, Zhang Y, Wang Z, Mari GM, et al. A simple and rapid immunochromatography test based on readily available filter paper modified with chitosan to screen for 13 sulfonamides in milk. J Dairy Sci 2021;104:126–33. doi:10.3168/jds.2020-18987.

[151] Liu J, Wang B, Huang H, Jian D, Lu Y, Shan Y, et al. Quantitative ciprofloxacin on-site rapid detections using quantum dot microsphere based immunochromatographic test strips. Food Chem 2021;335:127596. doi:10.1016/J.FOODCHEM.2020.127596.

[152] Bosma R, Devasagayam J, Singh A, Collier CM. Microchip capillary electrophoresis dairy device using fluorescence spectroscopy for detection of ciprofloxacin in milk samples. Sci Reports 2020 101 2020;10:1–8. doi:10.1038/s41598-020-70566-1.

[153] Zong L, Jiao Y, Guo X, Zhu C, Gao L, Han Y, et al. Paper-based fluorescent immunoassay for highly sensitive and selective detection of norfloxacin in milk at picogram level. Talanta 2019;195:333–8. doi:10.1016/J.TALANTA.2018.11.073.

[154] Zhou T, Liu JJ, Xu Y, Wu ZY. Fast and sensitive screening detection of tetracyclines with a paper-based analytical device. Microchem J 2019;145:703–7. doi:10.1016/J.MICROC.2018.10.022.

[155] Wang X, Li J, Jian D, Zhang Y, Shan Y, Wang S, et al. Paper-based antibiotic sensor (PAS) relying on colorimetric indirect competitive enzyme-linked immunosorbent assay for quantitative tetracycline and chloramphenicol detection. Sensors Actuators, B Chem 2021;329:129173. doi:10.1016/j.snb.2020.129173.

[156] Zhang F, Liu M, Liu R, Li J, Sang Y, Tang Y, et al. A broad-spectrum sensing strategy for the tetracycline family of antibiotics based on an ovalbumin-stabilized gold nanocluster and its application in a pump-free microfluidic sensing platform. Biosens Bioelectron 2021;171:112701. doi:10.1016/J.BIOS.2020.112701.

[157] Zhao M, Li X, Zhang Y, Wang Y, Wang B, Zheng L, et al. Rapid quantitative detection of chloramphenicol in milk by microfluidic immunoassay. Food Chem 2021;339:127857. doi:10.1016/j.foodchem.2020.127857.

[158] Wang L, Zhu F, Zhu Y, Xie S, Chen M, Xiong Y, et al. Intelligent Platform for Simultaneous Detection of Multiple Aminoglycosides Based on a Ratiometric Paper-Based Device with Digital Fluorescence Detector Readout. ACS Sensors 2019;4:3283–90. doi:10.1021/ACSSENSORS.9B01845/SUPPL_FILE/SE9B01845_SI_001.PDF.

[159] He L, Shen Z, Wang J, Zeng J, Wang W, Wu H, et al. Simultaneously responsive microfluidic chip aptasensor for determination of kanamycin, aflatoxin M1, and 17β-estradiol based on magnetic tripartite DNA assembly nanostructure probes. Microchim Acta 2020;187:1–11. doi:10.1007/S00604-020-4155-5/FIGURES/4.

[160] Li X, Wen K, Chen Y, Wu X, Pei X, Wang Q, et al. Multiplex Immunogold Chromatographic Assay for Simultaneous Determination of Macrolide Antibiotics in Raw Milk. Food Anal Methods 2015;8:2368–75. doi:10.1007/S12161-015-0130-X/FIGURES/8.

[161] Parolo C, Sena-Torralba A, Bergua JF, Calucho E, Fuentes-Chust C, Hu L, et al. Tutorial: design and fabrication of nanoparticle-based lateral-flow immunoassays. Nat Protoc 2020 1512 2020;15:3788–816. doi:10.1038/s41596-020-0357-x.

[162] Gao S, Wang W, Wang B. Molecularly imprinted polymers as recognition elements in optical sensors. Mol Imprinted Mater Sci Technol 2004:701–26. doi:10.1201/9781420030303.

[163] Le T, He H, Niu X, Chen Y, Xu J. Development of an immunochromatographic assay for detection of tylosin and tilmicosin in muscle, liver, fish and eggs. Http://DxDoiOrg/101080/095401052012716025 2013;24:467–80. doi:10.1080/09540105.2012.716025.

[164] Liu Z, Chen J, Zhao S, Pang Y, Shen X, Lei H, et al. Immunochromatographic assays based on three kinds of nanoparticles for the rapid and highly sensitive detection of tylosin and tilmicosin in eggs. Microchim Acta 2022;189:1–11. doi:10.1007/S00604-021-05151-Y/TABLES/3.

[165] Thongchai W, Liawruangath B, Liawruangrath S, Greenway GM. A microflow chemiluminescence system for determination of chloramphenicol in honey with preconcentration using a molecularly imprinted polymer. Talanta 2010;82:560–6. doi:10.1016/J.TALANTA.2010.05.007.

[166] Song X, Zhou T, Li J, Su Y, Xie J, He L. Determination of macrolide antibiotics residues in pork using molecularly imprinted dispersive solid-phase extraction coupled with LC–MS/MS. J Sep Sci 2018;41:1138–48. doi:10.1002/JSSC.201700973.

[167] Song X, Id †, Zhou T, Li J, Zhang M, Xie J, et al. molecules Determination of Ten Macrolide Drugs in Environmental Water Using Molecularly Imprinted Solid-Phase Extraction Coupled with Liquid Chromatography-Tandem Mass Spectrometry n.d. doi:10.3390/molecules23051172.

[168] Harron DWG. Technical Requirements for Registration of Pharmaceuticals for Human Use: The ICH Process. Textb Pharm Med 2013;1994:447–60. doi:10.1002/9781118532331.ch23.

[169] Harrower J, McNaughtan M, Hunter C, Hough R, Zhang Z, Helwig K. Chemical Fate and Partitioning Behavior of Antibiotics in the Aquatic Environment—A Review. Environ Toxicol Chem 2021;40:3275–98. doi:10.1002/ETC.5191.

[170] Schroeder NE, MacGuidwin AE. Behavioural quiescence reduces the penetration and toxicity of exogenous compounds in second-stage juveniles of Heterodera glycines. Nematology 2010;12:277–87. doi:10.1163/138855409X12506855979712.

[171] Mchedlov-Petrossyan NO, Isaenko Y V, Vodolazkaya NA, Goga ST. Acid-Base Behavior of Fluorescein Isothiocyanate in Aqueous Media and in Micellar Surfactant Solutions. Http://PreprintChemwebCom/Physchem/0309005 2003;2003:93–101.

[172] Zarski P, Ryder AG. Super Stable Fluorescein Isothiocyanate Isomer i Monolayer for Total Internal Reflection Fluorescence Microscopy. Langmuir 2018;34:10913–23. doi:10.1021/acs.langmuir.8b02509.

[173] Sjöback R, Nygren J, Kubista M. Absorption and fluorescence properties of fluorescein. Spectrochim Acta Part A Mol Spectrosc 1995;51. doi:10.1016/0584-8539(95)01421-P.

[174] Wentworth S. LOD_Sensitivity 1996:1996.

[175] Korzhikova-Vlakh E, Antipchik M, Tennikova T. Macroporous polymer monoliths in thin layer format. Polymers (Basel) 2021;13. doi:10.3390/polym13071059.

[176] Hijazi HY, Bottaro CS. Molecularly imprinted polymer thin-film as a micro-extraction adsorbent for selective determination of trace concentrations of polycyclic aromatic sulfur heterocycles in seawater. J Chromatogr A 2020;1617. doi:10.1016/j.chroma.2019.460824.

[177] Sheybani S, Hosseinifar T, Abdouss M, Mazinani S. Mesoporous molecularly imprinted polymer nanoparticles as a sustained release system of azithromycin. RSC Adv 2015;5:98880–91. doi:10.1039/C5RA11970G.

[178] Mhatre AM, Chappa S, Ojha S, Pandey AK. Functionalized glass fiber membrane for extraction of iodine species. Sep Sci Technol 2019;54:1469–77. doi:10.1080/01496395.2018.1520729.

[179] Jradi K, Daneault C, Chabot B. Chemical surface modification of glass beads for the treatment of paper machine process waters. Thin Solid Films 2011;519:4239–45. doi:10.1016/j.tsf.2011.02.080.

[180] Li W, Chu K, Liu L. Multipurpose Zwitterionic Polymer-Coated Glass Fiber Filter for Effective Separation of Oil-Water Mixtures and Emulsions and Removal of Heavy Metals. ACS Appl Polym Mater 2021;3:1276–84. doi:10.1021/acsapm.0c00928.

[181] Liu Q, Patel AA, Liu L. Superhydrophilic and underwater superoleophobic poly(sulfobetaine methacrylate)-grafted glass fiber filters for oil-water separation. ACS Appl Mater Interfaces 2014;6:8996–9003. doi:10.1021/am502302g.

[182] Cha Y-H, Matsuno N, Ronkainen-Matsuno NJ, Jensen K, Gutow J. Comparison of plasma and piranha cleaning for surface preparation of gold (Au) prior to alkane thiol monolayer deposition using grazing incidence IR spectroscopy and microscopy n.d.:1–24.

[183] Zhang Y, Na Q, Chen N, Chen J, Zhou X, Bai L. Preparation and evaluation of melamine molecularly imprinted polymers by thermaland photo-initiation methods. J Chinese Chem Soc 2013;60:204–11. doi:10.1002/jccs.201200382.

[184] Lorenzo RA, Carro AM, Alvarez-Lorenzo C, Concheiro A. To remove or not to remove? The challenge of extracting the template to make the cavities available in molecularly imprinted polymers (MIPs). Int J Mol Sci 2011;12:4327–47. doi:10.3390/ijms12074327.

[185] Stoian IA, Iacob BC, Dudaș CL, Barbu-Tudoran L, Bogdan D, Marian IO, et al. Biomimetic electrochemical sensor for the highly selective detection of azithromycin in biological samples. Biosens Bioelectron 2020;155:112098. doi:10.1016/J.BIOS.2020.112098.

[186] Cao X, Ji S, Kuang W, Liao A, Lan P, Zhang J. Solubility determination and correlation for azithromycin monohydrate and dihydrate in solvent mixtures. J Mol Liq 2020;301:112398. doi:10.1016/J.MOLLIQ.2019.112398.

[187] Hasaneen N, Akhtarian S, Pulicharla R, Brar SK, Rezai P. Surface molecularly imprinted polymer-based sensors for antibiotic detection. TrAC - Trends Anal Chem 2024;170:117389. doi:10.1016/j.trac.2023.117389.

[188] Hasaneen N, Pulicharla R, Brar SK, Rezai P. Direct fluorescence and spectrophotometric-based detection of azithromycin using fluorescein isothiocyanate: Method development and comparative analysis. J Environ Chem Eng 2024;12:112803. doi:10.1016/j.jece.2024.112803.

Appendix

1. Image, table and calibration curve of the concentration-response for the spectrophotometric detection technique.

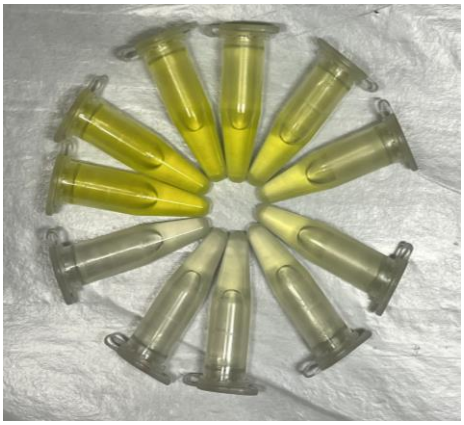

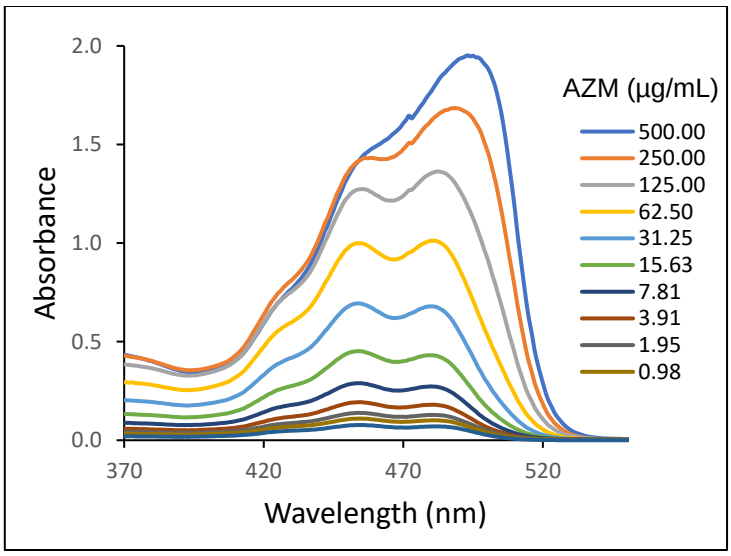

AZM (µg/mL)	31.25	25.00	15.63	15.00	7.81	5.00	3.91	1.95	0.98	0.00
Absorbance	0.66	0.58	0.44	0.42	0.28	0.21	0.19	0.13	0.11	0.07
SD	0.02	0.02	0.01	0.01	0.01	0.01	0.01	0.01	0.00	0.00

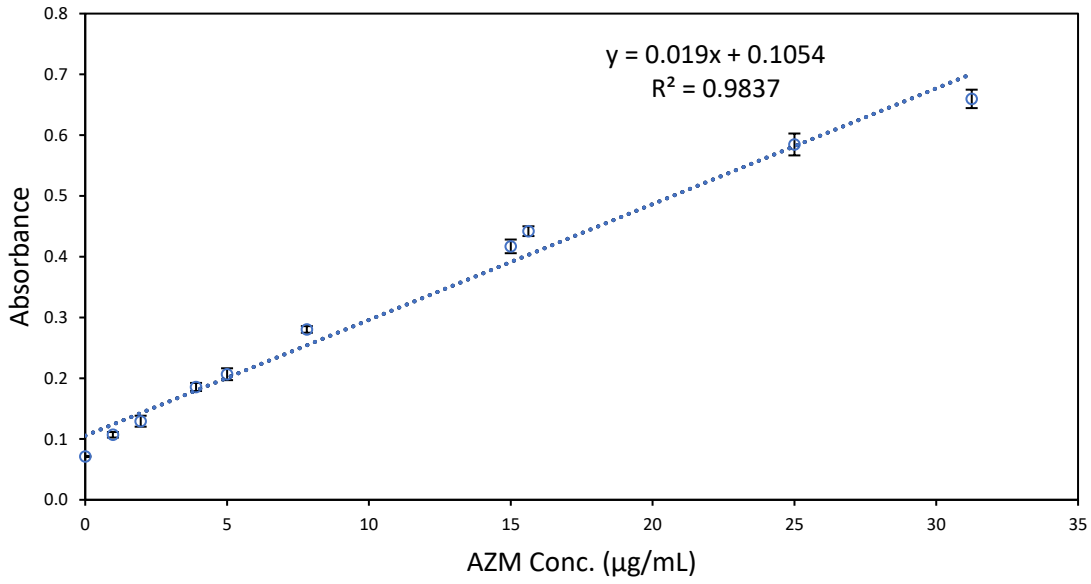

2. Image, table and calibration curve of the concentration-response for the fluorescence microscopic-based detection technique.

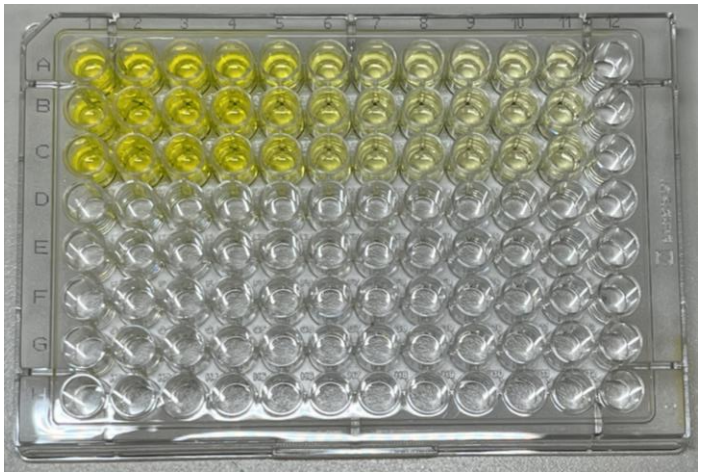

AZM (µg/mL)	31.25	25	15.63	15.00	7.81	5.00	3.91	1.95	0.00
Fluorescence intensity	68.84	53.28	39.73	35.26	22.80	15.45	13.32	7.67	4.01
SD	3.27	0.23	1.95	1.43	0.74	0.31	1.67	0.34	0.66

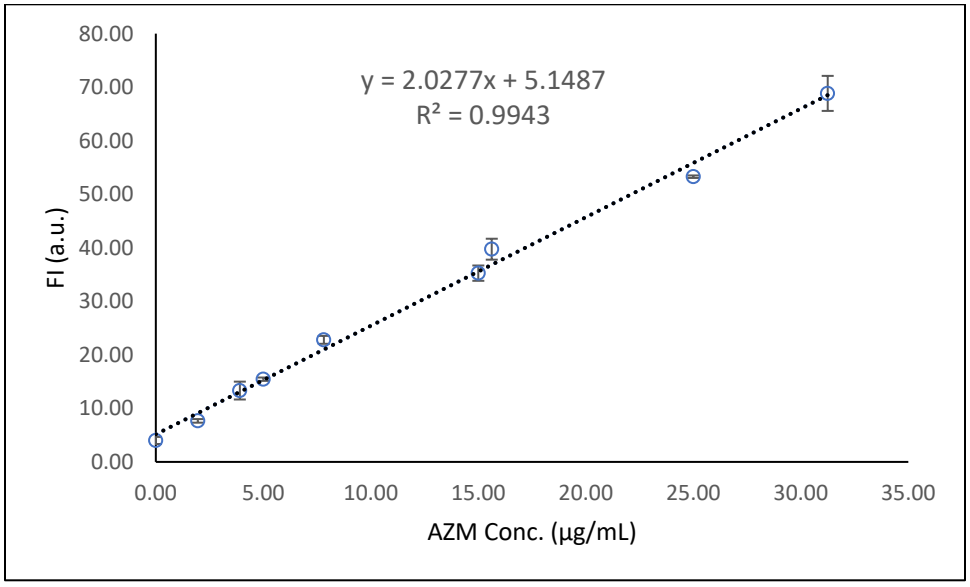

3. Evidence for ion-pair complex formation:

For ion-pair complex formation evidence, we mainly relied on the chemical characteristics of the two compounds where their ionization can be determined based on their pKa and the solution pH. FTIR only gave the peaks for methanol with no significant peaks for the complex nor the controls

for two individual compounds (AZM in methanol and FITC in methanol). We have used direct scan mass spectrometry for FITC in methanol (25 ug/ml) at 388 m/z, AZM in methanol (12.5 ug/ml) at 749.5 m/z, and for complex in methanol, where the concentration of the compounds kept constant in the controls and the complex. AZM solution was directly infused in the "+" mode and the same was done for FITC but in the "_" mode. Finally, the complex was determined in both "_" and "+" modes. Figure b and d showed a decrease in the peak total area at 388 m/z and 749.5 m/z in the complex compared to FITC and AZM (figure a and c), respectively. This decrease in the peaks total area in the complex compared to the corresponding peaks in the controls strongly suggests the formation of AZN-FITC ion pair complex which can stabilize the ions leading to their decreased abundance in the mass spectrum.

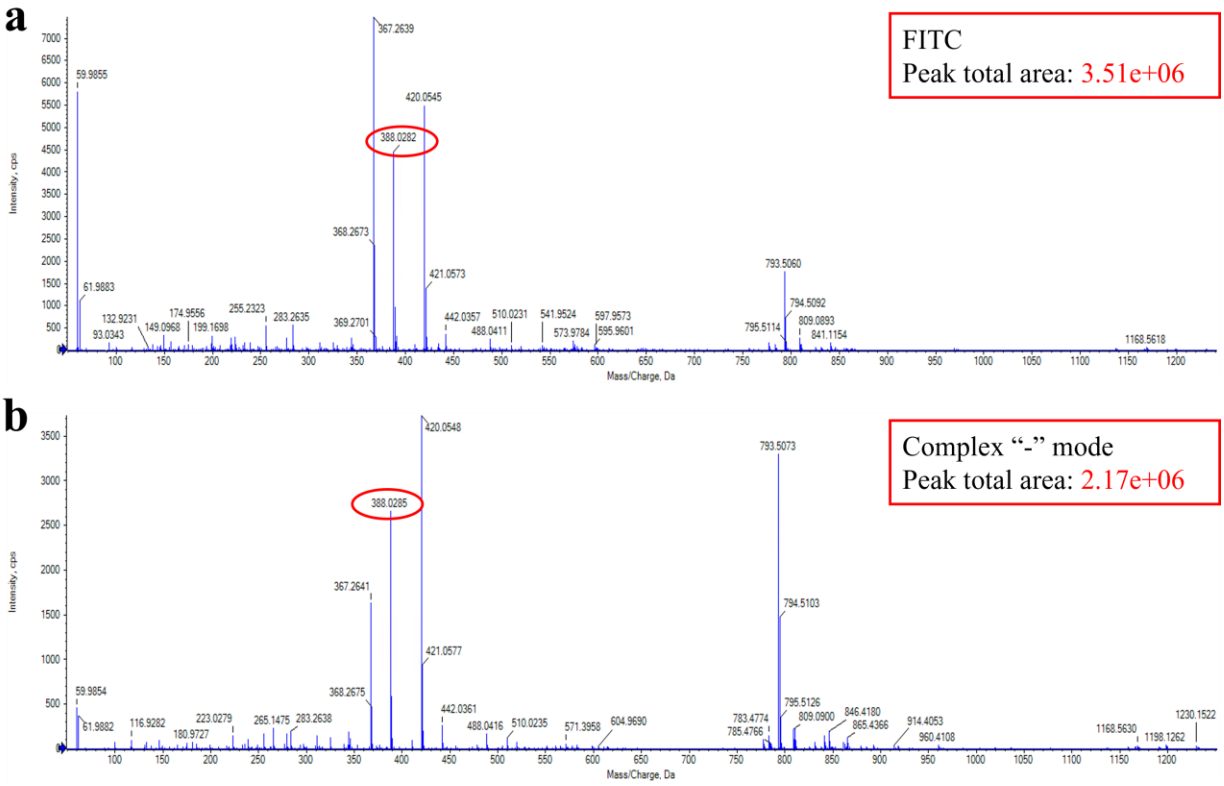

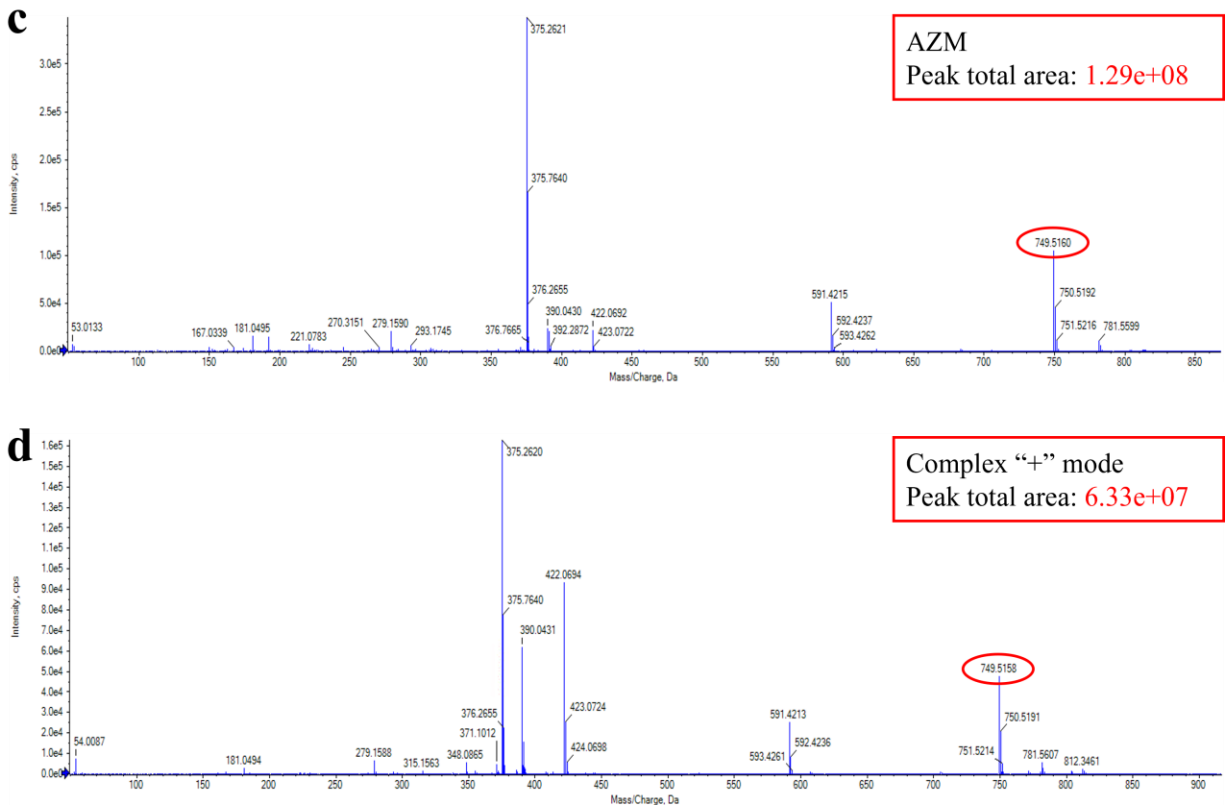

Mass spectrum of a. FITC 25 ug/ml in methanol, b. complex in "_" mode, c. AZM 12.5 ug/ml in methanol, d. complex in "+".

4. Polymer peeling off from the glass slides when not treated correctly.

5. Effect of changing the polymer recipe on the NIP:

Exp. No.	Monomer:Crosslinker	Monomer	Crosslinker	Solvent
1	1:3	MAA	EGDMA	ACN
2	1:4	MAA	EGDMA	ACN
3	1:5	MAA	EGDMA	ACN
4	1:10	MAA	EGDMA	ACN
5	1:3	MAA	EGDMA	DMSO
6	1:3	MMA	EGDMA	ACN
7	1:3	MMA	EGDMA	DMSO
8	1:10	MMA	EGDMA	ACN
9	1:3	MMA	DHEBA	DMSO
10	1:3	MAA	DHEBA	DMSO
11	1:2	MAA	EGDMA	ACN
12	1:1	MAA	EGDMA	ACN
13	1:2.5	MAA	EGDMA	ACN

MAA (Methacrylic acid)

MMA (Methyl methacrylate)

EGDMA (Ethyleneglycol dimethacrylate)

ACN (Acetonitrile)

DMSO (Dimethylsulfoxide)

DHEBA (Dihydroxyethylene bisacrylamide)

After 1 hour under UV

Start drying in

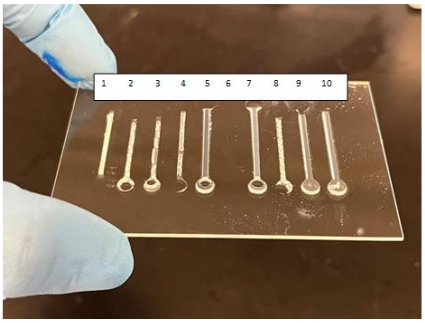

After washed with methanol and air dried

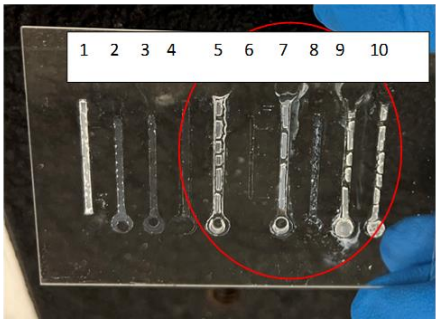

For 11, 12, and 13 experiments, no intact polymer was obtained and only white suspension was formed. When DMSO was used as a solvent in the prepolymerization solution, a transparent glassy polymer was obtained which can be easily cracked by washing as in experiment 5, 7, 9, and 10. The best composition to be used is the one in experiment 1 which gives white porous polymer.

6. 3D printed mold with different channels height and the resulted PDMS replica:

7. Set up during polymer washing using syringe pump:

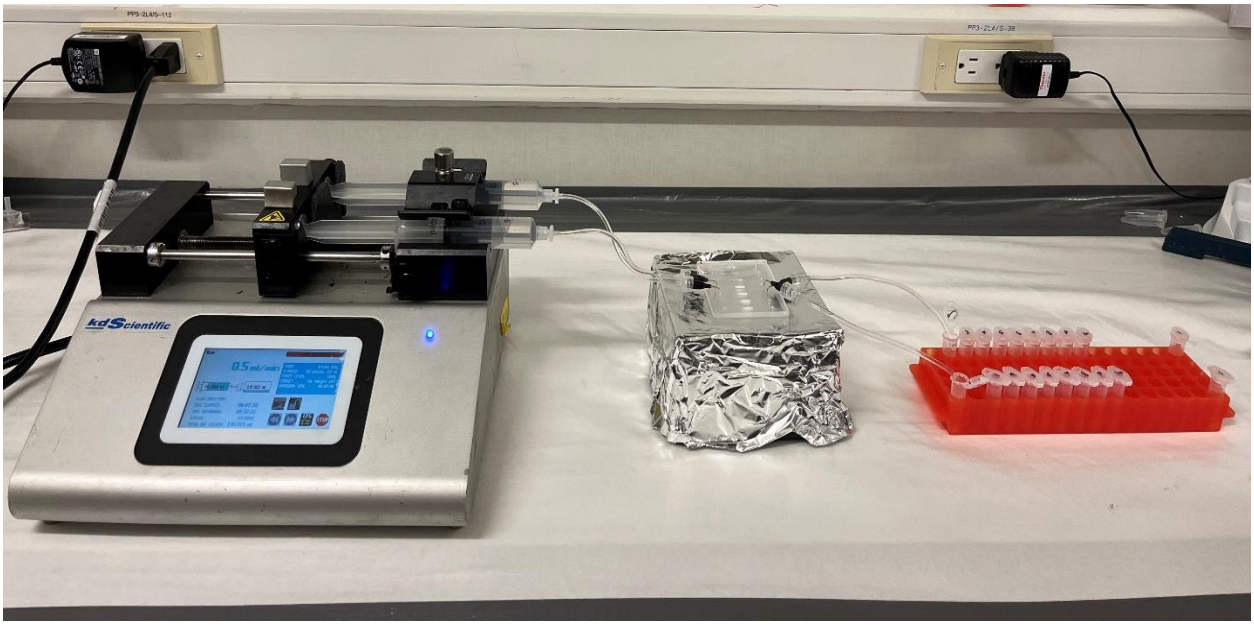

8. Table of fluorescence intensities (FI) and images of NIP and MIP after FITC application for the detection on ultrasonicated polymers (Experiment 1) in triplicate:

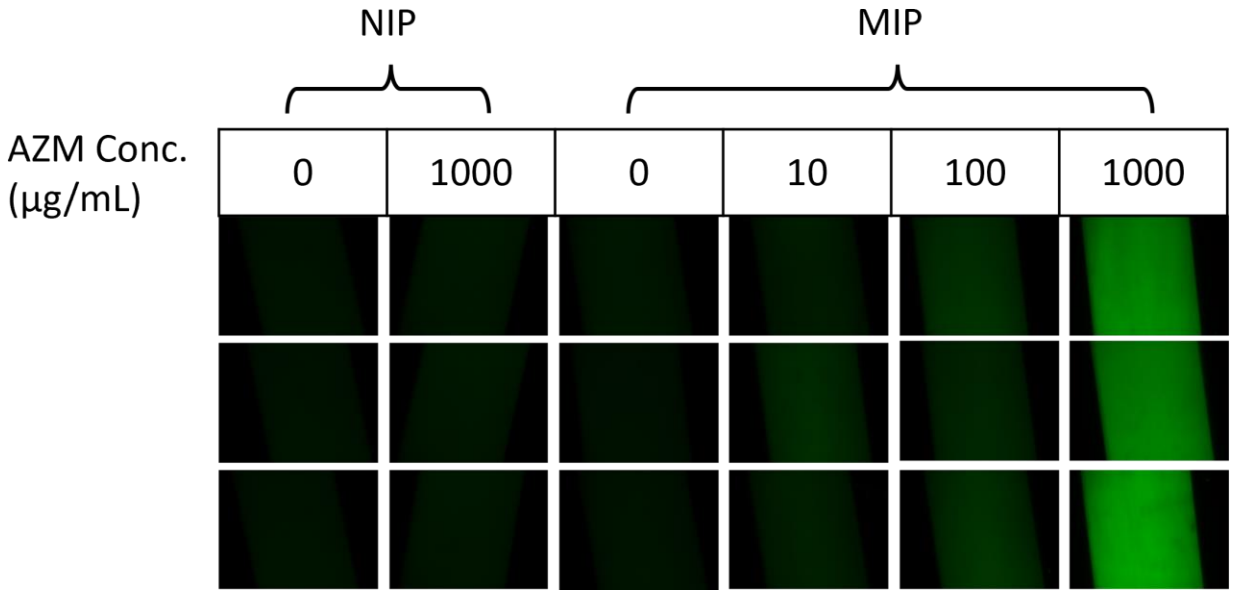

FI	5.51	6.983	7.193	8.668	10.92	37.396
	5.915	7.567	7.221	8.458	11.91	40.941
	5.763	7.023	5.779	9.43	14.538	38.996

9. Images, table and figure of fluorescence intensities (FI) after FITC application (Experiment 2) in triplicate where washing was done by a syringe pump:

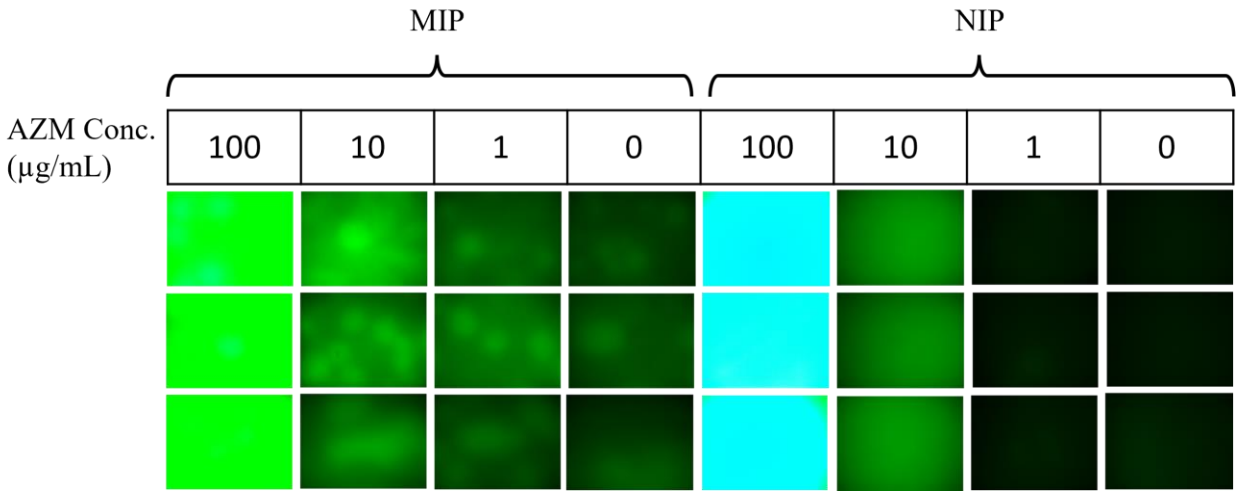

FI	91.178	57.935	29.192	20.043	168.288	42.625	6.985	6.695
	85.578	44.586	38.007	24.82	171.094	37.182	6.938	6.552
	85.433	35.238	23.509	18.565	167.611	42.174	7.457	9.497

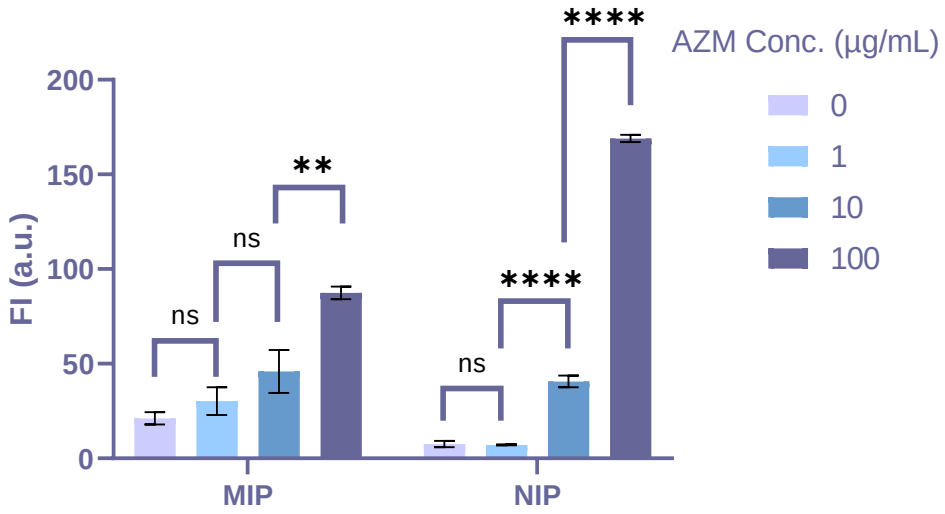

Fluorescence intensity graph (significance difference was calculated using $p<0.05$, ns: no significant difference, ** for p-value < 0.01, **** for p-value < 0.0001).